Universitat de les Illes Balears

Departament de Física

Time and Spatial Damping of Magnetohydrodynamic Waves in Partially Ionised Prominence Plasmas

Tesi Doctoral

Pep Forteza Ferrer

Tesi presentada per optar al Grau de Doctor en Física per la Universitat de les Illes Balears

Dirigida pels Profs. R. Oliver i J. L. Ballester

Palma de Mallorca, 22 de Novembre de 2012

Programa Oficial de Postgrau de Ciències Experimentals i Tecnologies (Física)

Universitat de les Illes Balears

Índex

Acknowledgements

En primer lloc voldria agraïr el suport financer rebut per part del Ministeri d'Educació i Ciència en forma de la beca de Formació de Professorat Universitari AP-2004-3806.

I also want to thank Maxim Khodachenko, Bernie Roberts and the rest of the Saint Andrews Solar Physics Group for their kind hospitality during my stay in Graz and Saint Andrews.

Molt especialment voldria agraïr als meus directors de tesi, Pep Lluís i Moncho, per haver-me donat la possibilitat d'experimentar en primera persona el món de la recerca i guiar-me en aquest procés. Sense la seva ajuda aquesta tesi no hauria vist la llum.

A tots els membres del grup de Física Solar de la UIB, Marc, Jaume, Íñigo, Toni, Manuel, Roberto i Samuel, agraïr-los haver estat uns grans companys de feina i viatge durant aquests anys, els berenars de grup, les discussions científiques i no científiques i el gran ambient de feina existent en el grup durant tot aquest temps.

Per acabar voldria agraïr als màxims responsables de que aquesta tesi hagi vist la llum: la meva familia i els meus amics, i en especial els meus pares. Sense el seu suport incondicional i els seus ànims aquesta etapa de la meva vida no hauria finalitzat.

Moltes gràcies!

Summary

Prominence oscillations are frequently detected by means of oscillatory variations in Doppler signals and spectral lines intensity. These oscillations seem to be strongly damped after a few periods. While oscillations have been interpreted in the context of the magnetohydrodynamic (MHD) theory in terms of the normal modes and propagating MHD waves supported by the filament, the mechanisms responsible for the damping are not well known and their investigation is the aim of the present research.

Prominence observations also indicate that these large scale coronal structures are formed by partially ionised plasma, although the quoted degree of ionization varies a lot from one work to another.

In this Thesis, the study of the effect of ion-neutral collisions on the damping of magnetohydrodynamic waves is started. First of all, we develop a set of one-fluid equations for a partially ionised plasma and use it in different plasma configurations.

As a first step in the study of partially ionised plasmas, the simplest plasma configuration is considered, an unbounded homogeneous partially ionised plasma. We study the temporal and spatial damping of magnetoacoustic waves (fast and slow) and Alfvén waves in the case of adiabatic and non-adiabatic plasmas. While the time damping of MHD waves in adiabatic partially ionised plasmas is due to ion-neutral collisions, in the non-adiabatic case it is possible to study the importance of each of the different damping mechanisms involved which are ion-neutral collisions, radiative losses and thermal conduction. On the other hand, in the case of spatial damping we have considered adiabatic and non-adiabatic MHD waves in fully ionised resistive as well as partially ionised plasmas, and we have also included the presence of flows. The consideration of all these effects has allowed us to obtain a more in-depth knowledge about their influence in the spatial damping of the studied MHD waves.

This work is intended to serve as a basis for future studies of more complex models such as the effect of the surrounding coronal material (slab configuration), the inclusion of threads or the influence of helium and its ions.

Resum en català

Les oscil·lacions de les protuberàncies són detectades freqüentment mitjançant variacions oscil·latòries en senyals Doppler i en la intensitat de les línies espectrals. Aquestes oscil·lacions pareixen fortament esmorteïdes després de pocs períodes. Mentre que les oscil·lacions s'han interpretat dins el context de la magnetohidrodinàmica (MHD) en termes de modes normals i ones MHD que es propaguen suportades pel filament, els mecanismes responsables de l'esmorteïment encara no es coneixen amb precissió i són objecte d'investigacions actuals.

Les observacions de protuberàncies mostren que aquestes estructures coronals de gran escala estan formades per plasmes parcialment ionitzats, tot i que el grau d'ionització varia molt entre els diferents estudis realitzats.

En aquesta Tesi s'inicia l'estudi de l'efecte de les col·lisions entre ions i àtoms neutres en l'esmorteïment de les ones magnetohidrodinàmiques. S'inicia l'estudi amb el desenvolupament de les equacions magnetohidrodinàmiques per un fluid considerant ionització parcial i s'aplica aquest conjunt d'equacions a diferents configuracions de plasmes.

Com a treball precursor, es considera la configuració geomètrica més simple, un plasma parcialment ionitzat, infinit i homogeni, i s'analitza l'esmorteïment temporal i espacial de les ones magnetoacústiques (ràpides i lentes) i les ones d'Alfvén tan en el cas de plasmes adiabàtics com en el cas de plasmes no adiabàtics. Mentre l'esmorteïment temporal de les ones MHD en plasmes adiabàtics parcialment ionitzats és degut a les col.lisions entre ions i neutres, en el cas no adiabàtic és possible estudiar l'importància de cada mecanisme d'esmorteïment involucrat. Aquests mecanismes són: col.lisions ions-neutres, pèrdues radiatives i la conducció tèrmica. Per altre banda, en el cas de l'esmorteïment espacial s'han estudiat també ones MHD adiabàtiques i no adiabàtiques en plasmes resistius totalment ionitzats així com en plasmes parcialment ionitzats, i hem inclós la presència de fluxes. La consideració de tots aquests efectes ha perms obtenir un coneixement molt més profund de la seva influència en l'esmorteïment espacial de les ones MHD estudiades.

Aquest treball forma una base per a l'estudi de models més complexes com ara l'efecte del material coronal, la inclusió d'estructura de fibres o la influència de la presència d'heli i dels seus ions.

Preface

People have worshipped the Sun and solar deities for all recorded history. Hence, many beliefs and legends have been formed around this worship, explaining several natural phenomena, such as the disappearance of the Sun at night, the shorter days during the winter or solar eclipses.

To understand the importance and respect that this body has generated on mankind, here there is a selection of some of the most relevant myths that involve the Sun.

In Egyptian mythology, the Sun god Ra (Figure 1c) passes through the Duat (the underworld) every night, in order to rise in the morning, in his solar barge, to avoid being extinguished by the waters. Each night he has to fight and defeat Apep (also known as Apophis in Greek), an evil demon personification of darkness and chaos.

In Hinduism, Surya (Figure 1b) was the solar deity and was represented with hair and arms of gold. His chariot was pulled by seven horses, a representation of the seven chakras. Occasionally, Surya was represented as an inanimate object, a shining gem placed in the midst of the heaven.

Amaterasu (Figure 1d) was the Japanese Sun goddess that hides herself in a cave, plunging the world into darkness, because she was angered, embarrassed or scared, depending on the source, by the behaviour of her brother Susanoo, the storm deity. With this myth, the Japanese mythology explained the shorter days during the winter.

In a Chinese myth, solar eclipses were caused by the dog of heaven biting off a piece of the Sun. In China there was the tradition of hitting pots and pans during a solar eclipse to drive away the dog with the noise.

In Norse mythology, Sol rode through the sky on her chariot pulled by two horses, Arvak and Alsvid. She was chased every day by the wolf Skoll, that wanted to devour her (while every night his brother Hati chased the Moon). Solar eclipses meant that Skoll had almost caught up to her. In Norse belief, the Sun did not give light, this was caused by the manes of the horses that pulled her chariot.

Helios (Figure 1a), the Greek god of the Sun, represented as a youth with a halo standing in a quadriga, rises each morning from the ocean in the east and rides his chariot drawn by four horses through the sky, to descend at night in the west. The great pride of Rhodes was the huge bronze statute in honour of the Sun god, reckoned as one of the Seven Wonders of the ancient

Figure 1: a) Helios ridding his quadriga in a Greek krater dated in 435 BC (British Museum, London). b) A representation of Surya on his chariot pulled by seven horses. c) Ra in the solar barge through Duat. d) Amaterasu emerging from a cave.

World.

Only with these few different examples of the rich mythology about the Sun one can see how some of these myths and stories are repeated in different mythologies with little changes: the Sun deity represented as an auriga or driving a barge, the explanation of eclipses as a bite on the solar disc, the daily chase of the Sun by a monster or demonic being, ...

There exist a lot more myths and legends related to the Sun and solar deities: Tama-nui-te-rā in Māori mythology, Maelare in the south coast of Papua New Guinea, Inti in Inca's beliefs, Tonatiuh for the Aztecs, ...

Making a complete and detailed list of all different myths and worships of the Sun and their influence in tradition, arts, constructions and heritage would extend over pages and pages. And, to add more difficulty to this titanic work, one needs to take into account the variation of the myths or deities over time. These were not immutable and far from this, mythology changed over the years. For instance, in late Greek mythology, Apollo became the Olympic Sun god, relegating Helios.

Chapter 1

The Sun

The Sun is an ordinary main sequence star of spectral type G2 V with an absolute bolometric magnitude of 4.74, and a surface temperature of, approximately, 5800 K. The only thing that makes this star so unique is its proximity to the Earth. This proximity allows us to study it in detail in order to understand the behaviour of stars.

Like other stars, the Sun is an autogravitating spheric object of plasma, with a radius of 700 000 km and an age of 4.5×10^9 years, located at 1 AU[1] from the Earth. The main physical parameters of the Sun are summarised in Table 1.1 together with a comparison with the Earth's ones.

The surface composition of the Sun is X = 0.74, Y = 0.24 and Z = 0.02 (mass fractions of hydrogen, helium and metals, respectively). The high abundance of heavy elements suggests that the Sun is a Population I, or third generation, star formed from the remains of former dead stars.

The Sun, as the other stars, generates energy by nuclear fusion and is in a hydrostatic balance state since pressure gradient balances the gravity force.

Parameter	Sun (⊙)	Earth (⊕)	Ratio (⊙/⊕)
Radius	6.96×10^8 m	6.371×10^6 m	109.24
Mass	1.99×10^{30} kg	5.97×10^{24} kg	333 333
Average density	1.5×10^5 kg m^{-3}	5.515 kg m^{-3}	0.255
Surface gravity	273.95 m s^{-2}	9.78 m s^{-2}	28.01
Escape velocity	617.6 m s^{-2}	11.19 m s^{-2}	55.19
Luminosity	3.827×10^{26} W		
Visual magnitude	−26.74		
Absolute magnitude	+4.83		
Equatorial rotation period	25.38 days	23 h 56 min	

Table 1.1: Sun's and Earth's main physical parameters.

---

[1] 1 AU (Astronomical Unit) $\cong 1.5 \times 10^8$ km.

1.1   Solar structure

1.1.1   Solar interior

The interior of the Sun is hidden from our view, only its surface layers can be seen. However, thanks to models and indirect observations, as the ones provided by helioseismology (the study of the internal oscillations of the Sun) and neutrino detection, we have been able to understand part of the solar interior behaviour and properties. In the solar interior, three different regions, namely, the core, the radiative zone and the convective zone (Figure 1.1) are considered. Some references include also the tachocline (the thin interface layer between the radiative and convective zones) as a fourth layer of the solar interior.
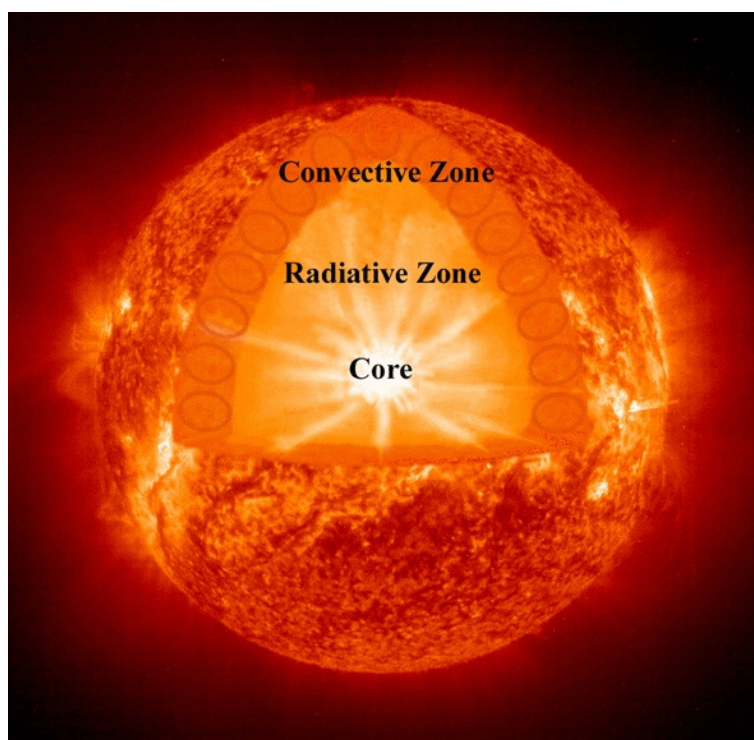
Figure 1.1: Scheme of the solar interior.

The core is the region where the nuclear fusion reactions take place, consuming $5,64 \times 10^8$ tons of hydrogen every second to form helium ($5,60 \times 10^8$ tons) and releasing energy (coming from the mass difference). This region contains half the mass of the Sun in only a radius of $0.25\ R_\odot$[2].

Nuclear fusion reactions require that individual hydrogen nuclei collide with each other with enough energy to overcome the repulsive electrical forces between them. The temperature at the centre of the Sun is estimated, according to models, at 15 000 000 K and the density at 150 000 $\mathrm{kg\,m^{-3}}$. Both

---

[2]$R_\odot$ is the symbol used to denote the solar radius.
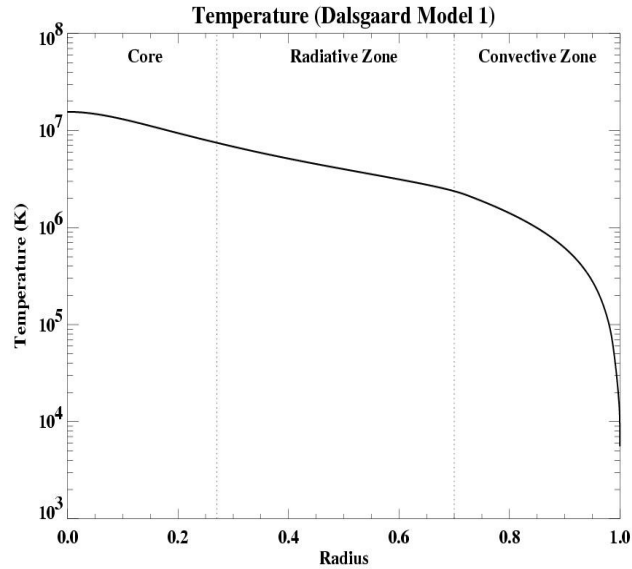
Figure 1.2: Solar interior temperature versus distance from the centre normalised to the solar radius.
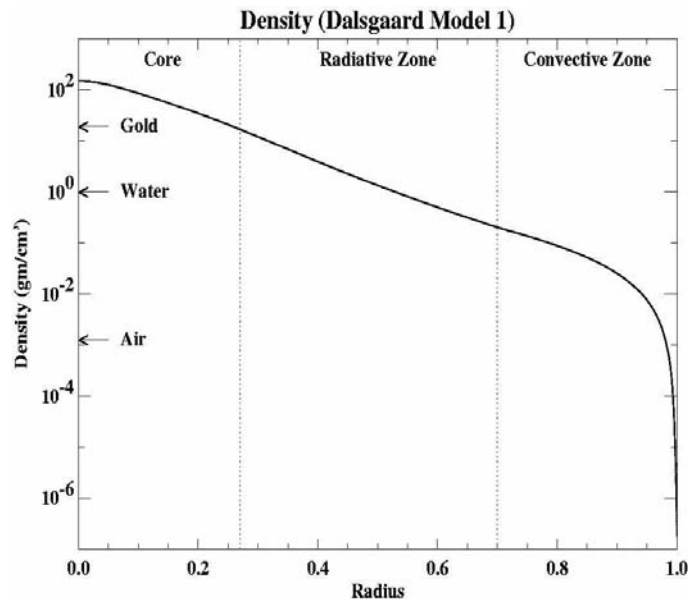
Figure 1.3: Solar interior density versus distance from the centre normalised to the solar radius.

temperature and density decrease as one moves outwards from the centre of the Sun (see Fig. 1.2 and 1.3).

The energy generated by the Sun in one second is enough to cover all human energetic needs, at the actual rate, for 50 000 years. This energy, generated in the core, is slowly transferred outwards by radiative diffusion across the radiative zone, which extends from the core to 0.7 $R_\odot$. The solar interior is

so opaque that a photon needs 10^7 years to complete the journey from the core to the surface because of the many times that it is absorbed and re-emitted. In comparison, an unimpeded photon would reach the solar surface in only two seconds. These constant emission, absorption and reemission of photons also increase the wavelength of the original γ-rays coming from the nuclear fusion up to visible light.

In the radiative zone the density drops from 20 000 kg m^{-3} down to 200 kg m^{-3}, while the temperature falls from seven to two milion degrees.

In our journey from the centre to the surface of the Sun, we next find the interface layer between the radiative and convective zones, the tachocline. The interest in this layer has increased in recent years because it is believed that the Sun's magnetic field is generated here by a combination of convection and rotation, a process known as the solar dynamo.

The outer layer of the solar interior, the convective zone, extends from the tachocline to a depth of 200 km from the surface. At the base of the convection zone, the plasma is cool enough to allow the heavier ions to keep some of their electrons, making the material more opaque and difficulting the radiation to get through. This makes the plasma unstable and convection sets in (such as water boiling in a pan). These convective motions carry heat quite rapidly to the surface, where the temperature and density drop to 5800 K and 2×10^{-4} kg m^{-3}, respectively.

1.1.2 Solar atmosphere

The solar atmosphere lies on top of the convective zone and is directly observable by means of its electromagnetic radiation. It consists of three regions with different physical properties: the photosphere, the chromosphere and the corona. Coronal material is continuously flowing away from the Sun forming the solar wind, that travels through the Solar System and eventually reaches the Earth and beyond. Aurorae and geomagnetic storms in the Earth are caused by strong perturbations of the solar wind.

The photosphere (Figure 1.4a) is the visible surface of the Sun, an extremely thin layer of only a few hundred kilometers thick (around 500 km), where most of the Sun's emission takes place.

The photosphere does not only emit in visible range, but it emits in a continuous spectrum in all frequencies, nearly like a black-body at a temperature of 5600 K, with absorption lines superimposed. The photospheric temperature decreases from 5800 K at the bottom to 4300 K at the top of the layer.

High resolution images of the photosphere show that it appears covered with irregularly shaped granules with a typical size of 1000 km and which are in continual motion. These granules correspond to the tops of the convective cells that overshoot the upper convective zone (Figure 1.4b).

Other remarkable features that can be observed in the photosphere are sunspots (Figure 1.4b), which are magnetic phenomena caused by the emer-
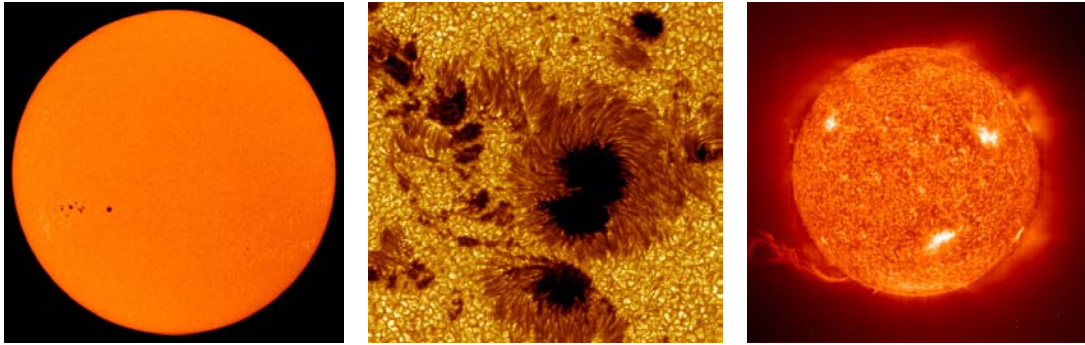
Figure 1.4: From left to right: a) the photosphere seen in visible light; b) a close look to a sunspot group, where granulation is also visible; c) image of the chromosphere at 304 Å (60 000–80 000 K) obtained with the EIT instrument onboard the SOHO spacecraft.
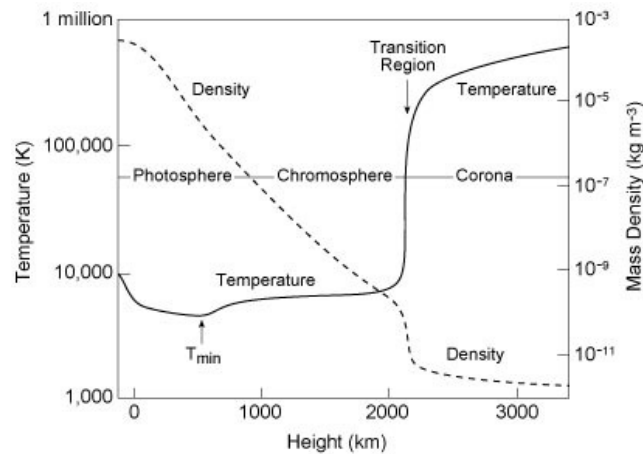
Figure 1.5: Evolution of the temperature and the mass density in the solar atmosphere as function of the distance above the convection zone given by the VALC model of Vernazza et al. (1981).

gence of magnetic flux tubes from the solar interior. At their centres, the magnetic field strength can reach 1000 G or more. At about 4000 K, sunspots are cooler than the rest of the photosphere and, because of this, they appear as dark features.

Above the photosphere the temperature surprisingly rises from 4300 K to about 20 000 K in a layer with a typical thickness of 2000 km called chromosphere. Using an adequate filter (Figure 1.4c) one can observe the chromosphere and identify new features like bright plages around sunspots and the chromospheric network. Prominences, made from chromospheric-like material, can be also observed using these filters although they are above the chromosphere (more information about prominences is given in Section 1.2).

Usually the temperature falls as one moves away from a heat source. This is true in the Sun's interior right up to the visible surface, but then, over a relatively thin layer, the chromosphere-corona transition region (CCTR), the temperature increases rapidly from around 10 000 K to temperatures of the

order of 10^6 K, where the corona begins. Figure 1.5 shows an schematic drawing of the density and the temperature as a function of height in the solar atmosphere. The mechanism responsible for this big increase of the temperature from the chromosphere to the corona is still unknown and the explanation of this phenomenon, commonly known as the coronal heating problem, has become one of the most important goals in solar physics.

The corona is the Sun's outer and by far the largest atmospheric layer. Due to the dazzling light of the photosphere, the corona is visible only during eclipses or using a coronograph (which is a disc that hides the solar disc emulating an eclipse) as a pearly white crown surrounding the Sun (Figure 1.6a). This white light is emitted by the photosphere and is scattered by the fast moving coronal electrons or emitted by the gas as spectral lines.

Early observations of the visible spectrum of the corona revealed a set of bright emission lines that did not correspond to known elements. The true nature of these lines remained unknown until it was determined that the temperature of the corona is of the order of one million degrees (Edlén & Swings 1942). At this temperature, only the heavier trace elements, like iron and calcium, are able to retain a few of their electrons. These highly ionised elements are responsible for the spectral lines that once were a mystery to astronomers.

Due to this high temperature, the corona emits in abundance in the ultraviolet, extreme-ultraviolet (EUV) and soft X-rays parts of the spectrum. This emission forces us to observe the corona by means of instruments in space, in order to avoid the shielding of the Earth's atmosphere at these wavelengths. The most oustanding missions with instruments working at these wavelengths are Yohkoh (1991–2005), SOHO (launched in 2005), TRACE (1998–2010), Hinode (launched in 2006), STEREO (launched in 2006) and SDO (launched in 2010). With the observations obtained by their telescopes (Figure 1.6b) it has become clear that the coronal plasma is dominated by the magnetic field, which emerges from below the photosphere and changes continuously. One can infer the geometry and strength of the coronal magnetic field by means of the analysis of the appearance of the corona.

Active regions are areas on the Sun where magnetic fields emerge through the photosphere into the chromosphere and corona. These regions appear bright in X-ray and ultraviolet images and may last for several weeks or even months. The magnetic field is stronger in an active region and is where sunspots can be formed.

There are two types of regions, depending on whether the magnetic field lines are open and connect to the interplanetary field (coronal holes) or closed over the surface, forming arches with their two endpoints in the photosphere. These closed regions are, in fact, composed of a great number of coronal loops, which delineate the magnetic field structure through the coronal plasma trapped within it, with a wide range of dimensions, densities and temperatures. Other structures, like prominences, streamers and plumes, are also
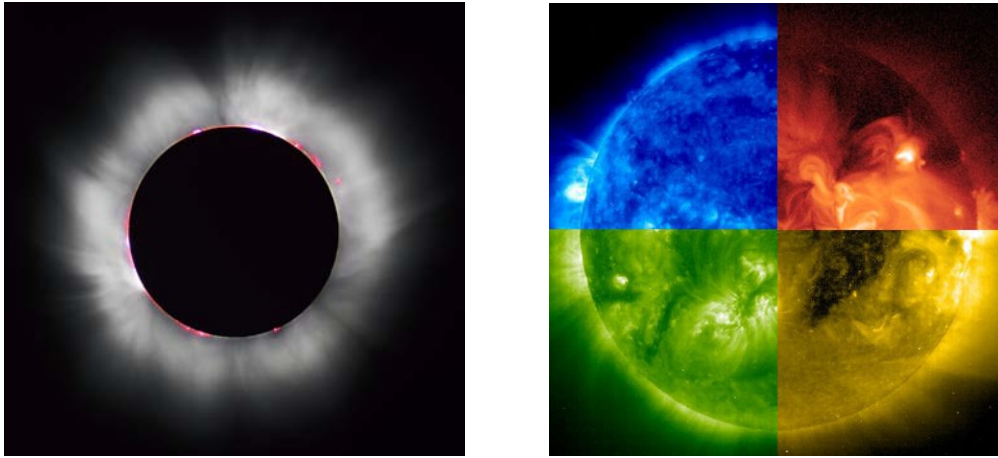
Figure 1.6:   From left to right: a) the corona seen during an eclipse. The red clouds are limb prominences such as those seen in Fig. 1.4c . b) A colour wheel with different views of the corona. Blue, green and yellow images have been obtained with EIT (onboard SoHO) and correspond to 171 Å (2–2.5 milion K), 195 Å (1.5 milion K) and 284 Å (0.9–1.0 milion K), respectively. The red-orange image has been obtained by Yohkoh in X-rays. The bright regions in these images are the coronal counterparts of the active regions seen in Fig. 1.4a, b.

common in the corona.

1.2   Prominences

In this section, we give a brief introduction to prominences and their properties. For a more detailed information about the physics of solar prominences we refer to recent reviews by Patsourakos & Vial (2002), Labrosse et al. (2010), and Mackay et al. (2010).

The first observations of prominences were undertaken during solar eclipses, and were explained as holes or clouds on the Moon. In 1239, Muratori interpreted them as 'burning holes' in the corona. Russian medieval chronicles mention prominences, but their first scientific description was not made until the eclipse of May 2, 1733. That day, Vassenius observed three or four prominences from Göteborg. He called them 'red flames' and believed that they were clouds in the Moon's atmosphere. It was not until 1842 when these observations of prominences were rediscovered.[3]

In 1851, more accurate descriptions of prominences began and with the introduction of photography in the Spanish eclipse of 1860 and spectrography in the eclipses of India and Malacca of 1868, the idea of prominences as big shining masses of gas was formed.

Now we know that prominences are coronal magnetic structures. Although they are embedded in the corona, they possess temperatures a hundred times

---

[3]*And some things that should not have been forgotten... were lost.* Cate Blanchett playing Galadriel in the film *The Lord of the Rings: The Fellowship of the Ring*, based on the book of J. R. R. Tolkien.
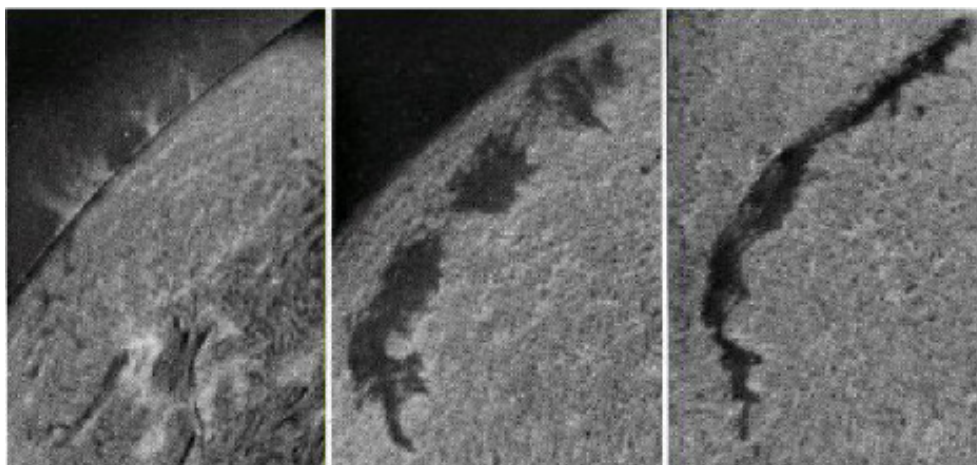
Figure 1.7: A prominence seen with an Hα filter at different times and changing its position because of solar rotation. In the first image it is seen as a bright prominence at the solar limb, while in the last one the same structure is clearly a dark filament on the disk.
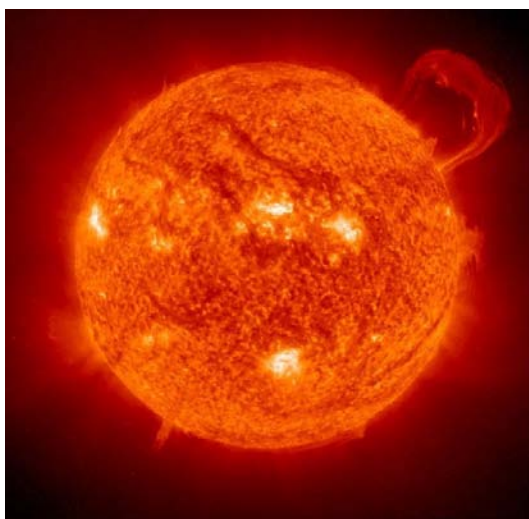
Figure 1.8: An eruptive prominence (SOHO-EIT, NASA & ESA)

smaller and densities a hundred or a thousand times larger than those of the surrounding corona.

The fact that their physical conditions are akin to those in the chromosphere suggests that prominences are made of chromospheric material which has been lifted up into the corona as a possible scenario to explain the prominence formation. Another proposed scenario to explain the origin of prominence material is condensation and cooling of plasma from the surrounding corona.

Prominences can be observed with an Hα filter as bright features above the solar limb and as thin, dark ribbons (called filaments) on the disc. In the beginning it was thought that filaments and prominences were different features, but with more careful observations it was discovered that the two

Parameter	Value
Density	$2 \times 10^{-12} - 5 \times 10^{-10}$ kg m^{-3}
Temperature	$5000 - 15\,000$ K
Magnetic field	$4 - 20$ G
Length	$60 - 600$ Mm
Height	$10 - 100$ Mm
Width	$4 - 30$ Mm
Thread's length	$3 - 28$ Mm
Thread's width	$100 - 600$ km

Table 1.2: Typical physical parameters of quiescent prominences and their fine structure. Adapted from Patsourakos & Vial (2002), Aschwanden (2004) and Lin (2004)

objects correspond to the same feature observed from different points of view (Figure 1.7). Now we use the words prominence and filament to refer indistinctly to both features.

Many models have been developed to explain how these cold clouds of dense plasma are supported against gravity and why they are thermally isolated from the hotter surrounding coronal medium. The key to these models is the magnetic field structure, which shields the prominence from the coronal medium and supports it in the corona.

The time-scale of prominence formation is about one day, and the lifetimes range from several months for quiescent prominences to only minutes or hours for active prominences (i.e. those located in active regions). At the end of their lives, some prominences suffer an instability that originates an eruption (Figure 1.8). Such eruptions are sometimes accompanied by flares or coronal mass ejections. Due to their longer life-time, quiescent prominences have been studied in more detail. Their typical parameters are summarised in Table 1.2.

High resolution images have revealed the fine structure of solar prominences. These fine structures, usually called threads, appear as a myriad of long (3000–28 000 km) and thin (100–600 km) dark ribbons in Hα images of filaments (see Figure 1.9) on the solar disk (Lin 2004; Lin et al. 2005, 2007, 2008, 2009), as well as in observations of prominences in the solar limb from the Solar Optical Telescope (SOT) aboard the Hinode spacecraft (Okamoto et al. 2007; Berger et al. 2008; Chae et al. 2008; Ning et al. 2009; Schmieder et al. 2010).

A considerable effort to measure prominence magnetic fields was started almost forty years ago (Leroy 1989; Paletou & Aulanier 2003), and the obtained results can be summarized as follows: The magnetic field in quiescent prominences has a strength of 3–15 G, is mostly horizontal, makes an acute angle of about 20 degrees with respect to the long axis of the prominence, and seems to increase slightly with height, indicating the presence of dipped field lines (Bommier & Leroy 1998). In the case of filament fine structure, statisti-
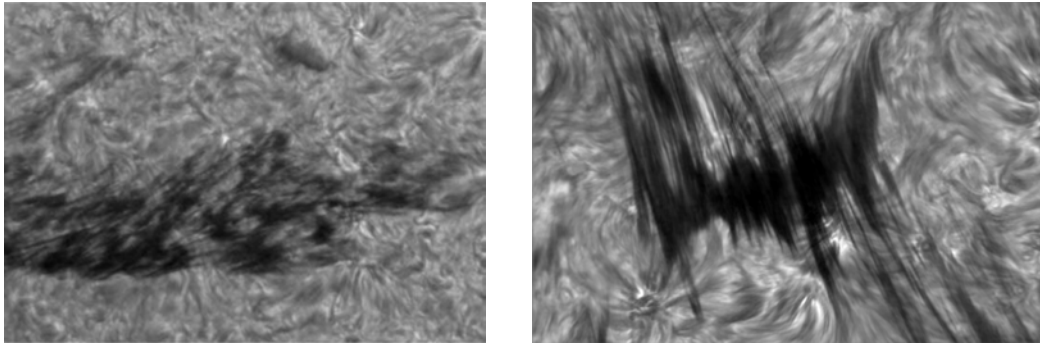
Figure 1.9: Two high resolution Hα images of quiescent prominences in which the fine structure can be appreciated. The images have been taken with the Swedish Solar Telescope on La Palma. From Lin et al. (2007).
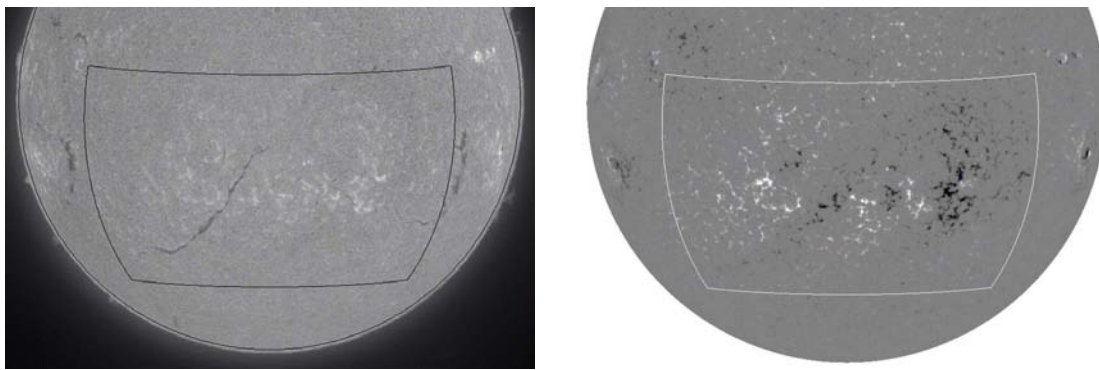
Figure 1.10: From left to right: a) An Hα image of a region of the solar disc where a filament is seen and b) a photospheric magnetogram of the same region. One can see that the filament is located between two regions of opposite magnetic polarity (black and white colours on the magnetogram).

cal studies show that the orientation of threads with respect to the filament long axis can significantly vary within the same filament (Lin 2004) and a mean value of 20 degrees has been reported.

It is also known that prominences exist above the polarity inversion line that separates two regions of opposite magnetic polarity in the photosphere (Figure 1.10), and because of the complex structures and the varied forms of prominences, it is difficult to establish definitive values for the different parameters (temperature, density, ionisation degree, magnetic field, ...). Vial (1998) points out three features as the reason for our limited knowledge about the nature of prominences:

- There is no such thing as a canonical prominence. Instead of that a wide range of parameters is observed in different objects.

- No prominence has a uniform structure. They are made of fibrils (thin threads) and different parameter values can be detected in different parts of the prominence.
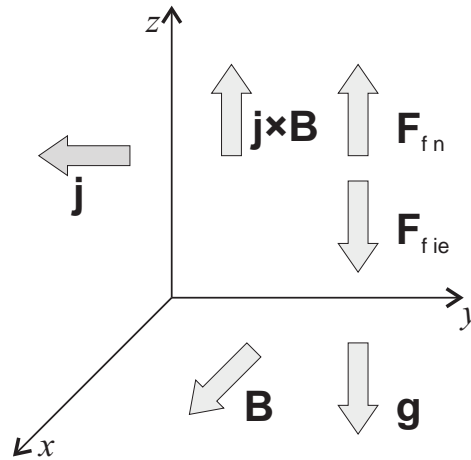
Figure 1.11: Coordinate system showing the simplified prominence magnetic field geometry assumed in Gilbert et al. (2002), together with directions of secondary drifts in the *y*-direction and the tertiary drifts in the positive and negative *z*-direction. The horitzontal gravitational drift is in the same direction as the horitzontal ion drift produced by the frictional interaction with the downflowing neutrals.

- No structure is really isolated. One needs to understand the interaction between the prominence and the corona at their interface.

On the other hand, it is also known that the prominence plasma is only partially ionised for typical prominence temperatures. The hydrogen ionisation degree could probably vary in different prominences or even in different regions within the same prominence (Patsourakos & Vial 2002).

In the past, the equilibrium of solar prominences within the solar corona has been explained in terms of a fully ionised plasma supported against gravity, and compressed, by magnetic forces (Kippenhahn & Schlüter 1957). With the consideration of a partially ionised plasma, the support needs to be understood in terms of the frictional coupling between the neutral and ionised components of the prominence plasma. In that way it is possible to explain the support of the neutral fraction of the plasma. Gilbert et al. (2002) describe a simple model in which the magnetic field, **B**, is in the *x*-direction and the gravitational acceleration, **g**, is in the negative *z*-direction, and also assumes no flow along the magnetic field lines (Figure 1.11).

In this scenario, the ions drift in the negative *y*-direction (in the direction of $\mathbf{g} \times \mathbf{B}$), while the electrons drift in the opposite direction. These drifts produce a current density, **j**, and a consequent $\mathbf{j} \times \mathbf{B}$ force that just balances the downward gravitational force on the ions and electrons. The neutral atoms do not sense the magnetic field, and thus fall downward in the direction of the gravitational force. The downward flow of neutral atoms relative to the ionised components of the plasma creates frictional forces between the neutral and ionised components: specifically, the ions and electrons exert upward frictional forces on the neutrals, meanwhile the neutrals exert equal and opposite downward forces on the ions and electrons. The downward frictional forces on

the ions and electrons enhance the drift current produced by the downward gravitational force. Under the condition of equilibrium the net drift current is such that the upward $\mathbf{j} \times \mathbf{B}$ force just balances the total downward gravitational force on the entire prominence plasma. It is in this way that the magnetic field supplies support for the entire prominence plasma including the neutrals, which do not directly feel its effect.

1.3   Prominence seismology

Oscillations are present everywhere in the Sun, the 5-minute photospheric oscillation being the most significant example. The existence of oscillations reflects a dynamic behaviour of the Sun and provides us with tools to understand the properties of our star.

Solar atmospheric seismology aims to determine physical parameters that are difficult to measure by direct means in magnetic and plasma structures. It is a remote diagnosis method that combines observations of oscillations and waves in magnetic structures, together with theoretical results from the analysis of oscillatory properties of given theoretical models. The philosophy behind this discipline is akin to that of Earth seismology, the sounding of the Earth interior using seismic waves, and helio-seismology, the acoustic diagnostic of the solar interior. The main difference between solar atmospheric seismology and helioseismology (which deals with the modes of oscillations of the whole Sun) is that single features studied in the corona can only be investigated for a short period of time, whereas the Sun as a whole remains practically unchanged over much longer intervals, which it can be observed. Solar atmospheric seismology was first suggested by Uchida (1970) and Roberts et al. (1984), in the coronal context, and by Roberts & Joarder (1994) and Tandberg-Hanssen (1995) in the prominence context, and the increase in the number and quality of high resolution observations in the 1990s has lead to its rapid development.

The branch of solar atmospheric seismology that deals with oscillations in prominences is also known as prominence seismology. The first reports about the presence of oscillations in prominences go back to the 1960s. The application of inversion techniques to prominence seismology is less developed. This is due to the complexity of these objects in comparison to, e.g., coronal loops. The recent refinement of theoretical models that incorporate the fine structuring of prominences and the high resolution observations of small amplitude oscillations have produced an increase in prominence seismology studies. Several techniques for the inversion of physical parameters have been developed that make use of observational estimates for quantities such as phase velocities, periods, damping times and flow speeds. In general, the solution to the inverse problem cannot provide a single value for all the physical parameters of interest. However, important information about unknown physical quantities can be obtained using this method.

Using different theoretical models as well as damping mechanisms, seismological studies have been performed using large and small amplitude prominence oscillations. These studies have allowed to estimate physical properties of prominences such as prominence Alfvén and kink speeds, thickness of inhomogeneous layers, angle of the vector magnetic field with the prominence long axis, magnetic field, etc.

A thorough review about the current state of prominence seismology can be found in Arregui et al. (2012).

1.3.1   Observational background

From the observational point of view, prominence oscillations can be classified into two groups according to the amplitude of periodic variations: large amplitude and small amplitude oscillations.

1.3.1.a   *Large amplitude oscillations*

Large amplitude oscillations arise when a disturbance, such as a Moreton wave (Moreton 1960) produced after a flare, impacts on a prominence and shakes its whole body. As a consequence of this large-scale perturbation, the prominence gas undergoes a large, horizontal displacement from its equilibrium position and the complete prominence vibrates with velocity amplitudes of the order of 20 km s^{-1} or higher during several periods until the oscillation is damped.

Because of the large velocities involved, large amplitude oscillations sometimes modify the absorption/emission wavelengths of the prominence. During the observations in Hα, the filament becomes visible when the prominence is at rest, i.e. when it reaches its maximum displacement from the unperturbed position. Meanwhile, when the line-of-sight velocity is sufficiently large, the emission from the material falls outside the bandpass of the filter and the prominence becomes invisible in Hα. The resulting optical effect gave rise to coining the term 'winking filament'.

Ramsey & Smith (1966) presented the first detailed study of the large amplitude oscillation motions although there are previous observations of 'winking filaments' (Dodson 1949). The work performed by H. E. Ramsey and S. F. Smith consists of the study of 11 flare-induced oscillations by using three narrow filters corresponding to the Hα centre line and two in the line wings at ±0.5 Å. They found no correlation between the period of the oscillations and filament dimensions, distance to the flare or its importance. Besides, a single filament was perturbed by four different flares during three consecutive days (June 25, 26 and 27, 1960) and the period was essentially the same in the four cases. So, the conclusion of this work was that prominences have their own frequency of oscillation and that this frequency cannot be related to the dimensions of the prominence or the characteristics of the triggering

flare. The amplitude of this oscillations is rapidly damped, disappearing after the observation of about four complete oscillations.

In spite of large amplitude oscillations being discovered half a century ago and the trigger for these motions being highly visible, unlike other types of solar oscillations, the topic has remained practically dormant for more than thirty years until the recent revival during the first years of the 21st century.

Modern observations of winking filaments indicate that the velocity of the plasma is in excess of 20 km s^{-1} (Eto et al. 2002; Okamoto et al. 2004) and that the filaments oscillate with periods from 30 minutes to 3 hours (Isobe & Tripathi 2006; Jing et al. 2006) and damping times of 2–3 times the corresponding period (Jing et al. 2006).

Recently, Jing et al. (2003, 2006) reported observations of periodic motions along the filament produced by a disturbance coming from a subflare at one end of the filament, whereas 'winking filaments' are activated by Moreton or EIT waves impinging on their sides.

On the other hand, large-amplitude oscillations have been also observed before or during prominence eruption (Isobe & Tripathi 2006; Isobe et al. 2007). These observations can be applied to diagnose the stability and the eruption mechanism.

Since the aim of this thesis is restricted to the study of small amplitude oscillations we refer the reader to Tripathi et al. (2009) for a complet review of both observational aspects and modelling efforts of large amplitude oscillations.

1.3.1.b *Small amplitude oscillations*

Quiescent prominences are also subject to small-amplitude oscillations, not related to flare activity and with velocity amplitudes much smaller than those observed in large-amplitude oscillations. In this case, the detected peak velocity ranges from the noise level (down to 0.1 km s^{-1} in some cases) to 2–3 km s^{-1}, although larger values have also been reported (Bashkirtsev & Mashnich 1984; Molowny-Horas et al. 1999; Terradas et al. 2002). These periodic changes in solar prominences do not normally affect the whole object at a time, but are of local nature instead.

Early observational studies revealed a wide range of characteristic periods that lead to classify small amplitude prominence oscillations according to their period in short ($P < 10$ min), intermediate ($10 < P < 40$ min) and long period oscillations ($P > 40$ min). However, recent reports of observations have induced a change into this classification adding two new categories: very short-period oscillations, with periods less than a minute (Balthasar et al. 1993), and ultra-long-periods of more than 8 h (Foullon et al. 2004).

This classification does not appear to reflect a different origin of the detected prominence perturbations for each of the period ranges. Presumably, periodic perturbations in prominences are produced by an external agent that

Reference	Period (min)	Structure
Harvey (1969)	$1 - 17$	Prominence
Bashkirtsev & Mashnich (1984)	$42 - 82$	Prominence
Tsubaki & Takeuchi (1986)	$2.7, 3.5$	Prominence
Yi et al. (1991)	$5, 9, 16$	Thread
Balthasar et al. (1993)	$0.5, 12, 20$	Prominence
Bashkirtsev & Mashnich (1993)	$5 - 90$	Prominence/Filament
Suetterlin et al. (1997)	$3 - 10, 20, 60$	Prominence
Terradas et al. (2002)	$30 - 40, 75$	Prominence
Foullon et al. (2004)	720	Filament
Lin (2004)	$4 - 20, 26, 42, 78$	Thread
Lin et al. (2007)	$3 - 9$	Thread

Table 1.3: Examples of observations of small-amplitude prominence oscillations, reported periods and structures in which observations were carried out.

excites different eigenmodes of the structure.

Some of the periods obtained in different works have been summarised in Table 1.3, which is only a representative compilation of values and by no means pretends to be exhaustive.

Unfortunately, on its own, a period reveals very little information about the conditions in the prominence since it corresponds to many combinations of density, temperature, magnetic field, etc.

On the other hand, there are also some determinations of wavelength and phase speed obtained from observations of oscillations in slab-like prominences. For instance, Molowny-Horas et al. (1997) determined a maximum value $\lambda_{\parallel} \simeq 20\,000$ km, while the corresponding phase speed was $v_{\mathrm{p}} \leq 44$ km s^{-1}. Terradas et al. (2002) analysed small amplitude oscillations in a polar crown prominence reporting the presence, along two selected paths in the prominence region, of two plane propagating waves, as well as a standing wave. The plane waves propagate in opposite directions with wavelengths of 67 500 and 50 000 km and phase speeds of 15 km s^{-1} and 12 km s^{-1}, while in the case of the standing wave, the estimated wavelength is of 44 000 km and the phase speed of 12 km s^{-1}. The reader is refered to Oliver & Ballester (2002), Wiehr (2004), and Engvold (2008), among other recent reviews, for more information about the observational background of small amplitude prominence oscillations

1.3.1.c   *Fine structure oscillations*

Individual oscillations of prominence fine structures have been frequently reported since telescopes with a high time and spatial resolution became available.

Threads have dynamics that can be easier to understand than that of the whole body. Early works (Yi et al. 1991; Yi & Engvold 1991) detected oscilla-
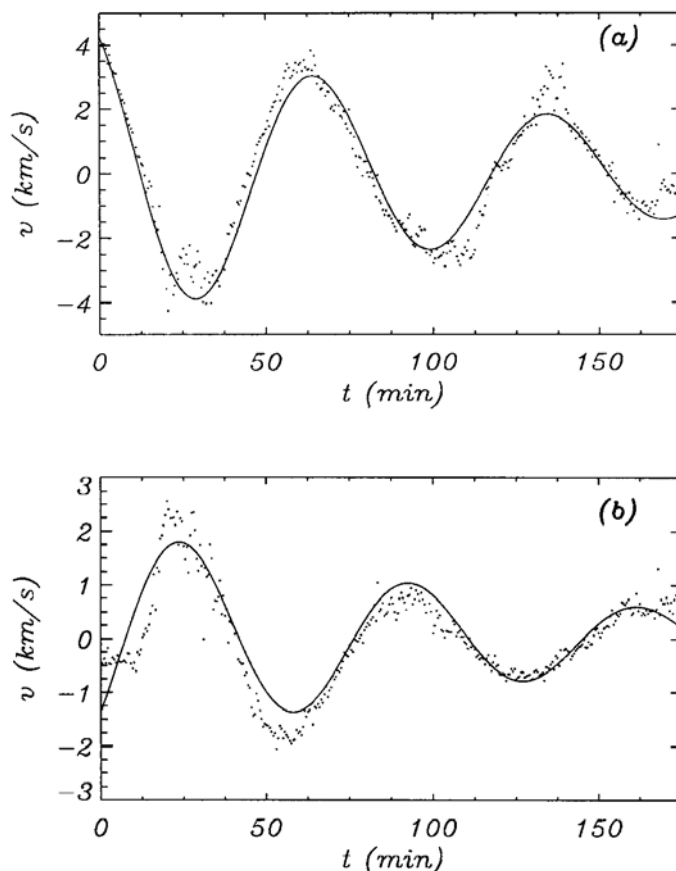
Figure 1.12: Observed Doppler velocity (dots) and fitted function (solid line) versus time at two different points in a quiescent prominence. The period is 70 min in both points and the damping time is 140 and 101 min, respectively. The function fitted to the observational data is of the form $v_0 \cos(\omega t + \phi) \exp(-t/\tau_D)$. Adapted from Molowny-Horas et al. (1999)

tory variations in Doppler signals and He I line intesity from threads in quiescent prominences and already noted the possible link between the prominence fine structure and the periodic motions in prominences. Furthermore, Yi et al. (1991) reported wavelengths greater than 20 000 km.

Later, Lin (2004), and Lin et al. (2007, 2009), using Hα and Doppler observations with better spatial resolution, found evidence of oscillations and propagating waves along quiescent prominence threads with wavelengths around 4000 km. In addition, observations from Hinode spacecraft have shown transverse oscillations of thread-like structures in both active region (Okamoto et al. 2007) and quiescent (Ning et al. 2009; Schmieder et al. 2010) prominences.

With these observations we can narrow the period of these oscillations to a range between 2 and 10 minutes, with velocity amplitudes smaller than ~3 km s^{-1}.

On the other hand, Yi et al. (1991), Lin et al. (2007), and Schmieder et al. (2010) suggested the presence of groups of neighboring threads that moved in

phase, which may be a signature of collective interactions and oscillations.

1.3.1.d Damping of small amplitude oscillations

The oscillatory amplitude tends to decrease in time in such a way that the periodicity totally disappears after a few periods (Oliver & Ballester 2002), just as observed in large amplitude oscillations. This is then interpreted as a signature of wave damping by some mechanism. The importance of observing and identifying the process of wave damping is that we can gain some information about the physical conditions and processes going on in the plasma. On the other hand, the ratio between the damping time τ_{D} and the period P, i.e. τ_{D}/P, gives us information about how fast oscillations are damped, and in prominence oscillations this ratio seems to be $\tau_{\mathrm{D}}/P < 10$.

The attenuation of the oscillations was previously suggested by some observations (Landman et al. 1977; Tsubaki & Takeuchi 1986) but it was first extensively investigated by Molowny-Horas et al. (1999) and Terradas et al. (2002). Molowny-Horas et al. (1999) and Terradas et al. (2002) derived reliable values of the damping time, τ_{D}, after fitting a sinusoidal function multiplied by a factor $\exp(-t/\tau_{\mathrm{D}})$ to Doppler velocity time series recorded simultaneously at different positions of a quiescent prominence (Figure 1.12). The values of τ_{D} thus obtained are usually between 1 and 3 times the corresponding period, and large regions of the prominence display similar damping times. Similar results were obtained in a more recent work by Mashnich et al. (2009). Furthermore, the analysis made by Terradas et al. (2002) suggests the presence of a propagating wave, which was interpreted as an slow mode, for which the amplitude of the oscillations spatially decreases in a substantial way in a distance of $2 - 5 \times 10^4$ km from the generation location. This distance can be considered as the typical spatial damping length, L_{d}, of the oscillations.

Although the spatial resolution in Molowny-Horas et al. (1999) and Terradas et al. (2002) was not enough to distinguish individual threads, one could assume that, as for large-scale oscillations, the individual and/or collective thread motions are also damped in time. This statement was recently confirmed by some high-resolution observations, which were able to resolve damped fine structure oscillations (Lin 2004; Ning et al. 2009).

The determination of the temporal decay law may have several implications, since it can give information about the physical damping mechanism, as different physical processes have their own decay profile.

1.3.1.e Flows

A typical feature of prominences is the presence of flows which are observed in Hα, UV and EUV lines (Labrosse et al. 2010). In Hα quiescent filaments, the observed velocities range from 5 to 20 km s^{-1} (Zirker et al. 1998; Lin et al. 2003, 2007) and, because of the physical conditions in filament plasmas, they seem to be field-aligned. In the case of active region prominences, flow speeds can be

higher than the previous values. Recent observations made with Hinode/SOT by Okamoto et al. (2007) reported the presence of synchronous vertical oscillatory motions in the threads of an active region prominence, together with the presence of flows along the same threads. However, in limb prominences different kind of flows are observed and, for instance, observations made by Berger et al. (2008) with Hinode/SOT have revealed a complex dynamics with vertical downflows and upflows.

Okamoto et al. (2007) studied six different threads observed in an active region prominence with the Hinode Solar Optical Telescope. They found flow velocities in the range 15–46 km s^{-1}, oscillatory periods in the range 135–250 s and thread lengths in the range 1700–16 000 km. Terradas et al. (2008) performed an independent seismological study of the same events assuming that the thread is a dense plasma moving along a horizontal and straight magnetic tube tied to the dense photosphere at its ends. They also consider low-β and linear approximations. They considered three different models: (a) the thin tube approximation with no flow, (b) the thin tube approximation with flow, and (c) the full ideal MHD equations with flow. The results of the models are in excellent agreement with the observations by Okamoto et al. (2007) and they conclude that the period of transverse oscillations is almost insensible to the presence of a flowing thread.

1.3.2   Theoretical background

The combination of observations and theoretical models of prominence oscillations constitutes a powerful diagnosis tool. With the help of this tool we can perform prominence seismology with the aim to determine difficult to measure prominence parameters.

1.3.2.a   Large amplitude oscillations

From the theoretical point of view, there is a lack of models explaining large amplitude oscillations. This lack is perfectly explained by the scarce number of observations of this kind of oscillations during the last third of the 20th century. Hyder (1966) proposed a model for the vertical motions in terms of harmonically damped oscillations. The restoring force was provided by the magnetic tension while coronal viscosity was considered the damping mechanism. Later, Kleczek & Kuperus (1969) proposed a similar model in order to explain the horizontal oscillations but considering that the damping was provided by the emission of acoustic waves.

Vršnak et al. (2007) applied the idea of prominence seismology to a prominence oscillation recorded on January 22th, 2002. They developed a simple model to deduce the poloidal and axial component of the magnetic field from the observed parameters obtaining an axial component of magnetic field of 10-30 G, which is a reasonable value for quiescent prominences.

Since the aim of this work is the study of small-amplitude oscillations we refer to Tripathi et al. (2009) for a complete review about large-amplitude oscillations, both observations and theory.

1.3.2.b *Small amplitude oscillations*

On the other hand, the great number of observations of small-amplitude oscillations have favoured an extense bibliography centred on theoretical models to explain these oscillations.

Simplified models for small-amplitude prominence oscillations were studied by Roberts (1991) considering the prominence as a point mass suspended on an elastic string, representing the locally deformed magnetic field which supports the prominence. This model provides with some insight into the period of vertical oscillations of the whole prominence, consistent with the 10–20 minute range of observed values. Another view of a quiescent prominence is the three-dimensional picture of a rectangular membrane. Once again, the periods obtained with this model are of the order of 30 minutes, which is consistent with observations.

More sophisticated studies, related to small-amplitude oscillations, have appeared since then, using the linearised magnetohydrodynamic equations. The inclusion of the magnetic field yields a magnetic pressure and magnetic tension as available restoring forces. The theoretical studies of magnetohydrodynamic waves in prominences reduces to solving the set of differential equations with the appropriate boundary conditions. Such theoretical studies can be divided into two groups depending on the equilibrium choice.

Global oscillations. The first group represents the prominence as an isothermal plasma slab of finite width. In this line, there are models which restrict to the prominence itself and do not consider the overlying arcade and the external coronal medium. Following this approach Oliver et al. (1992) studied the oscillatory modes of the Kippenhahn & Schlüter (1957) prominence model while Joarder & Roberts (1993) considered a Menzel (1951) prominence model in order to study the effect of gravity. Terradas et al. (2001) studied the effect of Newtonian cooling in the Kippenhahn-Schülter and Menzel equilibrium models.

Models in which the effect of the external medium is taken into account have also been developed. Joarder & Roberts (1992a,b) studied adiabatic perturbations of a prominence slab in a hot corona with a homogeneous magnetic field across and along the long axis of the slab. These authors created the distinction between internal, external and string modes. Oliver et al. (1993), analysing oscillations in the Poland & Anzer (1971) equilibrium model, found that the fundamental mode was internal and external at the same time, which lead to the term hybrid mode. Oliver et al. (1996) considered different prominence-corona transition regions (PCTR) and found that the former

classification in internal, external and hybrid modes could be maintained. Finally, Anzer (2009) has determined the basic modes of oscillation of simple 1D prominence configurations.

Fine structure oscillations.   The second group is formed by the models of oscillations that take into account the fine structure of the prominence and make use of a single fibril. The first theoretical study of this kind was carried out by Joarder et al. (1997) adapting the slab model of Joarder & Roberts (1992b). They considered a magnetic field oriented along the fine structure which was considered as a thin thread with finite width and length. Once again internal, external and hybrid modes are supported. A more in-depth study of the fibrils oscillations, including 3-dimensional prominence fibrils, was performed by Díaz et al. (2001, 2002, 2003, 2005) and Díaz (2004).

These models can reproduce the range of observed periods in prominences. Nevertheless, the ignorance of the precise values of prominence physical conditions and the little information available about some relevant oscillatory parameters prevents us from performing an unequivocal comparison between theoretical wave modes and observations. However, it seems that intermediate- and long-period oscillations are related to slow magnetoacoustic waves, whereas short-period oscillations can be connected to fast magnetoacoustic waves.

1.3.2.c   *Damping of the oscillations*

A number of recent works have studied, from a theoretical point of view, the attenuation of prominence oscillations attempting to explain the damped oscillations reported by Molowny-Horas et al. (1999) and Terradas et al. (2002). Several non-ideal damping mechanisms have been proposed to explain the damping of prominence oscillations. The complexity of the models has been improved from very simple configurations to more realistic models including prominence fine structures and flows.

Homogeneous and unbounded medium.   By removing the ideal assumption and including dissipative terms in the basic MHD equations, it is possible to study the attenuation of propagating waves in a homogeneous and unbounded medium. Carbonell et al. (2004, 2006) studied the time and spatial damping by non-adiabatic effects (optically thin radiation losses, thermal conduction, and plasma heating). These works concluded that only slow waves are efficiently damped by non-adiabatic effects, being radiative losses the dominant mechanism, while fast waves are slightly damped and Alfvén waves are unaffected. Carbonell et al. (2009) explored also the time damping of non-adiabatic slow and thermal waves in an unbounded prominence medium with a background flow.

Forteza et al. (2007, 2008) and Carbonell et al. (2010) have included partial ionisation in this type of models in order to study the influence of the ion-neutral collision mechanism in the attenuation of prominence oscillations. These works are extensively explained in this Thesis, therefore we refer the reader to the following chapters.

Slab models. In both the Kippenhahn & Schlüter (1957) and Menzel (1951) prominence models, Terradas et al. (2001) studied the damping of oscillations by radiative losses, based on the Newtonian cooling with a constant relaxation time, in Kippenhahn-Schülter and Menzel equilibrium models. Later, Terradas et al. (2008) assumed a more complete treatment of the non-adiabatic effects with the incorporation of optically thin radiation, heating and thermal conduction. The main conclusion that arises from these works is that only the slow wave is damped by the thermal effects in an efficient way, being the radiation the dominant attenuation mechanism in the range of typically observed wavelengths[4]; in contrast, the fast wave remains practically unaffected.

Soler et al. (2009c) considered a prominence slab embedded in the corona with magnetic field parallel to the slab axis and, performing a treatment of the non-adiabatic effects as in Terradas et al. (2005), obtained that the presence of the corona reduces the damping time of the fast waves due to the influence of coronal thermal conduction, although this effect is not enough to obtain damping times compatible with those observed. On the other hand, Soler et al. (2009e) studied the same configuration with the magnetic field perpendicular to the slab axis. In this case, fast modes may be thermally unstable for some wavelengths due to the heat transfer from the corona to the prominence slab along magnetic field lines.

Cylindrical models. The plasma density varies by about two orders of magnitude between a prominence and the surrounding corona. In such a highly inhomogeneous configuration, fast kink modes can be efficiently damped by transfering their energy to Alfvén modes through resonant absorption. Arregui et al. (2008) considered a transverse inhomogeneous transitional layer between a cylindrical filament thread and the corona, and investigated the damping by resonant absorption in the Alfvén continuum. The damping time obtained is approximately 3 periods for typical wavelengths of prominence oscillations and a typical density contrast between the prominence and the coronal plasma, meaning that resonant absorption is a plausible candidate to be the damping mechanism of transverse thread oscillations.

This study was extended by Soler et al. (2009a) by considering also resonant absorption in the slow continuum and by Soler et al. (2009d) that study the joint effect of resonant absorption and partial ionization.

---

[4]From 5000 km to 10^5 km according to Oliver & Ballester (2002).

Models including flows. Carbonell et al. (2009) explored the time damping of non-adiabatic slow and thermal waves in an unbounded prominence medium with a background flow in the case of field-aligned propagation. Fast mode is ignored in this work because non-adiabatic effects do not contribute in a significant way to its attenuation (Carbonell et al. 2004). The authors find that the period and damping per period show a strong dependence on the flow speed and also that the greatest period and damping per period of slow waves is obtained for flow speeds close to the real part of the non-adiabatic sound speed.

The thermal mode, which in the absence of flow does not propagate, becomes a propagating mode in the presence of a background flow. Therefore, may not be possible to determine whether an observed period and damping time is associated to a slow or thermal wave. In order to distinguish the origin of such wave it would be necessary to look at the temperature perturbation, which, for the thermal wave, should be larger than for the slow wave.

Soler et al. (2008) perform a similar study in the case of a single thread embedded in an unbounded corona considering flow motions parallel to a uniform magnetic field. This work points out that in the absence of flow, slow modes are efficiently damped by non-adiabatic effects, while fast kink modes are practically not affected.

Meanwhile, in the presence of flow, the damping time of slow and thermal waves is not affected, while for realistic values of the flow velocity, the larger the flow, the larger the attenuation of parallel fast kink modes, whereas the contrary occurs for antiparallel fast kink modes. Nevertheless, the values of the damping time obtained considering this model differ from the observed damping times of fast kink waves.

The observational and theoretical knowledge of waves and oscillations in solar prominences has been reviewed by Oliver (1999, 2004, 2009), Engvold (2001), Oliver & Ballester (2002), Ballester (2005, 2006, 2010), Banerjee et al. (2007), Tripathi et al. (2009), Labrosse et al. (2010), Mackay et al. (2010), Arregui & Ballester (2010), and Arregui et al. (2012).

1.4 Outlook of the Thesis

After having reviewed the current observational and theoretical backgrounds about prominence oscillations, it becomes clear that the study of how prominence oscillations are damped is of great interest. Therefore, the aim of this Thesis is to contribute to the theoretical understanding of the damping of prominence oscillations. In particular, we are going to focus in the effects of the ion-neutral collision mechanism in the damping of magnetohydrodynamic waves. The outline of the Thesis is as follows: In Chapter 2 we introduce the equations of magnetohydrodynamics and the wave equations, describing the different MHD modes. We end this chapter reviewing some of the classical results about oscillations in simple structures. In Chapter 3 we derive the

single-fluid MHD equations for a partially ionised plasma. In Chapter 4 we study the behaviour of Alfvén, fast and slow MHD waves in an unbounded, homogeneous, adiabatic and partially ionised plasma, which is the simplest configuration that can be used to understand the effect of ion-neutral collisions in the damping of MHD waves. In Chapter 5 we consider the same simple model but we include non-adiabatic effects in order to study the joint effect of ion-neutral collisions and thermal mechanisms on the damping of MHD waves. In Chapter 6, and using the same equilibrium model as before, we study the spatial damping of MHD waves in different kinds of plasmas (ideal, resistive and partially ionised) with and without background flows.

Finally, in Chapter 7 the results and conclusions of this work are presented, and a brief discussion of future developments and applications of these results is carried out.

Chapter 2

Magnetohydrodynamics

It is well known that matter in the Sun is in a plasma state, that is, an ionised gas with enough abundance of free charges. One way to have a reasonable description of the plasma under solar conditions, among other applications, is magnetohydrodynamics, or MHD for short. This chapter is devoted to present the MHD equations and some relevant simple plasma configurations which will be used as initial equilibrium configurations in the following chapters.

2.1 But... what is a plasma?

Some estimations suggest that up to 99% of the matter of the visible Universe is in plasma state: stars, nebulae, the solar wind, the interstellar hydrogen, the Van Allen belts, ... So, we are living on the other 1%, the small fraction of the Universe where plasmas are not produced naturally. It is because of this that most people think that there are only three states of matter, i.e. solid, liquid and gas. But the truth is that plasma can be considered the fourth state of matter with its own properties.

A plasma is, essentialy, a fluid composed by charged particles (electrons, ions and neutrals), or, in other words, an ionised gas. Nevertheless, there are others, more accurate definitions as the one given by Chen (1974): *a plasma is a* [macroscopic] *quasi-neutral gas of charged particles and neutral particles which exhibits collective behaviour*. So, besides the fact that a plasma is electrically neutral, the existence of charged particles means that it can support electric currents and interact with electric and magnetic fields.

The main difference between a neutral gas and a plasma is that the first one is dominated by two-body billiard-ball-like collisions, that are strong and short range forces, while in a plasma, a charged particle interacts through the Coulomb force with the other charged particles of the plasma and, in addition to this, a moving charged particle creates a magnetic field which also interacts with the other charged particles. Since the electromagnetic forces are weak

and of long range, in comparison with the forces dominant in a neutral gas, a charged particle interacts with a large number of other charged particles, resulting in a collective behaviour of the plasma.

In order to have this collective plasma behaviour the following conditions must be satisfied:

- The long-range Coulomb interaction between charged particles should dominate over the short-range binary collisions with neutrals.

- There should be frequent enough collisions between electrons and ions to establish a fluid behaviour.

- The length-scale of plasma dynamics should be much larger than the minimum size over which the condition of quasi-neutrality is satisfied. Thermal fluctuations can produce local charge imbalances and create huge electric fields. These electric fields cause the acceleration of particles, and the charge imbalance is neutralised almost instantaneously. This lenght-scale is definied by the Debye length, λ_{D}[1].

- For statistical considerations, the number of particles inside a Debye sphere (i.e. a sphere of radius λ_{D}) must be big enough.

2.2 Magnetohydrodynamic equations

It has previously been stated that the matter in the conditions present in the Sun is in plasma state. Under these conditions, the macroscopic behaviour of the plasma in certain regions can be reasonably well described by Magneto-HydroDynamics (MHD). This theory can be introduced from two different formalisms. The first one starts directly from Boltzmann kinetic theory and combines it with Maxwell's equations of electromagnetism, taking into account certain approximations and properties of the plasma state. This derivation can be followed in Goossens (2003). The second formalism introduces MHD from fundamental equations of fluid dynamics together with Maxwell's equations, considering that a plasma is a fluid made of charged particles permeated by electric and magnetic fields. This second approach can be followed in Priest (1984) and is the one we use throughout this chapter in order to introduce the MHD equations. We want to note that we need to consider several fundamental assumptions to obtain the general equations for MHD. These assumptions are:

---

[1]The Debye length is defined as

$$\lambda_{\mathrm{D}} \sim \sqrt{\frac{\varepsilon_0 k_{\mathrm{B}} T}{e^2 n}},$$

where ε_0 is the electric permittivity, n is the number density, e is the electron charge and k_{B} is Boltzmann's constant.

- The plasma is treated as a continuum. This is valid because the length scale for variations is larger than the typical internal plasma lengths, characterised by the ion cyclotron radius.

- The plasma is assumed to be in thermodynamic equilibrium with distribution functions close to Maxwellian. This holds for time-scales much larger than the collision times and length-scales much longer than the mean free paths.

- Most of the plasma properties are assumed isotropic.

- The plasma is treated as a single fluid. This means that global plasma magnitudes are considered, which are computed as the sum of the magnitudes of each species present in the plasma (i.e. ions, electrons and neutrals).

- The equations are written in an inertial frame.

- Relativistic effects are neglected since the typical plasma velocities (flow, sound and Alfvén speeds) are much smaller than the speed of light.

- In many processes in the solar atmosphere the plasma can be considered as electrically neutral to a high degree of approximation, that is $n_i - n_e \ll n$, with n the total number density and n_i and n_e the ion and electron number densities. In practice, a local charge imbalance produces an electric field with a spatial range given by the Debye length, which is a measure of the distance over which the charge density can deviate appreciably. In fact, as we have previously said, a plasma may be defined as an ionised gas for which λ_D is much smaller than all other scales of interest.

Taking into account all the previous considerations one can obtain the set of non-adiabatic MHD equations. Now we summarise the non-adiabatic MHD equations:

$$\frac{\partial \rho}{\partial t} + \nabla \cdot (\rho \mathbf{v}) = 0, \tag{2.1}$$

$$\rho \frac{d\mathbf{v}}{dt} = -\nabla p + \frac{1}{4\pi} (\nabla \times \mathbf{B}) \times \mathbf{B} + \rho \mathbf{g}, \tag{2.2}$$

$$\frac{dp}{dt} - \frac{\gamma p}{\rho} \frac{d\rho}{dt} = -(\gamma - 1)\mathfrak{L}, \tag{2.3}$$

$$\frac{\partial \mathbf{B}}{\partial t} = \nabla \times (\mathbf{v} \times \mathbf{B}), \tag{2.4}$$

$$\nabla \cdot \mathbf{B} = 0, \tag{2.5}$$

$$p = \frac{\rho R T}{\tilde{\mu}}, \tag{2.6}$$

namely the continuity equation (Eq. [2.1]), the equation of motion (Eq. [2.2]), the energy equation (Eq. [2.3]), the induction equation (Eq. [2.4]), the solenoidal condition (Eq. [2.5]) and the equation of state (Eq. [2.6]), with ρ the density, $\mathbf{v}$ the velocity, p the pressure, $\mathbf{B}$ the magnetic field, $\mathbf{g}$ the gravitatory field, γ the adiabatic index, $\mathcal{L}$ the energy loss function, T the temperature and $\tilde{\mu}$ the ionisation fraction.

The energy loss function $\mathcal{L}$ in Eq. (2.3) has different terms which represent the rate of energy loss or gain. Heat flux due to particle conduction, radiation or ohmic dissipation and any other sources or sinks are included in the energy loss function. Formally, $\mathcal{L}$ is negligible when the time-scale for changes in pressure, density and temperature is much smaller than the time-scales for the different mechanisms considered in the energy loss function. This situation is often valid for rapid changes associated with, for example, waves, so that all changes of state can be considered adiabatic. In this case, the energy loss function is set to zero (adiabatic approximation) and the plasma is considered thermally isolated, i.e. there is no exchange of heat, and so the entropy is conserved.

Non-adiabaticity can be considered by introducing a more complete form of the energy loss function such as

$$\mathcal{L} = \nabla \cdot (\kappa \cdot \nabla T) - L_{\mathrm{r}} - j^2/\sigma + H, \qquad (2.7)$$

where κ is the thermal conduction tensor, L_{r} is the radiation term, j^2/σ stands for the ohmic dissipation, with σ being the conductivity, and H groups other heating terms, such as viscous dissipation or heating by waves or reconnection. In the case of a perfect conducting plasma ($\sigma \to \infty$) the ohmic dissipation term vanishes.

2.3 Magnetohydrodynamic waves

In a gas, sound waves propagate due to the presence of a pressure restoring force: local compression or rarefactions of the gas set up a pressure gradient in opposition to the motion, which tries to restore the original equilibrium. When the gas is uniform, the waves propagate isotropically at the sound speed of the medium, denoted by c_{s}.

These waves carry energy away from the source but they possess such a small amplitude that the gas is only slightly disturbed. When this amplitude is large enough, the wave may steepen into a shock wave, as in the case of the sonic boom from a supersonic aircraft.

In the presence of a magnetic field, variations in the gas pressure generally lead to disturbances of magnetic lines, and any attempt to propagate sound waves results in variations in the magnetic field, which also exert a restoring force.

Oscillations, interpreted in terms of MHD waves, have been observed in many solar structures, such as sunspots, prominences, coronal loops and others, so MHD waves are important to understand the Sun's dynamics.

The basic theory of wave motion in the presence of a magnetised plasma can be found in Cowling (1976), among other references. The mathematical discussion of wave motion adopted in this work follows a standard pattern, consisting of considering an equilibrium situation and then perturbing it slightly in order to see whether linear disturbances propagate as waves.

2.3.1 Linearised equations

Since we only consider small-amplitude oscillations in prominences, nonlinear effects are not very important and it is enough to consider the linear regime. After this linearisation, the set of equations reduces to a more simplified form and it is even possible to obtain analytical solutions to some simple problems.

Before linearising the equations we need to define an equilibrium background. As a background model, we use a homogeneous unbounded medium threaded by a uniform magnetic field along the x-direction, and with no background flow. The equilibrium magnitudes of the medium are given by

$$p_0 = \text{const.}, \quad \rho_0 = \text{const.}, \quad T_0 = \text{const.},$$

$$\mathbf{B_0} = B_0 \hat{e}_x,$$

with $B_0 = $ const.

Next, we assume that physical variables suffer small displacements from their equilibrium values in the form

$$\mathbf{B} = \mathbf{B}_0 + \tilde{\mathbf{B}}(\mathbf{r}, t),$$

$$\mathbf{v} = \tilde{\mathbf{v}}(\mathbf{r}, t),$$

$$p = p_0 + \tilde{p}(\mathbf{r}, t),$$

$$\rho = \rho_0 + \tilde{\rho}(\mathbf{r}, t),$$

$$T = T_0 + \tilde{T}(\mathbf{r}, t), \tag{2.8}$$

where the subscript 0 denotes equilibrium quantities and the tildes, the perturbed quantities. Now, we insert these physical quantities into the continuity, momentum, energy, induction and state equations (Eqs. [2.1]–[2.6]) and linearise them neglecting products of the perturbed quantities, which are assumed to be small in comparison with the equilibrium values (i.e. $|\tilde{\mathbf{B}}|/|\mathbf{B}_0| \ll 1$, $|\tilde{p}/p_0| \ll 1$, $|\tilde{\rho}/\rho_0| \ll 1$, $|\tilde{T}/T_0| \ll 1$).

Neglecting gravity effects we end up with the following set of linearised equations

$$\frac{\partial \tilde{\rho}}{\partial t} + \rho_0 \nabla \cdot \tilde{\mathbf{v}} = 0, \tag{2.9}$$

$$\rho_0 \frac{\partial \tilde{\mathbf{v}}}{\partial t} = -\nabla \tilde{p} + \frac{1}{4\pi} (\nabla \times \tilde{\mathbf{B}}) \times \mathbf{B}_0, \tag{2.10}$$

$$\frac{\partial \tilde{p}}{\partial t} - \frac{\gamma p_0}{\rho_0} \frac{\partial \tilde{\rho}}{\partial t} = (\gamma - 1) \left\{ \frac{\kappa_{0\parallel}}{B_0^2} \nabla \cdot \left[\left(\mathbf{B_0} \cdot \nabla \tilde{T} \right) \mathbf{B_0} \right] - \rho_0 \left(L_\rho \tilde{\rho} + L_T \tilde{T} \right) \right\}, \tag{2.11}$$

$$\frac{\partial \tilde{\mathbf{B}}}{\partial t} = \nabla \times (\tilde{\mathbf{v}} \times \mathbf{B}_0), \tag{2.12}$$

$$\nabla \cdot \tilde{\mathbf{B}} = 0, \tag{2.13}$$

$$\frac{\tilde{p}}{p_0} - \frac{\tilde{\rho}}{\rho_0} - \frac{\tilde{T}}{T_0} = 0, \tag{2.14}$$

where L_ρ and L_T are the partial derivatives of the heat-loss function with respect to density and temperature, respectively,

$$L_\rho = \left(\frac{\partial L}{\partial \rho} \right)_T, \qquad L_T = \left(\frac{\partial L}{\partial T} \right)_\rho, \tag{2.15}$$

with T and p held constant, respectively, at the equilibrium state.

2.3.2 Adiabatic magnetohydrodynamic waves

In the adiabatic case, i.e. in the absence of radiative losses, thermal conduction and heating, Eq. (2.11) becomes,

$$\frac{\partial \tilde{p}}{\partial t} - c_s^2 \frac{\partial \tilde{\rho}}{\partial t} = 0, \tag{2.16}$$

where the sound speed squared is defined by

$$c_s^2 = \frac{\gamma p_0}{\rho_0}. \tag{2.17}$$

Now we consider that perturbations are in the form of plane waves, so one can Fourier-analyse perturbed quantities as follows

$$\tilde{f}(\mathbf{r}, t) = f_1 e^{i(\omega t + \mathbf{k} \cdot \mathbf{r})}, \tag{2.18}$$

where f_1 is the perturbation amplitude and, with no loss of generality, we choose the wave vector in the xz-plane, $\mathbf{k} = k_x \hat{\mathbf{x}} + k_z \hat{\mathbf{z}}$. Then, the set of linear adiabatic equations reduces to the following set of scalar expressions,

$$\omega \rho_1 + \rho_0 (k_x v_{1x} + k_z v_{1z}) = 0, \tag{2.19}$$

$$\omega \rho_0 v_{1x} + k_x p_1 = 0, \tag{2.20}$$

$$\omega \rho_0 v_{1y} - \frac{B_{0x}}{4\pi} k_x B_{1y} = 0, \tag{2.21}$$

$$\omega \rho_0 v_{1z} + k_z p_1 + \frac{B_{0x}}{4\pi}(k_z B_{1x} - k_x B_{1z}) = 0, \tag{2.22}$$

$$i\omega \left(p_1 - c_s^2 \rho_1 \right) = 0, \tag{2.23}$$

$$\omega B_{1x} + B_{0x} k_z v_{1z} = 0, \tag{2.24}$$

$$\omega B_{1y} - B_{0x} k_x v_{1y} = 0, \tag{2.25}$$

$$\omega B_{1z} - B_{0x} k_x v_{1z} = 0, \tag{2.26}$$

$$k_x B_{1x} + k_z B_{1z} = 0. \tag{2.27}$$

Alfvén waves

Eqs. (2.21) and (2.25) are decoupled from the rest and from them we can obtain the dispersion relation for Alfvén waves

$$\omega^2 - k_x^2 v_a^2 = 0, \tag{2.28}$$

where the Alfvén speed squared is defined by

$$v_a^2 = \frac{B_0^2}{4\pi \rho_0}. \tag{2.29}$$

Alfvén waves propagate with a constant phase speed along magnetic field lines, $\omega/k_x = v_a$, and are driven by tension and pressure forces with no pressure or density variations (they are incompressible). This last fact makes Alfvén waves insensible to non-adiabatic effects.

Plasma motions associated to this mode are transverse to both the magnetic field and the direction of propagation. It is a highly anisotropic mode, unable to propagate across the field, with energy flowing along field lines at the Alfvén speed.

Magnetoacoustic waves

Eqs. (2.19)–(2.27) excluding (2.21) and (2.25) describe slow and fast magnetoacoustic modes. The slow wave is essentially an acoustic wave modified by the magnetic field, while the fast wave is a magnetic wave driven by magnetic pressure and weakly affected by acoustic effects (Goossens 2003).

Next, it is possible to obtain a general dispersion relation for magnetoacoustic waves by imposing that the determinant of this algebraic system be zero. This provides us with the well-known dispersion relation for magnetoacoustic waves,

$$\omega^4 - \left(c_s^2 + v_a^2 \right) k^2 \omega^2 + k^4 c_s^2 v_a^2 \cos^2 \theta = 0, \tag{2.30}$$

with $k^2 = k_x^2 + k_z^2$ and the propagation angle θ being the angle between the equilibrium magnetic field, $\mathbf{B}_0$, and the propagation direction, $\mathbf{k}$. The analytical solution of Eq. (2.30) is,

$$\omega^2 = \frac{k^2}{2}\left[\left(c_s^2 + v_a^2\right) \pm \sqrt{\left(c_s^2 + v_a^2\right)^2 - 4c_s^2 v_a^2 \cos^2\theta}\right], \tag{2.31}$$

where the positive sign corresponds to the fast magnetoacoustic wave while the negative sign corresponds to the slow magnetoacoustic wave.

In the low β plasma approximation (i.e. for $c_s \ll v_a$), that is suitable for a prominence plasma, the solutions to the dispersion relation become

$$\omega = k_x c_s, \tag{2.32}$$

for the slow wave and

$$\omega = k v_a, \tag{2.33}$$

for the fast wave.

The slow mode is driven by tension and pressure forces, with pressure and density variations. It is an anisotropic mode, unable to propagate across the magnetic field lines, and the energy flow is confined to the vicinity of certain magnetic field lines.

The fast mode, like the slow mode, is driven by tension and pressure forces, with pressure and density variations. This mode is roughly isotropic, although it propagates faster across the magnetic field.

It should be pointed out that in other conditions, the distinction between the three modes (Alfvén, fast and slow) is not clear, because they become coupled. Anyway, in general it is still possible to identify the characteristics of a wave and to classify it by comparing with the most suitable mode in an infinite homogeneous medium.

2.3.3 Non-adiabatic magnetohydrodynamics

With the inclusion of non-adiabatic effects the previous MHD modes are modified and a fourth mode appears, the thermal mode.

Now, we proceed as in the previous section but considering the non-adiabatic terms. Then, we end up with the following set of scalar equations,

$$\omega \rho_1 + \rho_0(k_x v_{1x} + k_z v_{1z}) = 0, \tag{2.34}$$

$$\omega \rho_0 v_{1x} + k_x p_1 = 0, \tag{2.35}$$

$$\omega \rho_0 v_{1y} - \frac{B_{0x}}{4\pi} k_x B_{1y} = 0, \tag{2.36}$$

$$\omega \rho_0 v_{1z} + k_z p_1 + \frac{B_{0x}}{4\pi}(k_z B_{1x} - k_x B_{1z}) = 0, \tag{2.37}$$

Regime	χ^*	α	Reference
Prominence (1)	1.76×10^{-6}	7.4	Hildner (1974)
Prominence (2)	1.76×10^{-46}	17.4	Milne et al. (1979)
Prominence (3)	7.01×10^{-97}	30	Rosner et al. (1978)
Corona	1.97×10^{31}	-1	Hildner (1974)

Table 2.1: Parameter values (in cgs units) of the radiative loss function considering different plasma optical thicknesses. The three prominence regimes represent different plasma optical thicknesses, Prominence (1) being valid for an optically thin plasma, Prominence (2) for optically thick and Prominence (3) for very thick plasmas. An optically thin plasma is assumed for the coronal regime.

$$i\omega\left(p_1 - c_s^2\rho_1\right) + (\gamma - 1)\left(\kappa_\parallel k_x^2 + \rho 0 L_T\right)T_1 + (\gamma - 1)(L + \rho_0 L_\rho)\rho_1 = 0, \tag{2.38}$$

$$\omega B_{1x} + B_{0x}k_z v_{1z} = 0, \tag{2.39}$$

$$\omega B_{1y} - B_{0x}k_x v_{1y} = 0, \tag{2.40}$$

$$\omega B_{1z} - B_{0x}k_x v_{1z} = 0, \tag{2.41}$$

$$k_x B_{1x} + k_z B_{1z} = 0, \tag{2.42}$$

$$\frac{p_1}{p_0} - \frac{\rho_1}{\rho_0} - \frac{T_1}{T_0} = 0. \tag{2.43}$$

Again, Eqs. (2.36) and (2.40) are decoupled from the rest and govern Alfvén waves, which are not affected by non-adiabatic effects.

From the rest of equations and imposing that the determinant of this algebraic system be zero we obtain the general dispersion relation for thermal and magnetoacoustic waves,

$$a_5\omega^5 + a_4\omega^4 + a_3\omega^3 + a_2\omega^2 + a_1\omega + a_0 = 0, \tag{2.44}$$

whose coefficients are given by:

$$a_0 = -\frac{ik^2 k_x^2 v_a^2}{\rho_0}(AT_0 - H\rho_0),$$

$$a_1 = k^2 k_x^2 c_s^2 v_a^2,$$

$$a_2 = ik^2 \left[\frac{AT_0 - H\rho_0}{\rho_0} + \frac{AT_0 v_a^2}{p_0}\right],$$

$$a_3 = -k^2 \left(c_s^2 + v_a^2\right),$$

$$a_4 = -i\frac{AT_0}{p_0},$$

$$a_5 = 1, \tag{2.45}$$

with

$$A = (\gamma - 1)\left(\kappa_\parallel k_x^2 + \rho_0 L_T\right), \tag{2.46}$$
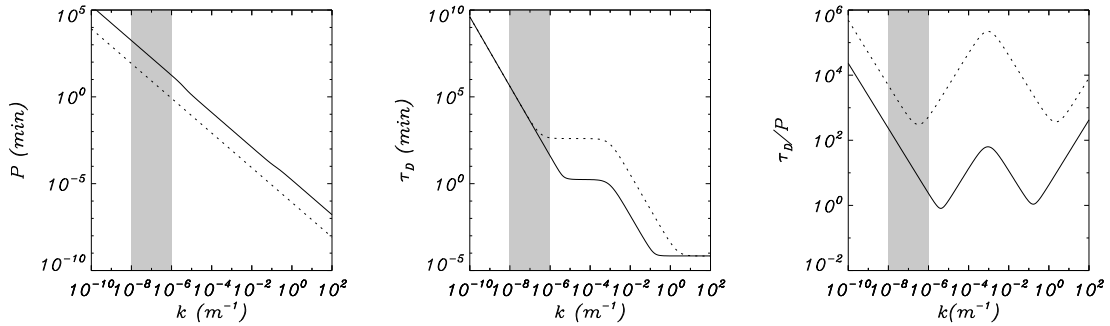
Figure 2.1: Period, damping time and ratio of the damping time to the period versus the wavenumber k for fast (dotted line) and slow (solid line) waves. Eq. (2.44) has been solved considering typical prominence conditions ($T_0 = 8000$ K, $\rho_0 = 5 \times 10^{-11}$ kg cm^{-3}, $\tilde{\mu} = 0.5$), $B_0 = 10$ G, Prominence (1) regime radiation conditions (Table 2.1) and constant heating per unit volume ($a = b = 0$). Adapted from Carbonell et al. (2004).

$$H = (\gamma - 1)(L + \rho_0 L_\rho). \tag{2.47}$$

The solutions of this dispersion relation were studied by Carbonell et al. (2004). Considering a real wavenumber, k, the solutions for the frequency are complex, $\omega = \omega_R + i\omega_I$. Hence, the amplitude of the perturbations is multiplied by a factor $\exp(-\omega_I t)$. For $\omega_I > 0$ oscillations are damped in time, while, on the contrary, if $\omega_I < 0$ oscillations are amplified. The dispersion relation, Eq. (2.44), has one purely imaginary root, corresponding to the thermal or condensation mode which is a non-propagating solution (Field 1965). The rest of roots correspond to wave modes and consist of two pairs, one representing the slow mode and the other corresponding to the fast mode.

In the adiabatic limit, $A = H = 0$, Eq. (2.44) becomes the well-known dispersion relation for adiabatic perturbations (Eq. [2.30]).

Carbonell et al. (2004) solved Eq. (2.44) for a wide range of wavenumbers and for different values of equilibrium physical conditions akin to those of prominences. They also considered different optical thicknesses of the prominence plasma and several heating mechanisms (Table 2.1). One of the main results of this work is that waves are always attenuated ($\omega_I > 0$) for prominence conditions[2].

The period P, the damping time τ_D and the ratio of the period to the damping time can be computed from the real and imaginary part of the frequency; respectively:

$$P = \frac{2\pi}{\omega_R}, \qquad \tau_D = \frac{1}{\omega_I}, \qquad \frac{\tau_D}{P} = \frac{\omega_R}{2\pi\omega_I}. \tag{2.48}$$

Figure 2.1 reproduces some results from Carbonell et al. (2004). We can observe that both magnetoacoustic waves are damped by non-adiabatic effects,

---

[2]They also found that waves can be amplified ($\omega_I < 0$) in time for the prominence-corona transition region (PCTR) and coronal conditions in some ranges of k depending on the heating scenario. This situation corresponds to a thermal instability (Field 1965).

the slow wave being more attenuated than the fast wave. For the wavenumbers corresponding to the observed range of wavelengths (shaded regions of the figures), the theoretical value of τ_D/P is compatible with observations in the case of the slow wave, but larger values are obtained in the case of the fast wave.

Chapter 3

Partially ionised plasma: one-fluid MHD equations[*]

Prominences seem to be constituted by partially ionised plasmas since neutral hydrogen lines are observed. The ionisation degree of prominences varies over a wide range, with the ratio of electron to neutral hydrogen density roughly between 0.1 and 10 (Patsourakos & Vial 2002). Therefore, we should consider this fact and a new set of MHD equations, including the effect of collisions between ions and neutrals present in the plasma, is needed.

The frictional damping of magnetoacoustic waves in a partially ionised plasma is much stronger than in a fully ionised plasma because the presence of neutral atoms causes the Joule heating dissipation to increase as a result of collisions of electrons with neutrals and ions and, what is more important, of collisions of ions with neutrals (Khodachenko et al. 2004). The cause for the collisions between ions and neutrals is in Alfvén's frozen flux theorem: if a perturbation gives rise to a transverse displacement of the magnetic field, charged particles move bodily with magnetic field lines, while neutrals stay motionless. This comparative study of the role of ion-neutral damping of MHD waves and their damping due to viscosity and thermal conductivity was made by Khodachenko et al. (2004, 2006) and it was found that collisional damping is dominant. It is well known that the role of neutrals can be very relevant in a cold plasma ($T \sim 10\,000$ K), such as has been found by Leake & Arber (2006) in the context of the magnetic flux emergence from the solar interior into the corona. These authors found that the chromospheric partial ionisation leads to an increased rate of flux emergence and, more importantly, that the magnetic field becomes force-free after crossing the chromosphere.

The goal of this chapter is to add to the single-fluid MHD equations (presented in the previous chapter) the effect of the ion-neutral collision mechanism, i.e. to derive a set of single-fluid MHD equations for partially ionised

---

[*]This Chapter is based on: Forteza, P., Oliver, R., Ballester, J. L., & Khodachenko, M. L. 2007, "Damping of oscillations by ion-neutral collisions in a prominence plasma", Astronomy and Astrophysics, 461, 731.

plasmas.

3.1   General assumptions

We consider the prominence material as a partially ionised hydrogen plasma with T_α, ρ_α, n_α, p_α and $\mathbf{v}_\alpha$ respectively representing the temperature, density, number density, pressure and velocity of the different plasma species: electrons ($\alpha = $ e), ions ($\alpha = $ i) and neutrals ($\alpha = $ n). Obviously, in a hydrogen plasma the number density of ions and electrons is equal, i.e $n_e = n_i$. Moreover, the density can be defined as $\rho_\alpha = m_\alpha n_\alpha$, with m_α the particle mass.

The total density, total pressure and centre of mass velocity are defined as

$$\rho = \rho_e + \rho_i + \rho_n \approx \rho_i + \rho_n, \tag{3.1}$$

$$p = p_e + p_i + p_n = 2p_i + p_n, \tag{3.2}$$

$$\mathbf{v} = \frac{\sum_{\alpha=e,i,n} \rho_\alpha \mathbf{v}_\alpha}{\rho} \approx \xi_i \mathbf{v}_i + \xi_n \mathbf{v}_n, \tag{3.3}$$

where the assumptions $\rho_e|\mathbf{v}_e| \ll \rho_i|\mathbf{v}_i|$ and $\rho_e|\mathbf{v}_e| \ll \rho_n|\mathbf{v}_n|$ have been made. Here the relative densities of ions and neutrals are defined as

$$\xi_i = \frac{\rho_i}{\rho} \approx \frac{n_i}{n_i + n_n},$$

$$\xi_n = \frac{\rho_n}{\rho} \approx \frac{n_n}{n_i + n_n}. \tag{3.4}$$

The degree of ionisation of the plasma is characterised by the ionisation fraction defined as the mean atomic weight (the average mass per particle in units of the proton mass, m_p),

$$\tilde{\mu} = \frac{1}{1 + \xi_i}. \tag{3.5}$$

This definition implies that $\tilde{\mu} = 0.5$ for a fully ionised plasma and $\tilde{\mu} = 1$ for a neutral gas. Although we retain the relative densities of ions and neutrals in the following, these can be expressed in terms of the ionisation fraction as $\xi_i = 1/\tilde{\mu} - 1$ and $\xi_n = 2 - 1/\tilde{\mu}$.

Is important to note that here we do not include the effects of particle ionisation and recombination, so the number of ions, neutrals and electrons in the plasma remains constant, and also assume a strong thermal coupling between the different species, which leads electrons, ions and neutrals to have the same temperature ($T_e = T_i = T_n = T$). Then, it makes no sense to consider separate continuity, momentum and energy equations for the three components. The separate governing equations for the three species can be easily substituted by a set of one-fluid equations for the whole partially ionised plasma. In the following sections we outline the derivation of this set of expressions.

3.2   Continuity equation

To obtain the continuity equation of a partially ionised plasma one only needs to add the individual continuity equations for the different species present in the plasma (i.e. electrons, ions and neutrals):

$$\frac{\partial \rho_e}{\partial t} + \nabla \cdot (\rho_e \mathbf{v}_e) = 0, \tag{3.6}$$

$$\frac{\partial \rho_i}{\partial t} + \nabla \cdot (\rho_i \mathbf{v}_i) = 0, \tag{3.7}$$

$$\frac{\partial \rho_n}{\partial t} + \nabla \cdot (\rho_n \mathbf{v}_n) = 0. \tag{3.8}$$

The addition of these three equations together with the definitions of the density (Eq. [3.1]) and the centre of mass velocity of the partially ionised plasma (Eq. [3.3]) yields

$$\frac{\partial \rho}{\partial t} + \nabla \cdot (\rho \mathbf{v}) = 0. \tag{3.9}$$

3.3   Momentum equation

The general form of the momentum equation, neglecting gravity effects, is

$$n_\alpha m_\alpha \frac{d_\alpha \mathbf{v}_\alpha}{dt} = -\nabla p_\alpha + n_\alpha Z_\alpha e \left(\mathbf{E} + \frac{1}{c} \mathbf{v}_\alpha \times \mathbf{B} \right) + \sum_\beta \mathbf{R}_{\beta\alpha}, \tag{3.10}$$

where $d_\alpha / dt \equiv \partial/\partial t + \mathbf{v}_\alpha \cdot \nabla$ and Z_α is the charge of the particles (i.e., in our case $Z_e = -1$, $Z_i = 1$ and $Z_n = 0$). In addition,

$$\mathbf{R}_{\beta\alpha} = n_\alpha m_\alpha \nu'_{\alpha\beta} (\mathbf{v}_\beta - \mathbf{v}_\alpha) \tag{3.11}$$

is the momentum interchange between the species α and the other species, $\beta \neq \alpha$, present in the plasma. Using the fact that momentum is conserved in a collision we find

$$\mathbf{R}_{\beta\alpha} = -\mathbf{R}_{\alpha\beta}, \qquad \alpha_{\alpha\beta} = \alpha_{\beta\alpha}. \tag{3.12}$$

The effective collision frequency $\nu'_{\alpha\beta}$ can be obtained from

$$\nu'_{\alpha\beta} = \frac{m_\beta}{m_\alpha + m_\beta} \nu_{\alpha\beta}, \tag{3.13}$$

where $\nu'_{\alpha\beta} = \nu'_{\beta\alpha}$ and $\nu_{\alpha\beta} = \nu_{\beta\alpha}$ and only the three collision frequencies ν_{ei}, ν_{en} and ν_{in} need to be computed using the following expressions

$$\nu_{ei} = 5.89 \times 10^{-24} \frac{n_i \ln \Lambda_C Z^2}{(k_B T)^{3/2}}, \tag{3.14}$$

$$\nu_{en} = n_n \sqrt{\frac{8k_B T}{\pi m_{en}}} \Sigma_{en}, \tag{3.15}$$

$$\nu_{in} = n_n \sqrt{\frac{8k_B T}{\pi m_{in}}} \Sigma_{in}, \tag{3.16}$$

where $\Sigma_{en} \sim 7{\times}10^{-16}$ cm^2 and $\Sigma_{in} \sim 5{\times}10^{-15}$ cm^2 are the electron-neutral and ion-neutral collisional cross-sections, $m_{\alpha n} = m_\alpha m_n/(m_\alpha + m_n)$ with $\alpha = $ e, i and $\ln \Lambda_C$ is the Coulomb logarithm, whose value has a weak dependence on temperature and density (Priest 1984) and usually takes values between 5 and 10.

One can define

$$\alpha_{\alpha\beta} = n_\alpha m_\alpha \nu'_{\alpha\beta}, \tag{3.17}$$

$$\alpha_n = \alpha_{in} + \alpha_{en}. \tag{3.18}$$

Now, introducing the relative ion-neutral velocity and the electric current density,

$$\mathbf{w} = \mathbf{v}_i - \mathbf{v}_n, \tag{3.19}$$

$$\mathbf{j} = n_i e(\mathbf{v}_i - \mathbf{v}_e), \tag{3.20}$$

one can write the momentum equations for electrons, ions and neutrals for our partially ionised plasma as follows

$$n_i m_e \frac{d_e \mathbf{v}_e}{dt} = -\nabla p_e - n_i e \left(\mathbf{E} + \frac{1}{c} \mathbf{v}_e \times \mathbf{B} \right) + (\alpha_{ei} + \alpha_{en}) \frac{\mathbf{j}}{n_i e} - \alpha_{en} \mathbf{w}, \tag{3.21}$$

$$n_i m_i \frac{d_i \mathbf{v}_i}{dt} = -\nabla p_i + n_i e \left(\mathbf{E} + \frac{1}{c} \mathbf{v}_i \times \mathbf{B} \right) - \alpha_{ei} \frac{\mathbf{j}}{n_i e} - \alpha_{in} \mathbf{w}, \tag{3.22}$$

$$n_n m_i \frac{d_n \mathbf{v}_n}{dt} = -\nabla p_n - \alpha_{en} \frac{\mathbf{j}}{n_i e} + (\alpha_{in} + \alpha_{en}) \mathbf{w}. \tag{3.23}$$

Adding these three equations, taking into account Eqs. (3.2) and (3.20) and neglecting the electrons inertia term, we obtain the momentum equation for the whole partially ionised plasma

$$n_i m_i \frac{d_i \mathbf{v}_i}{dt} + n_n m_i \frac{d_n \mathbf{v}_n}{dt} = -\nabla p + \frac{1}{c} \mathbf{j} \times \mathbf{B}. \tag{3.24}$$

After some algebra[1] the momentum equation leads to

$$\rho \frac{d\mathbf{v}}{dt} = -\nabla p + \frac{1}{c} \mathbf{j} \times \mathbf{B} - \nabla \cdot (\xi_i \xi_n \rho \mathbf{w}\mathbf{w}). \tag{3.25}$$

---

[1]See Appendix A for a detailed derivation of the momentum equation.

where $d/dt \equiv \partial/\partial t + \mathbf{v} \cdot \nabla$.

The term containing $\mathbf{w}$ is caused by the species inertia and can be usually neglected in solar applications and also vanishes in the linear regime. An expression for $\mathbf{w}$ is given in Section 3.6.

3.4   Energy equation

We start with the energy equation of each species, neglecting thermal effects

$$\frac{\partial p_e}{\partial t} + \mathbf{v}_e \cdot \nabla p_e + \gamma p_e \nabla \cdot \mathbf{v}_e = (\gamma - 1)Q_e, \tag{3.26}$$

$$\frac{\partial p_i}{\partial t} + \mathbf{v}_i \cdot \nabla p_i + \gamma p_i \nabla \cdot \mathbf{v}_i = (\gamma - 1)Q_i, \tag{3.27}$$

$$\frac{\partial p_n}{\partial t} + \mathbf{v}_n \cdot \nabla p_n + \gamma p_n \nabla \cdot \mathbf{v}_n = (\gamma - 1)Q_n. \tag{3.28}$$

Adding the three equations we obtain

$$\frac{\partial p}{\partial t} + \sum_\alpha (\mathbf{v}_\alpha \cdot \nabla p_\alpha + \gamma p_\alpha \nabla \cdot \mathbf{v}_\alpha) = (\gamma - 1) \sum_\alpha Q_\alpha, \tag{3.29}$$

where the $Q_\alpha = \sum_\beta Q_{\alpha\beta}$ and $Q_{\alpha\beta}$ is the heat generated in a gas of particles of species α as a consequence of collisions with particles of species β.

Considering

$$Q_{\alpha\beta} + Q_{\beta\alpha} = -\mathbf{R}_{\beta\alpha} \cdot (\mathbf{v}_\alpha - \mathbf{v}_\beta), \tag{3.30}$$

and Eqs. (3.19) and (3.20) we can write the right-hand side summatory of Eq. (3.29) as

$$Q_e + Q_i + Q_n = \frac{\alpha_e}{e^2 n_i^2} j^2 + \alpha_n w^2 - 2\frac{\alpha_{en}}{en_i}\mathbf{w} \cdot \mathbf{j}. \tag{3.31}$$

After some algebraic manipulations[2] we end up with the energy equation for the whole partially ionised plasma

$$\frac{dp}{dt} + \gamma p \nabla \cdot \mathbf{v} + \gamma \nabla \cdot (2\xi_n p_i \mathbf{w} - \xi_i p_n \mathbf{w}) - \gamma \mathbf{j} \cdot \nabla \left(\frac{p_i}{en_i}\right) = (\gamma - 1)q_{\text{Joule}}, \tag{3.32}$$

which considering Eq. (3.9) can be written as

$$\frac{dp}{dt} - \frac{\gamma p}{\rho}\frac{d\rho}{dt} + \gamma \nabla \cdot (2\xi_n p_i \mathbf{w} - \xi_i p_n \mathbf{w}) - \gamma \mathbf{j} \cdot \nabla \left(\frac{p_i}{en_i}\right) = (\gamma - 1)q_{\text{Joule}}. \tag{3.33}$$

---

[2]See Appendix B for a complete derivation of the energy equation.

Now, one can generalise this energy equation in order to obtain a more general expression including the thermal effects,

$$\frac{dp}{dt} - \frac{\gamma p}{\rho}\frac{d\rho}{dt} + \gamma \nabla \cdot (2\xi_n p_i \mathbf{w} - \xi_i p_n \mathbf{w}) - \gamma \mathbf{j} \cdot \nabla\left(\frac{p_i}{e n_i}\right) = -(\gamma-1)\left[\rho L(\rho, T) - \nabla \cdot (\kappa \cdot \nabla T) - q_{\text{Joule}}\right].$$

(3.34)

3.4.1 Radiation and heating

The heat-loss function represents the difference between an arbitrary heat imput, H, and radiative losses, L_r,

$$L(\rho, T) = L_r(\rho, T) - H(\rho, T).$$

(3.35)

Radiative losses can be written following Priest (1984) as

$$L_r = \frac{n_e n_H}{\rho} Q(T),$$

(3.36)

where the electron density, n_e, and the density of hydrogen atoms and neutrals, $n_H = n_i + n_n$, can be expressed in terms of ξ_i by means of using Eq. (3.4).

The function $Q(T)$ has been evaluated by different authors (Cox & Tucker 1969; Tucker & Koren 1971; McWhirter et al. 1975; Raymond & Smith 1977) and can be aproximated by

$$Q(T) = m_p^2 \chi^* T^\alpha,$$

(3.37)

whith χ^* and α being piecewise functions that depend on the temperature.

This approach was taken by Hildner (1974) who assumed an optically thin plasma. While the use of this approach seems reasonable for coronal conditions, it may not be valid for prominence conditions because they are, at least in part, optically thick. The radiative losses from the internal part of prominences are greatly reduced and this can be represented by changing the values of χ^* and α in the cooling function (see Table 2.1).

The processes involved in the solar atmospheric heating are still not well known, so several possible heating mechanisms or scenarios have been proposed, like heating by acoustic or Alfvén waves or by current dissipation. In some works (Rosner et al. 1978; Dahlburg & Mariska 1988), the heating function is written as

$$H(\rho, T) = h\rho^a T^b.$$

(3.38)

and the values taken into account for the exponents a and b are

1. Constant heating per unit volume ($a = b = 0$).

2. Constant heating per unit mass ($a = 1$, $b = 0$).

3. Heating by coronal current disipation ($a = 1$, $b = 1$).

4. Heating by Alfvén mode/mode conversion ($a = b = 7/6$).

5. Heating by Alfvén mode/anomalous conduction damping ($a = 1/2$, $b = -1/2$).

So, the heat-loss function for a partially ionised plasma takes the form

$$L(\rho, T) = \xi_i \rho \chi^* T^\alpha - h \rho^a T^b. \tag{3.39}$$

Finally, the constant h in Eq. (3.39) can be obtained by considering an equilibrium with uniform temperature ($L(\rho_0, T_0) = 0$) and one of the heating scenarios. In our investigation we have chosen a constant heating per unit volume ($a = b = 0$), so

$$h = \xi_i \rho_0 \chi^* T_0^\alpha. \tag{3.40}$$

3.4.2 Thermal conduction

Now, we need an expression for the thermal conduction in a partially ionised plasma. Following Parker (1953) and Ibáñez & Mendoza (1990), the thermal conduction coefficient in a partially ionised plasma can be expressed as the sum of the contributions of electrons and neutrals

$$\boldsymbol{\kappa} = \boldsymbol{\kappa}_e + \boldsymbol{\kappa}_n. \tag{3.41}$$

In typical coronal and prominence conditions the magnetic field is strong enough to make the perpendicular component of the electron's conductivity tensor negligible ($\kappa_\parallel \gg \kappa_\perp$), so

$$\boldsymbol{\kappa}_e = \kappa_{e\parallel} \hat{\mathbf{b}}\hat{\mathbf{b}}, \tag{3.42}$$

with

$$\kappa_{e\parallel} = 1.84 \times 10^{-5} \frac{\xi_i T^{5/2}}{\ln \Lambda_C}. \tag{3.43}$$

On the other hand, the neutrals contribution to thermal conduction is isotropic since neutrals do not sense the magnetic field, so

$$\boldsymbol{\kappa}_n = \kappa_n \mathbf{I}, \tag{3.44}$$

with

$$\kappa_n = 2.5 \times 10^3 (1 - \xi_i). \tag{3.45}$$

3.5   Equation of state

The equation of state is only needed to determine the temperature from the number density, n, and pressure, p, of the plasma. It is given by the sum of the equations of state of electrons, ions and neutrals

$$p_\mathrm{e} = n_\mathrm{e} k_\mathrm{B} T = n_\mathrm{i} k_\mathrm{B} T, \tag{3.46}$$

$$p_\mathrm{i} = n_\mathrm{i} k_\mathrm{B} T, \tag{3.47}$$

$$p_\mathrm{n} = n_\mathrm{n} k_\mathrm{B} T, \tag{3.48}$$

so, the equation of state for the partially ionised plasma is

$$p = p_\mathrm{e} + p_\mathrm{i} + p_\mathrm{n} = (2 n_\mathrm{i} + n_\mathrm{n}) k_\mathrm{B} T = n k_\mathrm{B} T. \tag{3.49}$$

3.6   Ohm's law

The first step to obtain the generalised Ohm's law is to calculate an expression for **w** by adding the momentum equations of electrons and ions (Eqs. [3.21] and [3.22]) multiplied by ξ_n and the momentum equation of neutrals (Eq. [3.23]) multiplied by $-\xi_\mathrm{i}$. The result is

$$\mathbf{w} = -\frac{\mathbf{G}}{\alpha_\mathrm{n}} + \frac{\xi_\mathrm{n}}{c \alpha_\mathrm{n}} \mathbf{j} \times \mathbf{B} + \frac{\alpha_\mathrm{en}}{\alpha_\mathrm{n}} \frac{\mathbf{j}}{e n_\mathrm{i}} - \frac{\xi_\mathrm{n} \xi_\mathrm{i}}{\alpha_\mathrm{n}} \rho \left(\frac{d_\mathrm{i} \mathbf{v}_\mathrm{i}}{dt} - \frac{d_\mathrm{n} \mathbf{v}_\mathrm{n}}{dt} \right), \tag{3.50}$$

where **G** is the pressure function (defined in Braginskii 1965),

$$\mathbf{G} = \xi_\mathrm{n} \nabla (p_\mathrm{e} + p_\mathrm{i}) - \xi_\mathrm{i} \nabla p_\mathrm{n}. \tag{3.51}$$

Taking into account that the partial pressures of the different species are

$$p_\mathrm{e} = p_\mathrm{i} = \frac{\xi_\mathrm{i}}{1 + \xi_\mathrm{i}} p, \qquad p_\mathrm{n} = \frac{\xi_\mathrm{n}}{1 + \xi_\mathrm{i}} p, \tag{3.52}$$

the pressure function can be cast as

$$\mathbf{G} = 2 \xi_\mathrm{n} \nabla \left(\frac{\xi_\mathrm{i}}{1 + \xi_\mathrm{i}} p \right) - \xi_\mathrm{i} \nabla \left(\frac{\xi_\mathrm{n}}{1 + \xi_\mathrm{i}} p \right). \tag{3.53}$$

From Eqs. (3.3), (3.19) and (3.20) we can write

$$\mathbf{v}_\mathrm{e} = \mathbf{v} + \xi_\mathrm{n} \mathbf{w} - \frac{\mathbf{j}}{e n_\mathrm{i}}. \tag{3.54}$$

Now, considering Eqs. (3.21), (3.50) and (3.54) and neglecting the term containing derivatives of $\mathbf{v}_\mathrm{i}$ and $\mathbf{v}_\mathrm{n}$ in the formula of **w** one obtains

$$\mathbf{E}^* \equiv \mathbf{E} + \frac{1}{c}\mathbf{v} \times \mathbf{B} = \frac{\varepsilon\mathbf{G} - \nabla p_{\mathrm{e}}}{e n_{\mathrm{i}}} + \frac{\mathbf{j}}{\sigma} + \frac{1 - 2\varepsilon\xi_{\mathrm{n}}}{e n_{\mathrm{i}} c}\mathbf{j} \times \mathbf{B}$$
$$+ \frac{\xi_{\mathrm{n}}}{c\alpha_{\mathrm{n}}}\left[\mathbf{G} \times \mathbf{B} - \frac{\xi_{\mathrm{n}}}{c}(\mathbf{j} \times \mathbf{B}) \times \mathbf{B}\right], \tag{3.55}$$

where $\varepsilon = \alpha_{\mathrm{en}}/\alpha_{\mathrm{n}} \ll 1$ and

$$\sigma = \frac{n_{\mathrm{i}}e^2}{m_{\mathrm{e}}\left[\nu'_{\mathrm{ei}} + (1 - \varepsilon)\nu'_{\mathrm{en}}\right]} \approx \frac{n_{\mathrm{i}}e^2}{m_{\mathrm{e}}\left(\nu'_{\mathrm{ei}} + \nu'_{\mathrm{en}}\right)} \tag{3.56}$$

is the conductivity.

The Joule heating term, that appears in the energy equations (3.32) or (3.34) can be cast using Eq. (3.55) as

$$q_{\mathrm{Joule}} \equiv \mathbf{E}^* \cdot \mathbf{j} = \frac{\varepsilon\mathbf{G} - \nabla p_{\mathrm{e}}}{n_{\mathrm{i}}} \cdot \mathbf{j} + \frac{j^2}{\sigma} - \frac{\xi_{\mathrm{n}}}{c\alpha_{\mathrm{n}}}(\mathbf{j} \times \mathbf{B}) \cdot \mathbf{G} + \frac{\xi_{\mathrm{n}}^2}{c^2\alpha_{\mathrm{n}}}(\mathbf{j} \times \mathbf{B})^2. \tag{3.57}$$

3.7   Induction equation

To obtain the induction equation we need to take the curl of Eq. (3.55) and insert it into Faraday's law[3], so one can obtain the general form of the induction equation[4]

$$\frac{\partial \mathbf{B}}{\partial t} = \nabla \times (\mathbf{v} \times \mathbf{B}) - \frac{c}{e}\nabla \times \left(\frac{\varepsilon\mathbf{G} - \nabla p_{\mathrm{e}}}{n_{\mathrm{i}}}\right) - \nabla \times (\eta\nabla \times \mathbf{B})$$
$$- \nabla \times \left(\frac{\xi_{\mathrm{n}}}{\alpha_{\mathrm{n}}}\mathbf{G} \times \mathbf{B}\right) - \frac{c}{4\pi e}\nabla \times \left[\frac{1 - 2\varepsilon\xi_{\mathrm{n}}}{n_{\mathrm{i}}}(\nabla \times \mathbf{B}) \times \mathbf{B}\right] \tag{3.58}$$
$$+ \nabla \times \left\{\frac{\xi_{\mathrm{n}}^2}{4\pi\alpha_{\mathrm{n}}}[(\nabla \times \mathbf{B}) \times \mathbf{B}] \times \mathbf{B}\right\},$$

where the coefficient of magnetic diffusivity is defined as

$$\eta = \frac{c^2}{4\pi\sigma}, \tag{3.59}$$

and the quantity $\xi_{\mathrm{n}}^2/(4\pi\alpha_{\mathrm{n}})$ is sometimes written as (Khodachenko et al. 2004; Leake et al. 2005; Khodachenko et al. 2006)

$$\frac{\xi_{\mathrm{n}}^2}{4\pi\alpha_{\mathrm{n}}} = \frac{\eta_{\mathrm{C}} - \eta}{|\mathbf{B}|^2}. \tag{3.60}$$

---

[3] $\nabla \times \mathbf{E} = -\frac{1}{c}\frac{\partial \mathbf{B}}{\partial t}$.

[4] Here $\mathbf{j} = \frac{c}{4\pi}\nabla \times \mathbf{B}$ has been used.

Here the Cowling's coefficient of magnetic diffusivity, η_C, is defined in a similar way as η, but with the Cowling electroconductivity σ_C instead of σ,

$$\sigma_C = \frac{\sigma}{1 + \frac{\xi_n^2 B_0^2 \sigma}{\alpha_n c^2}}. \tag{3.61}$$

The terms on the right-hand side of Eq. (3.58) are known in the literature as the convective term, Biermann's battery, Ohm's diffusion, diamagnetic current term, Hall's diffusion and ambipolar diffusion, respectively. Among these terms, Biermann's battery is the less important in solar atmospheric plasmas, since it is only relevant when large pressure gradients are present, whereas this term is identically zero in a homogeneous plasma.

Ohm's diffusion is mainly governed by electron-ion collisions and ambipolar diffusion is mostly caused by ion-neutral collisions. On the other hand, Hall's effect is also present in the fully ionised case and is enhanced by ion-neutral collisions since they tend to decouple ions from the magnetic field while electrons remain able to drift with the magnetic field (Pandey & Wardle 2008). The diamagnetic current term couples the magnetic field evolution with pressure gradients and its effect is larger for intermediate values of the ionization fraction since **G** vanishes when we consider the fully ionised or the fully neutral limits.

3.8   Summary of single-fluid MHD equations for partially ionised plasmas

Thus, to describe the behavior of a partially ionised plasma one must consider the set of one-fluid Eqs. (3.9), (3.25), (3.34), (3.49) and (3.58), where q_{Joule} is obtained from Eq. (3.57). The terms containing **w** are usually neglected in solar applications and they also vanish in the linear regime. Therefore, the plasma variables in these formulae are ρ, p, T, **v** and **B** and so the set of nine scalar equations contains nine scalar dependent variables. The one-fluid MHD equations for a non-adiabatic partially ionised plasma reduce to their counterparts for a non-adiabatic fully ionised plasma by taking $\xi_i = 1$ (and $\xi_n = 0$) and a perfectly conducting plasma ($\eta_C = \eta = 0$). To retrieve the equations for an ideal plasma we need to neglect the non-adiabatic terms.

Following Leake et al. (2005) the Hall term can be dropped from the generalised Ohm's law if the plasma is magnetised, i.e. if the ions and electrons are tightly bound to the magnetic field. This condition can be written in terms of the ion-gyrofrequency and the collision time as $\omega_i \tau \gg 1$. Using the definition of the ion-neutral collision frequency this is equivalent to

$$\frac{eB}{cm_i} \sqrt{\frac{\pi m_i}{16 k_B T}} \frac{1}{n_n \Sigma_{in}} \gg 1, \tag{3.62}$$

which depends on the strength of the magnetic field as well as the temperature and number density. Since this condition is satisfied in prominences one can neglect the Hall term of the induction equation.

In summary, assuming a homogeneous plasma, isotropic pressure, neglecting gravity, viscosity and species inertia in Eq. (3.25), and neglecting also the Biermann's battery and Hall's current term in Eq. (3.58), our set of single-fluid MHD equations for partially ionised plasmas is,

$$\frac{\partial \rho}{\partial t} + \nabla \cdot (\rho \mathbf{v}) = 0, \tag{3.63}$$

$$\rho \frac{d\mathbf{v}}{dt} = -\nabla p + \frac{1}{c} \mathbf{j} \times \mathbf{B}, \tag{3.64}$$

$$\frac{dp}{dt} + \gamma p \nabla \cdot \mathbf{v} - \gamma \frac{\mathbf{j}}{en_{\mathrm{i}}} \cdot \nabla p_{\mathrm{i}} = -(\gamma - 1) \left[\rho L(\rho, T) - \nabla \cdot (\kappa \cdot \nabla T) - q_{\mathrm{Joule}} \right], \tag{3.65}$$

$$\nabla \cdot \mathbf{B} = 0, \tag{3.66}$$

$$\frac{\partial \mathbf{B}}{\partial t} = \nabla \times (\mathbf{v} \times \mathbf{B}) + \eta \nabla^2 \mathbf{B} - \Xi \nabla \times (\nabla p \times \mathbf{B})$$
$$+ \frac{\eta_{\mathrm{C}} - \eta}{|\mathbf{B}|^2} \nabla \times \{ [(\nabla \times \mathbf{B}) \times \mathbf{B}] \times \mathbf{B} \}, \tag{3.67}$$

$$p = \frac{\rho R T}{\tilde{\mu}}, \tag{3.68}$$

with the parameter Ξ defined as

$$\Xi = \frac{\xi_{\mathrm{i}} \xi_{\mathrm{n}}^2}{(1 + \xi_{\mathrm{i}}) \alpha_{\mathrm{n}}}, \tag{3.69}$$

and where $L(\rho, T)$, κ and q_{Joule} are obtained from Eqs. (3.35), (3.41) and (3.57), respectively.

At this point, it could be worth to keep in mind that in order to study MHD waves in partially ionised plasmas other approaches could be taken. For instance, Zaqarashvili et al. (2011) have considered two-fluid, one made of ions and electrons and the other one made by neutrals. In order to obtain the set of MHD equations applicable to this case, they start from three fluid equations (Braginskii 1965; Goedbloed & Poedts 2004) plus Maxwell's equations, and, after neglecting the electron inertia and viscosity effects, they derived a set of two-fluid MHD equations for partially ionised plasmas. Once derived, this set of equations can be used for the study of MHD waves in the two-fluid approach. The interest of this approach is related with the time-scales of the phenomena under study since for timescales longer than the ion-neutral collision time, the system can be considered as a single-fluid. However, when the time-scales are near or shorter than the ion-neutral collision time, two-fluid equations should be considered. Taking into account that in prominence oscillations the observed periods are much larger than the ion-neutral collision time-scale, it is fully justified to use of a single-fluid approach for our study.

3.9   Non-adiabatic and linear MHD waves in a flowing partially ionised prominence plasma

As a background model, we use a homogeneous unbounded medium threaded by a uniform magnetic field along the x-direction, and with a field-aligned background flow. The equilibrium magnitudes of the medium are given by

$$p_0 = \text{const.,} \quad \rho_0 = \text{const.,} \quad T_0 = \text{const.,}$$

$$\mathbf{B_0} = B_0 \hat{e}_x, \quad \mathbf{v}_0 = v_0 \hat{e}_x,$$

with $B_0 = \text{const.}$, and $v_0 = \text{const.}$.

To obtain the dispersion relation for linear MHD waves in presence of a flow, we consider small perturbations from the equilibrium in the form

$$\mathbf{B} = \mathbf{B}_0 + \tilde{\mathbf{B}}(\mathbf{r}, t),$$

$$\mathbf{v} = \mathbf{v}_0 + \tilde{\mathbf{v}}(\mathbf{r}, t),$$

$$p = p_0 + \tilde{p}(\mathbf{r}, t),$$

$$\rho = \rho_0 + \tilde{\rho}(\mathbf{r}, t),$$

$$T = T_0 + \tilde{T}(\mathbf{r}, t), \tag{3.70}$$

and we linearise the single fluid basic equations. Since the medium is unbounded, as in Chapter 2, we perform a Fourier analysis in plane waves assuming that perturbations behave as

$$\tilde{f} = f_1 e^{i(\omega t - \mathbf{k} \cdot \mathbf{r})}. \tag{3.71}$$

Choosing the z-axis so that the wavenumber $\mathbf{k}$ lies in the xz-plane ($\mathbf{k} = k_x \hat{\mathbf{x}} + k_z \hat{\mathbf{z}}$) the operator $\frac{\partial}{\partial t} + \mathbf{v}_0 \cdot \nabla$ becomes $i(\omega + k_x v_0)$, which points out that in the presence of a background flow the frequency suffers a Doppler shift given by $k_x v_0$ and that the wave frequency, ω, for the non-adiabatic case with flow can be obtained from

$$\omega = \Omega + k_x v_0, \tag{3.72}$$

Ω being the wave frequency for the non-adiabatic case without flow. Also, these frequencies can be described in a different manner: Ω corresponds to the frequency measured by an observer linked to the flow intertial rest frame, while ω corresponds to the frequency measured by an observer linked to an external inertial rest frame.

After the Fourier analysis, the following linearised scalar equations are obtained.

$$\Omega \rho_1 - \rho_0 (k_x v_{1x} + k_z v_{1z}) = 0, \tag{3.73}$$

$$\Omega \rho_0 v_{1x} - k_x p_1 = 0, \tag{3.74}$$

$$\Omega \rho_0 v_{1y} + \frac{B_{0x}}{4\pi} k_x B_{1y} = 0, \tag{3.75}$$

$$\Omega \rho_0 v_{1z} - k_z p_1 + \frac{B_{0x}}{4\pi}(k_x B_{1z} - k_z B_{1x}) = 0, \tag{3.76}$$

$$i\Omega \left(p_1 - c_s^2 \rho_1\right) + (\gamma - 1)\left(\kappa_{e\parallel} k_x^2 + \kappa_n k^2 + \rho_0 L_T\right)T_1 + (\gamma - 1)(L + \rho_0 L_\rho)\rho_1 = 0, \tag{3.77}$$

$$B_{1x}\left(i\Omega + k_x^2 \eta + k_z^2 \eta_C\right) + (\eta - \eta_C)k_x k_z B_{1z} - B_{0x}k_z(iv_{1z} - k_z \Xi p_1) = 0, \tag{3.78}$$

$$B_{1y}\left(i\Omega + k_x^2 \eta_C + k_z^2 \eta\right) + iB_{0x}k_x v_{1y} = 0, \tag{3.79}$$

$$B_{1z}\left(i\Omega + k_x^2 \eta_C + k_z^2 \eta\right) + (\eta - \eta_C)k_x k_z B_{1x} + +B_{0x}k_x(iv_{1z} - k_z \Xi p_1) = 0, \tag{3.80}$$

$$k_x B_{1x} + k_z B_{1z} = 0, \tag{3.81}$$

$$\frac{p_1}{p_0} - \frac{\rho_1}{\rho_0} - \frac{T_1}{T_0} = 0. \tag{3.82}$$

Equations (3.75) and (3.79) are decoupled from the rest and lead to the following dispersion relation for Alfvén waves in a partially ionised plasma with background flow

$$\Omega^2 - i\Omega k^2(\eta_C \cos^2 \theta + \eta \sin^2 \theta) - v_a^2 k^2 \cos^2 \theta = 0, \tag{3.83}$$

From Eq. (3.83) we can define a modified and complex Alfvén speed,

$$\Gamma(\theta)^2 = v_a^2 + i\Omega \left(\eta_C + \eta \tan^2 \theta\right). \tag{3.84}$$

Then, the dispersion relation for Alfvén waves becomes,

$$\Omega^2 - \Gamma(\theta)^2 k^2 \cos^2 \theta = 0. \tag{3.85}$$

From the remaining linearised equations, and after imposing that the determinant of the algebraic system must be zero, we obtain our general dispersion relation for thermal and magnetoacoustic waves in presence of a background flow, which is given by,

$$(\Omega^2 - k^2 \Lambda^2)(ik^2 \eta_C \Omega - \Omega^2) + k^2 v_a^2 (\Omega^2 - k_x^2 \Lambda^2) + ik^2 k_z^2 v_a^2 \Lambda^2 \Xi \rho_0 \Omega = 0, \tag{3.86}$$

where Λ is the non-adiabatic sound speed[5] defined by

$$\Lambda^2 = \frac{\frac{T_0}{\rho_0}A - H + ic_s^2 \Omega}{\frac{T_0}{\rho_0}A + i\Omega}. \tag{3.87}$$

Here

---

[5]A modified sound speed was introduced by Soler et al. (2007) for the non-adiabatic fully ionised case, and by Carbonell et al. (2009) for the non-adiabatic fully ionised case with background flow.

$$A = (\gamma - 1)\left(\kappa_{e\parallel}k_x^2 + \kappa_n k^2 + \rho_0 L_T\right), \tag{3.88}$$

$$H = (\gamma - 1)(L + \rho_0 L_\rho), \tag{3.89}$$

and L_ρ and L_T are defined as in Eq. (2.15), and using the propagation angle, θ, between $\mathbf{k}$ and $\mathbf{B}_0$ the wavenumber components can be expressed as $k_x = k\cos\theta$ and $k_z = k\sin\theta$.

On the other hand, setting $A = H = v_0 = 0$, we obtain the dispersion relation for Alfvén and magnetoacoustic adiabatic waves in a partially ionised and non-flowing plasma. Setting $\xi_n = 0$ and $\eta = 0$, we recover the dispersion relations for Alfvén and magnetoacoustic adiabatic waves in a fully ionised ideal plasma.

3.10 Prominence plasma parameters

Since our aim is to study MHD waves in a partially ionised prominence plasma, the chosen values for the different parameters correspond to those commonly used in prominence studies. Therefore, and unless otherwise is stated, we consider the magnetic field $B_0 = 10$ G, density $\rho_0 = 5 \times 10^{-11}$ kg m^{-3} and temperature $T_0 = 8000$ K. Furthermore, for the radiative loss function we use the parameter values corresponding to Prominence (1) regime in Table 2.1, and the ionisation fraction, $\tilde{\mu}$, is a free parameter in our calculations which enables us to consider from fully ionised to almost neutral plasmas. Another important issue for our study is the numerical value of the sound (c_s) and Alfvén speeds (v_a) and their dependence on the parameter values. In the case of a fixed density and a fixed magnetic field, the Alfvén speed has a constant numerical value of 126.15 km/s. However, since the sound speed depends on the gas pressure, which is a function of the number densities of ions and neutrals, its numerical value is not constant but depends on the ionisation fraction considered. For a fully ionised plasma, the sound speed is 14.84 km/s, while for a partially ionised plasma with $\tilde{\mu} = 0.95$ its value decreases to 10.76 km/s.

Chapter 4

MHD waves in an adiabatic partially ionised prominence plasma[*]

Once we have defined our general dispersion relation for linear non-adiabatic MHD waves in a partially ionised plasma, it is time to start with the study of MHD wave propagation.

In this chapter we will study the propagation of adiabatic MHD waves in an unbounded, homogeneous and partially ionised plasma with physical properties akin to those of solar prominences. This is the simplest configuration which can be studied and the most convenient one to start the research about the effect of ion-neutral collisions in the damping of MHD waves.

4.1 Dispersion relation

Setting the flow velocity and the non-adiabatic terms to zero ($v_0 = 0$, $A = H = 0$) in Eqs. (3.85), (3.86) and (3.87), we obtain the dispersion relation for adiabatic magnetoacoustic waves in a partially ionised plasma,

$$\omega^4 - ik^2\eta_C\omega^3 - k^2\left(c_s^2 + v_a^2\right)\omega^2 + ik^2c_s^2\left(k^2\eta_C - k_z^2v_a^2\Xi\rho_0\right)\omega + k^2k_x^2c_s^2v_a^2 = 0, \qquad (4.1)$$

as well as for Alfvén waves,

$$\omega^2 - k_x^2\Gamma(\theta)^2 = 0. \qquad (4.2)$$

---

[*]This Chapter is based on Forteza, P., Oliver, R., Ballester, J. L., & Khodachenko, M. L. 2007, "Damping of oscillations by ion-neutral collisions in a prominence plasma", Astronomy and Astrophysics, 461, 731 and Forteza, P., Oliver, R., & Ballester, J. L. 2008, "Time damping of non-adiabatic MHD waves in an unbounded partially ionised prominence plasma", Astronomy and Astrophysics, 492, 223.
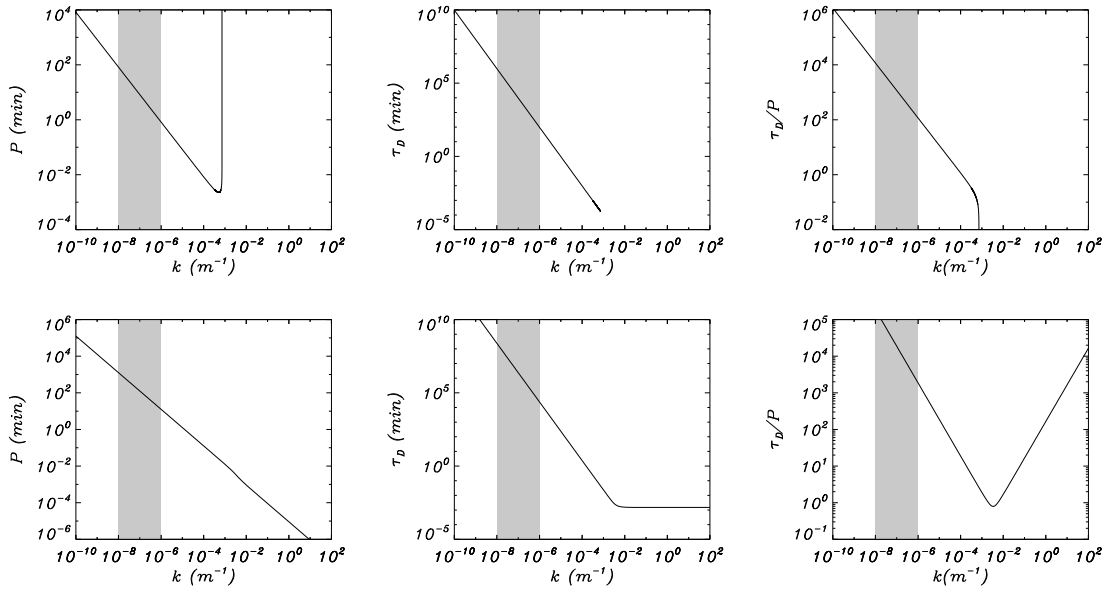
Figure 4.1: Period, damping time and ratio of the damping time to the period for the fast (*top*) and slow (*bottom*) waves in an adiabatic partially ionised plasma with $\tilde{\mu} = 0.8$. In all figures, the shaded region corresponds to the interval of observed wavelengths of prominence oscillations. The parameter values are: $T_0 = 8000$ K, $\rho_0 = 5 \times 10^{-11}$ kg cm^{-3}, $B_0 = 10$ G and $\tan \theta = 0.2/\pi$ ($k_x x_0 = \pi/2$ and $k_z x_0 = 0.1$).

with

$$\Gamma(\theta)^2 = v_{\mathrm{a}}^2 + i\omega \left(\eta_{\mathrm{C}} + \eta \tan^2 \theta \right), \tag{4.3}$$

which is the modified Alfvén speed in absence of flow.

On the other hand, since we are interested in the time damping of magnetoacoustic waves we consider the wavenumber, k, to be real and seek for complex solutions of the frequency ω expressed as $\omega = \omega_{\mathrm{R}} + i\omega_{\mathrm{I}}$. Then, the period and damping time of the waves can be calculated as $P = 2\pi/\omega_{\mathrm{R}}$ and $\tau_{\mathrm{D}} = 1/\omega_{\mathrm{I}}$. We also calculate the ratio of the damping time to the period, τ_{D}/P, in order to compare theoretical results with observations.

4.2 Magnetoacoustic waves

Figure 4.1 shows the period, the damping time and the ratio of the damping time to the period computed from the numerical solution of Eq. (4.1) for a partilly ionised plasma with $\tilde{\mu} = 0.8$. The values of τ_{D}/P reveal that ion-neutral collisions, which are the main cause for the damping of magnetoacoustic waves in the present scenario, are more important for fast waves than for slow waves; for $\tilde{\mu} = 0.8$ a difference of an order of magnitude can be appreciated.

Perhaps the most interesting feature is that above a certain wavenumber ($\sim 7 \times 10^{-4}$ m^{-1}) the fast wave disappears. In order to understand this effect, let

us consider the dispersion relation Eq. (4.1) for parallel propagation ($k_z = 0$, $k = k_x$),

$$\left(\omega^2 - k_x^2 \Gamma(0)^2\right)\left(\omega^2 - k_x^2 c_s^2\right) = 0, \tag{4.4}$$

so that the fast and slow waves decouple. In this case, the fast wave becomes an Alfvén wave, and its frequency is obtained by imposing that the first factor of the previous equation vanishes. Then, solving this dispersion relation for ω we obtain,

$$\omega = \frac{ik^2 \eta_C}{2} \pm \frac{k}{2}\sqrt{4v_a^2 - k^2 \eta_C^2}.$$

In order to have $\omega_R \neq 0$, $4v_a^2 - k^2 \eta_C^2$ must be greater than zero, which leads to

$$k < \frac{2v_a}{\eta_C} \equiv k_c. \tag{4.5}$$

Hence, in a partially ionised plasma the fast mode only exists as a damped propagating wave for wavenumbers below the critical value, k_c. For wavenumbers greater than this critical value we have a damped disturbance instead of a propagating wave.

Using the parameter values mentioned before we obtain $k_c \sim 7.3 \times 10^{-4}$ m^{-1}, very similar to the value $\sim 7 \times 10^{-4}$ m^{-1} derived from Fig. 4.1. Given that Eq. (4.5) has been derived for parallel propagation, $\theta = 0$, this agreement indicates that non-parallel propagation does not produce a substantial modification of k_c.

On the other hand, Eq. (4.4) points out that, in the case of parallel propagation, the slow waves are not affected by resistive effects.

4.2.1   Exploring the space parameter

In this section we study the dependence of the fast and slow wave solutions on different parameters of the equilibrium configuration. These parameters are the ionisation fraction, the propagation angle, the density and the magnetic field. The reason behind this study is the fact that these quantities are not very well known for prominences.

Ionisation fraction

Figure. 4.2 presents the variation of the period, the damping time and the ratio of the damping time to the period when the ionisation fraction of the plasma is changed. It is clear that the damping of both waves, fast and slow, becomes stronger for plasmas with a larger proportion of neutrals. For nearly fully neutral plasmas ($\tilde{\mu} \to 1$) the values of τ_D/P for the fast wave in the region of observed wavelengths in prominence oscillations are compatible with
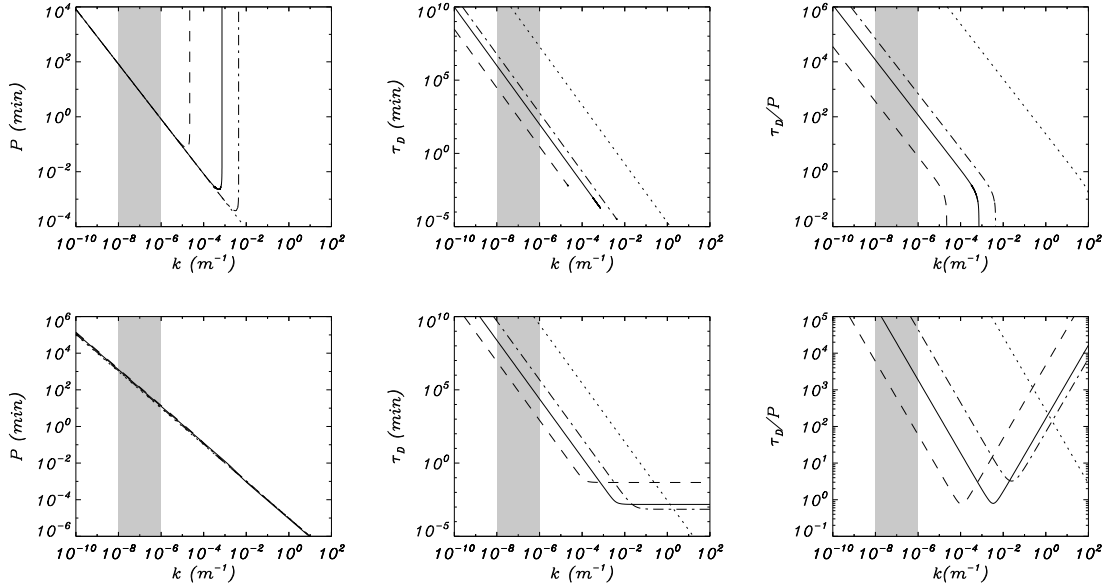
Figure 4.2: Period, damping time and ratio of the damping time to the period for the fast (*top*) and slow (*bottom*) waves for different ionisation fractions: $\tilde{\mu} = 0.5$ (dotted), $\tilde{\mu} = 0.6$ (dash-dotted), $\tilde{\mu} = 0.8$ (solid) and $\tilde{\mu} = 0.99$ (dashed). All other parameter values are the same as those in Fig. 4.1.
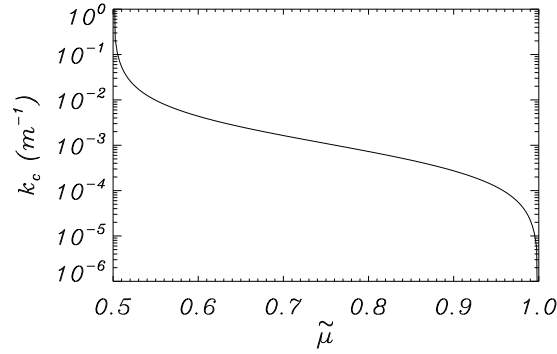

Figure 4.3: Variation of the fast wave critical wavenumber, k_c, versus the ionisation fraction, $\tilde{\mu}$, in the case of parallel propagation. All other parameter values are the same as those in Fig. 4.1.

observations. On the other hand, the slow wave damping ratio is much larger than the observed one even for the largest considered value of $\tilde{\mu}$.

There is also a dependence of the fast wave critical wavenumber on the ionisation fraction. This can be appreciated in Fig. 4.3, where the critical wavenumber for the fast wave, and for parallel propagation (Eq. [4.5]), has been plotted versus the ionisation fraction of the plasma. When the fraction of neutrals is increased, Cowling's magnetic diffusivity increases and the critical wavenumber decreases.
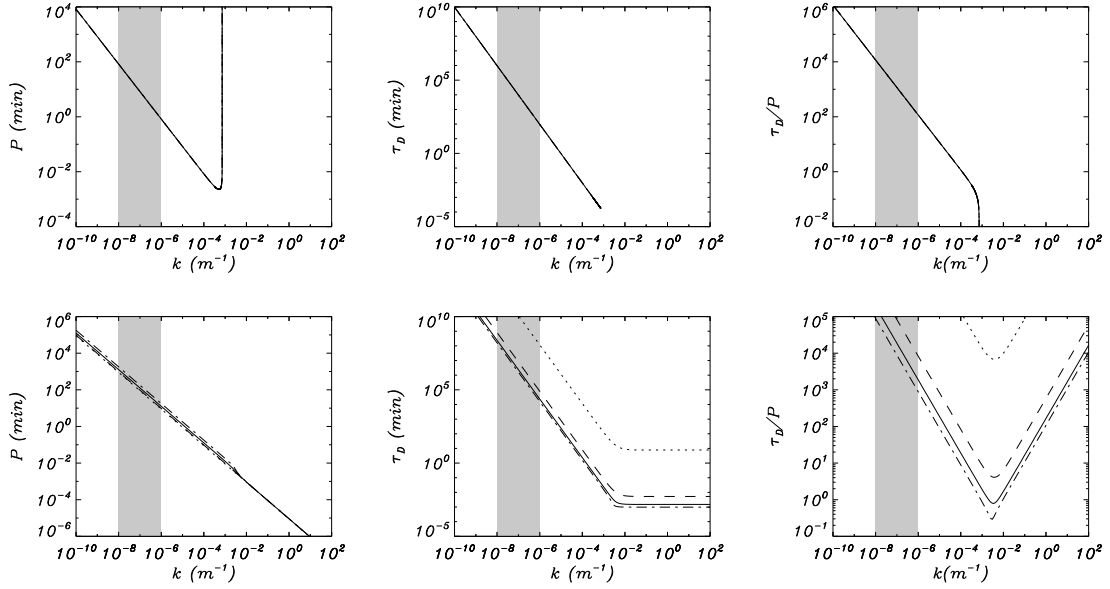
Figure 4.4: Period, damping time and ratio of the damping time to the period for the fast (*top*) and slow (*bottom*) waves for an adiabatic partially ionised plasma with $\tilde{\mu} = 0.8$ for $\theta = 0.01$ (dotted), $\theta = \pi/8$ (dashed), $\theta = \pi/4$ (solid) and $\theta = \pi/3$ (dash-dotted). All other parameter values are the same as those in Fig. 4.1.

Propagation angle

Figure 4.4 shows the dependence on the propagation angle of the period, the damping time and the ratio of the damping time to the period for fast and slow waves. We observe that all these quantities are not affected by the propagation angle for the fast wave, while for the slow wave the main influence of the propagation angle appears in the damping time, the period only being slightly affected. Of course, τ_D/P shows also a strong dependence with θ, and in Fig. 4.4 a variation of five orders of magnitude in τ_D/P, when the propagation angle is varied between $\theta = 0.01$ and $\theta = \pi/3$, can be observed.

Density and magnetic field

Figure 4.5 shows that when the plasma density is modified the behaviour of the fast wave is strongly affected since the values of the Alfvén speed and of both magnetic diffusivities are modified. In particular, when the density is decreased, small values of the damping time and damping ratio, τ_D/P, are obtained. Something similar happens for slow waves since the sound speed is also modified. In this case, there is also a displacement of the minima of τ_D/P to small wavenumbers when the density decreases. All this means that the efficiency of the ion-neutral collisions mechanism increases in low density plasmas.

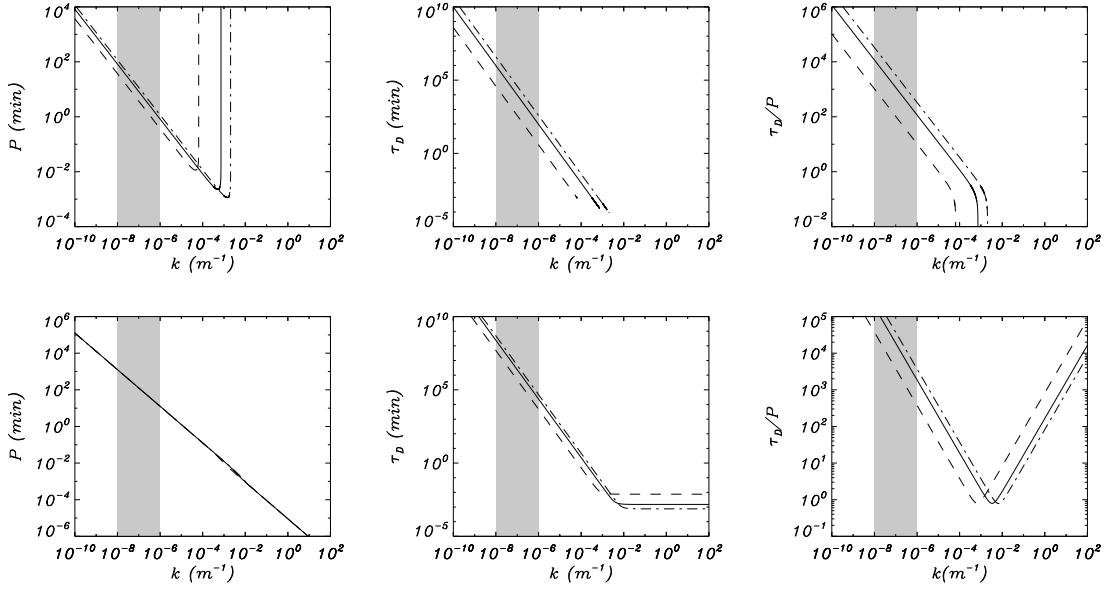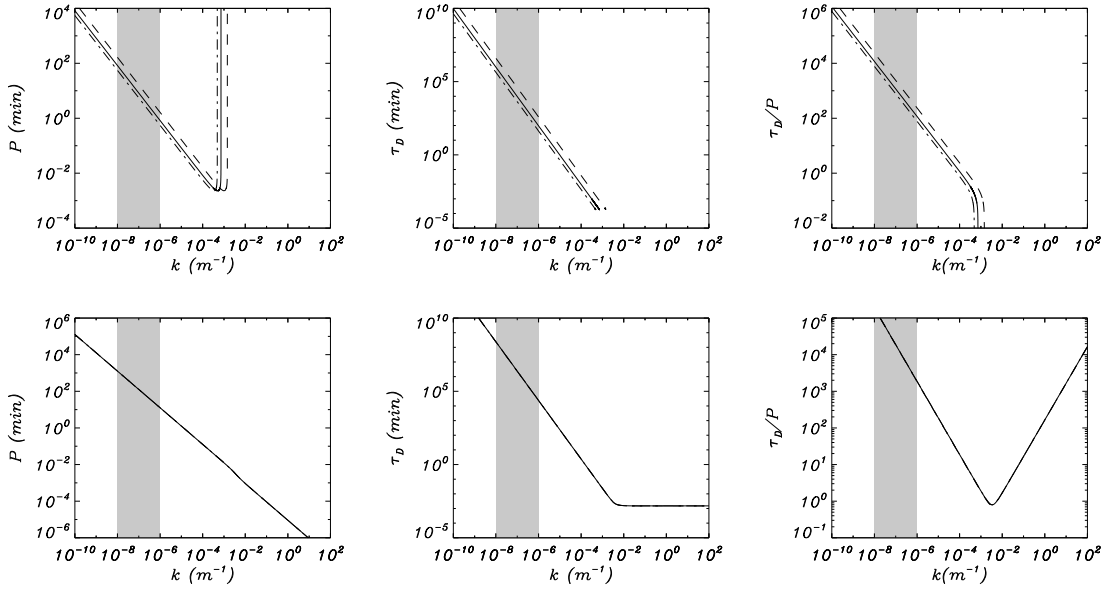Figure 4.6 shows the behavior of magnetoacoustic wave parameters when

Figure 4.5: Period, damping time and ratio of the damping time to the period for the fast (*top*) and slow (*bottom*) waves for an adiabatic partially ionised plasma ($\tilde{\mu} = 0.8$) with $\rho_0 = 10^{-14}$ g/cm^3 (dashed), $\rho_0 = 5 \times 10^{-14}$ g/cm^3 (solid) and $\rho_0 = 10^{-13}$ g/cm^3 (dash-dotted). All other parameter values are the same as those in Fig. 4.1.

Figure 4.6: Period, damping time and ratio of the damping time to the period for the fast (*top*) and slow (*bottom*) waves for an adiabatic partially ionised plasma ($\tilde{\mu} = 0.8$) with $B_0 = 5$ G (dashed), $B_0 = 10$ G (solid) and $B_0 = 15$ G (dash-dotted). All other parameter values are the same as those in Fig. 4.1.

the value of the magnetic field is modified. The slow wave is not sensitive to these variations, while the fast wave presents a slight dependence on B_0 due to

the modification of the Alfvén speed and Cowling's magnetic diffusivity. From this behaviour, we can conclude that, in the case of fast waves, ion-neutral collisions mechanism becomes more efficient in presence of strong magnetic fields.

4.2.2 Perturbations

Since we are in the linear regime, to determine the perturbed variables once the frequency has been computed one can impose an arbitrary value to one of them. Then, all other perturbations can be computed from

$$v_x = \frac{c_s^2 k_x k_z}{\omega^2 - c_s^2 k_x^2} v_z, \tag{4.6}$$

$$p = -\frac{\rho_0 \omega}{k_x} v_x, \tag{4.7}$$

$$B_z = \frac{k_x \left[B_0^2 \left(i v_z + k_x \Xi p \right) + 4\pi (\eta - \eta_C)(k_z p + \rho_0 \omega v_z) \right]}{B_0 \left(k^2 \eta + i\omega \right)}, \tag{4.8}$$

$$B_x = \frac{B_0 k_x B_z - 4\pi (k_z p + \rho_0 \omega v_z)}{B_0 k_z}. \tag{4.9}$$

In Fig. 4.7 we plot the moduli of the perturbed variables computed from Eqs. (4.6)–(4.9) (solid lines) together with the solutions for the ideal, fully-ionised plasma (squares), computed from the ideal expressions for the perturbations. Regarding the fast wave, we find that perturbations coincide for the two cases. Although this may seem a surprising behavior for values of $\tilde{\mu}$ close to 1, for which the interactions with neutrals result in the largest modification to the fast wave properties, an explanation can be found from Eq. (4.8). All the non-ideal terms and the influence of the neutral component of the plasma are concentrated in this formula, and are absent in the expressions of the other perturbed variables. In addition, the largest contribution in this expression comes from the term with $k_z \Xi p$ and, since the pressure perturbation is quite small for fast waves, Eq. (4.8) results in a B_z that is similar for the two cases represented in Fig. 4.7. Then, since B_z does not change much, all other perturbed quantities are similar in the fully ionised ideal case and in the partially ionised, non-ideal case.

As for the slow wave, the two sets of perturbations are rather different and, again, the pressure perturbation is crucial to understand this behavior. To plot the slow mode perturbations we have fixed v_x, so by virtue of Eq. (4.7) the pressure is fixed to its ideal value (such as found in Fig. 4.7). Now, the slow wave is characterised by a large pressure perturbation compared to that of the fast wave, so p has an amplification effect on the value of B_z, and therefore of B_x, compared to the corresponding ideal value. This effect is more noticeable for propagation with a large angle with respect to $\mathbf{B}_0$ because of the presence of k_z in the term $k_z \Xi p$ in Eq. (4.8).
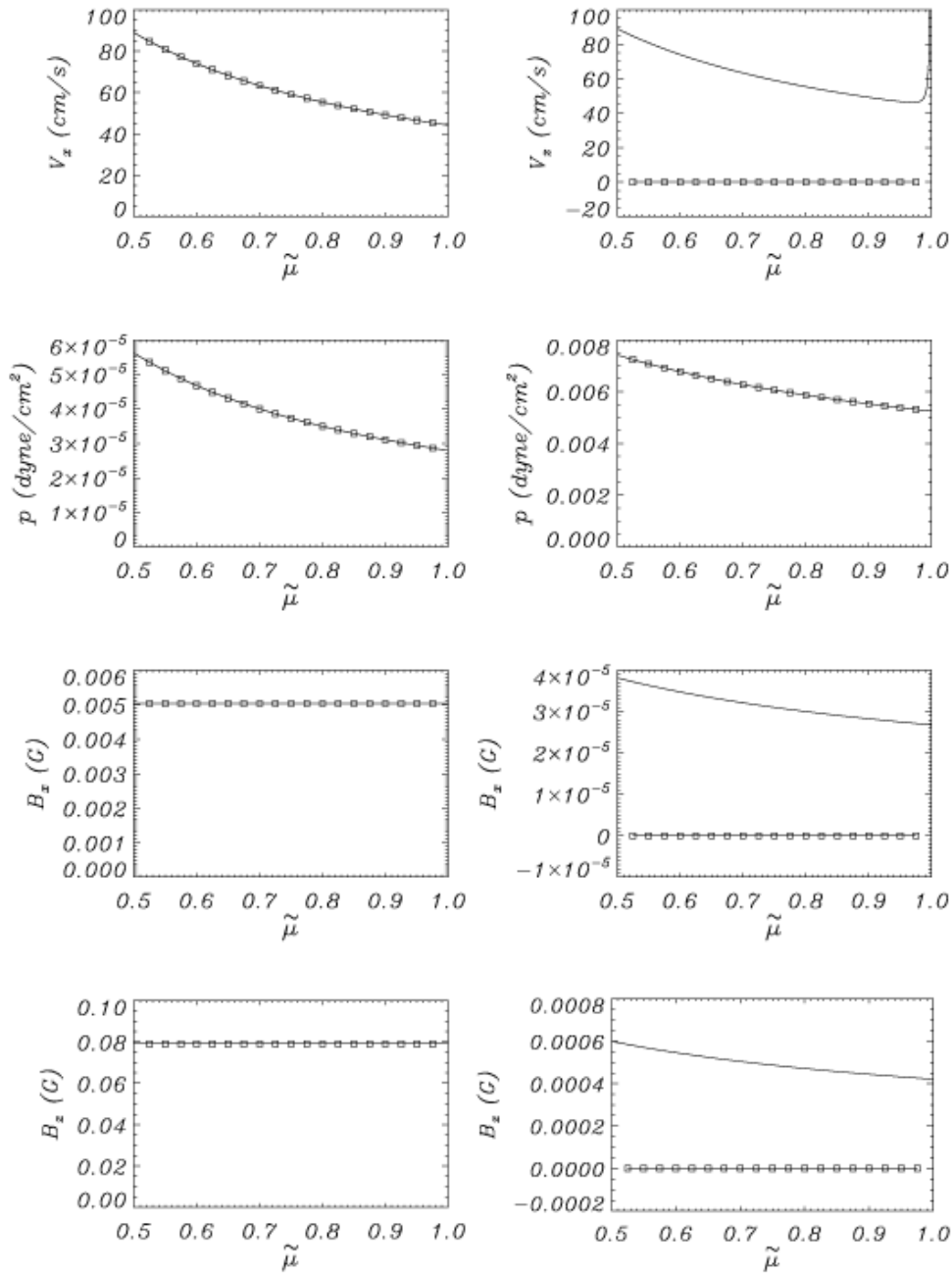
Figure 4.7: Perturbation amplitude of the velocity, the pressure and the x- and z-components of the magnetic field for the fast wave (*left*) and the slow wave (*right*). The solid line corresponds to a partially ionised plasma, while squares correspond to a fully ionised ideal plasma. The perturbed B_x and B_z for the slow wave in the fully ionised ideal plasma are several orders of magnitude smaller than the values computed for partially ionised plasma; for this reason they seem to be zero in the two plots on the right. All other parameter values are the same as those in Fig. 4.1. In addition, for fast and slow waves the arbitrary amplitudes, $v_z = 1$ km/s, $v_x = 1$ km/s have been respectively considered.

Another conclusion one can extract from Fig. 4.7 is that the inclusion of partial ionisation and non-ideal effects does not influence the predominant polarisation of the magnetoacoustic wave motions since $v_x \gg v_z$ for slow waves and $v_z \gg v_x$ for fast waves.

4.2.3 Approximate solution

We can obtain approximate expressions for the real and imaginary parts of the frequency obtained from Eq. (4.1). For this we need to write $\omega = \omega_R + i\omega_I$ and split the dispersion relation into its real and imaginary parts,

$$
\begin{aligned}
&\omega_I^4 - 6\omega_I^2\omega_R^2 + \omega_R^4 + k^2\left[-\eta_C\omega_I\left(\omega_I^2 - 3\omega_R^2\right) + v_a^2\left(\omega_I^2 - \omega_R^2\right)\right] \\
&+c_s^2k^2\left[\omega_I^2 + k_x^2\left(v_a^2 - \eta_C\omega_I\right) + k_z^2\left(-\eta_C + v_a^2\Xi\rho_0\right)\omega_I - \omega_R^2\right] = 0,
\end{aligned}
\tag{4.10}
$$

$$
\begin{aligned}
&k^2c_s^2\left(2\omega_I - k^2\eta_C + k_z^2v_a^2\Xi\rho_0\right) + 4\omega_I\left(\omega_I^2 - \omega_R^2\right) \\
&+k^2\left[2v_a^2\omega_I + \eta_C\left(\omega_R^2 - 3\omega_I^2\right)\right] = 0.
\end{aligned}
\tag{4.11}
$$

If we consider the case of weak damping, which means that the imaginary part of the frequency is much smaller than the real part ($\omega_I \ll \omega_R$), then the real part of the dispersion relation, Eq. (4.10), leads to the dispersion relation for magnetoacoustic waves in an ideal plasma, Eq. (2.30). This means that for $c_s \ll v_a$ the real part of the frequency can be calculated from Eqs. (2.32) and (2.33),

$$
\omega_R^{\text{slow}} \approx k_x c_s, \qquad \omega_R^{\text{fast}} \approx k v_a.
\tag{4.12}
$$

On the other hand, the imaginary part of the dispersion relation, Eq. (4.11), leads to the following expression

$$
k^2c_s^2\left(2\omega_I - k^2\eta_C + k_z^2v_a^2\Xi\rho_0\right) - 4\omega_I\omega_R^2 + k^2\left(2v_a^2\omega_I + \eta_C\omega_R^2\right) = 0,
\tag{4.13}
$$

that allows to derive the following expression for the imaginary part of the frequency,

$$
\omega_I \approx \frac{k^2k_z^2c_s^2v_a^2\Xi\rho_0 + \eta_Ck^2\left(\omega_R^2 - k^2c_s^2\right)}{4\omega_R^2 - 2k^2\left(c_s^2 + v_a^2\right)}.
\tag{4.14}
$$

And after substituting the value of ω_R from Eqs. (4.12) we obtain expressions for the imaginary part of ω for the slow waves

$$
\omega_I^{\text{slow}} \approx \frac{1}{2}\left(\frac{c^2}{4\pi\sigma}\frac{c_s^2}{v_a^2}k_z^2 + \frac{\rho_0c_s^2}{\alpha_n}\frac{\xi_n^2}{1+\xi_i}k_z^2\right),
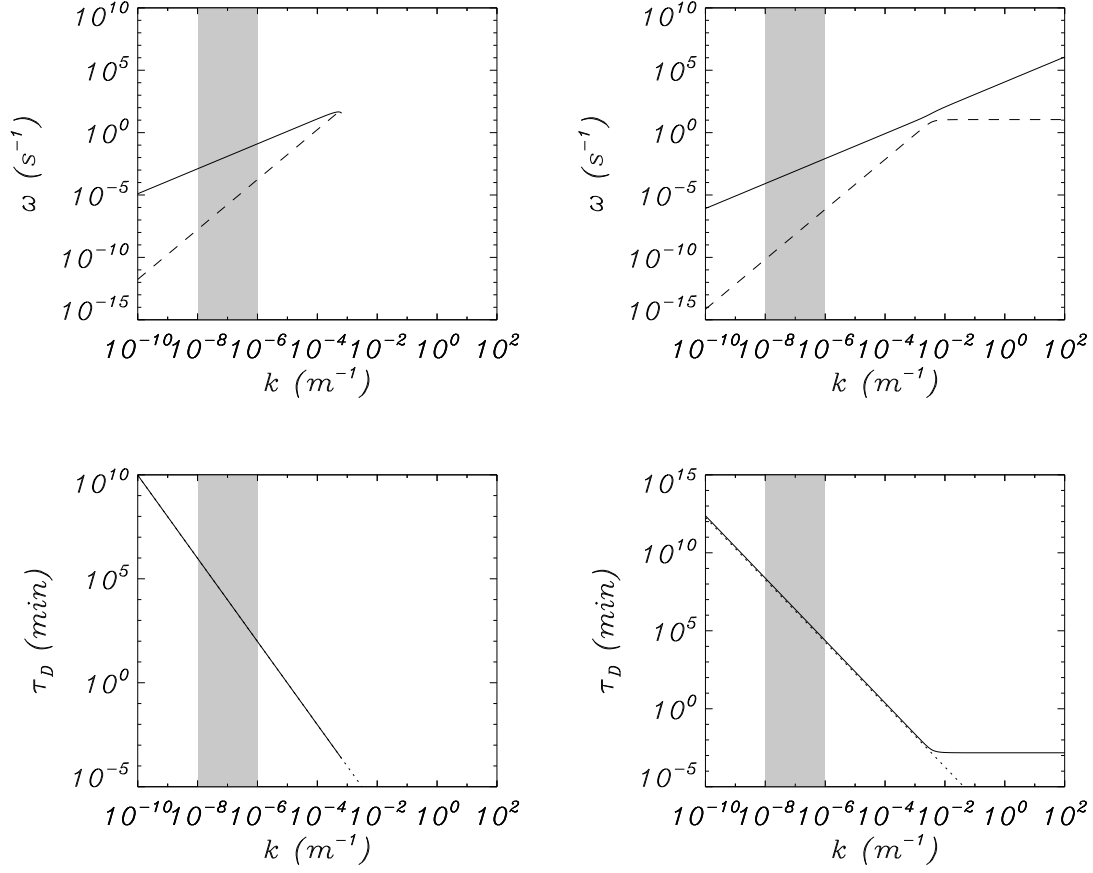\tag{4.15}
$$

and fast waves

Figure 4.8: Top panels: Real (solid) and imaginary (dashed) part of the frequency obtained from Eq. (4.1) for fast (*left*) and slow (*right*) waves. Bottom panels: The dashed lines correspond to the damping times for fast (*left*) and slow (*right*) waves obtained from Eq. (4.1). The solid lines correspond to the approximate solutions.

$$\omega_I^{\text{fast}} \approx \frac{1}{2}\left[\frac{c^2 k^2}{4\pi\sigma} + \frac{\xi_n^2 B_0^2}{4\pi\alpha_n}\left(k^2 + \frac{c_s^2}{v_a^2}k_z^2\frac{\xi_i}{1+\xi_i}\right)\right] \approx \frac{1}{2}\left(\frac{c^2 k^2}{4\pi\sigma} + \frac{\xi_n^2 B_0^2}{4\pi\alpha_n}k^2\right) = \frac{1}{2}k^2\eta_C. \quad (4.16)$$

In Fig. 4.8 we have represented the numerical solution of the dispersion relation (Eq. [4.1]) together with the approximate expressions derived in this section. We can conclude that there is a perfect agreement between the numerical and the approximate solutions for small wavenumbers, including the interval of observed wavelengths. The approximate expressions are not valid in the range of large wavenumbers because the weak damping approximation is valid no more (Fig. 4.8). The wavenumber where this happens is similar to k_c, the wavenumber where the fast wave becomes a damped oscillation instead of a propagating wave.

4.2.4   Comparison with Braginskii (1965)

Braginskii (1965) gives approximate expressions for the logarithmic damping decrement, $\delta \equiv \omega_{\mathrm{I}}/\omega_{\mathrm{R}}$, of the magnetoacoustic and Alfvén modes in an unbounded medium and in the low-β plasma limit. The path followed by this author in the derivation of δ is different from the way that led us to Eq. (4.1) or Eqs. (4.15) and (4.16), so a comparison between both results is necessary. Since we have neglected the viscous and conductive contributions, they are removed from Braginskii's expressions before performing the comparison.

For the fast mode, using Braginskii's Eqs. (8.38), (8.41) and (8.47b) we get

$$2\omega_{\mathrm{I}}^{\mathrm{fast}} = \frac{c^2}{4\pi\sigma}k^2 + \frac{c^2 k^2}{4\pi}\frac{\xi_{\mathrm{n}}^2 B_0^2}{\alpha_{\mathrm{n}} c^2}, \tag{4.17}$$

whereas for the slow waves Eqs. (8.38), (8.44) and (8.49) yield

$$2\omega_{\mathrm{I}}^{\mathrm{slow}} = \frac{c^2}{4\pi\sigma}k_{\perp}^2 \frac{c_{\mathrm{s}}^2}{v_{\mathrm{a}}^2} + \frac{\rho_0 c_{\mathrm{s}}^2 \xi_{\mathrm{n}}^2}{\alpha_{\mathrm{n}}}\left[k_{\parallel}^2 \frac{n_{\mathrm{i}}^2}{n^2} + k_{\perp}^2 \frac{(n_{\mathrm{i}} + n_{\mathrm{n}})^2}{n^2}\right]. \tag{4.18}$$

We rewrite these expressions in our own variables by making the substitutions $k_{\parallel} = k_x$ and $k_{\perp} = k_z$ and by also taking into account the definitions of the relative densities of ions and neutrals, Eq. (3.4). Then, the former formulae can be written as

$$\omega_{\mathrm{I}}^{\mathrm{fast}} = \frac{1}{2}\left[\frac{c^2}{4\pi\sigma}k^2 + \frac{\xi_{\mathrm{n}}^2 B_0^2}{4\pi\alpha_{\mathrm{n}}}k^2\right] = \frac{1}{2}k^2\eta_{\mathrm{C}}, \tag{4.19}$$

$$\omega_{\mathrm{I}}^{\mathrm{slow}} = \frac{1}{2}\left[\frac{c^2}{4\pi\sigma}\frac{c_{\mathrm{s}}^2}{v_{\mathrm{a}}^2}k_z^2 + \frac{\rho_0 c_{\mathrm{s}}^2}{\alpha_{\mathrm{n}}}\frac{\xi_{\mathrm{n}}^2}{(1+\xi_{\mathrm{i}})^2}\left(\xi_{\mathrm{i}}^2 k_x^2 + k_z^2\right)\right]. \tag{4.20}$$

Now, Braginskii's formulae can be easily compared with our analytical approximations for the imaginary part of the frequency (Eqs. [4.15] and [4.16]). It can be appreciated that in the case of the fast wave Eqs. (4.16) and (4.19) are identical, although, quite surprisingly, in the case of slow waves, Eqs. (4.15) and (4.20) disagree. The difference between these two expressions appears in the second term on the right-hand side, i.e. the one coming from the collisions of electrons and ions with neutrals, that correspond to the dominant term. To assess the importance of this discrepancy we plot the damping time obtained from the numerical solution of Eq. (4.1) together with the results obtained from Braginskii's expressions and our set of approximate equations (see Fig. 4.9). In the case of the fast wave there is a perfect agreement between the three results, as expected. Nevertheless, for the slow wave there is a divergence of τ_{D} as we move towards parallel propagation ($\theta = 0$). Braginskii's solution is such that for purely parallel propagation the slow wave has a finite damping time, whereas our developments, both numerical and approximate, lead to no damping of the slow wave for $\theta = 0$; the cause for this difference is the term proportional to k_x^2 in Eq. (4.20).
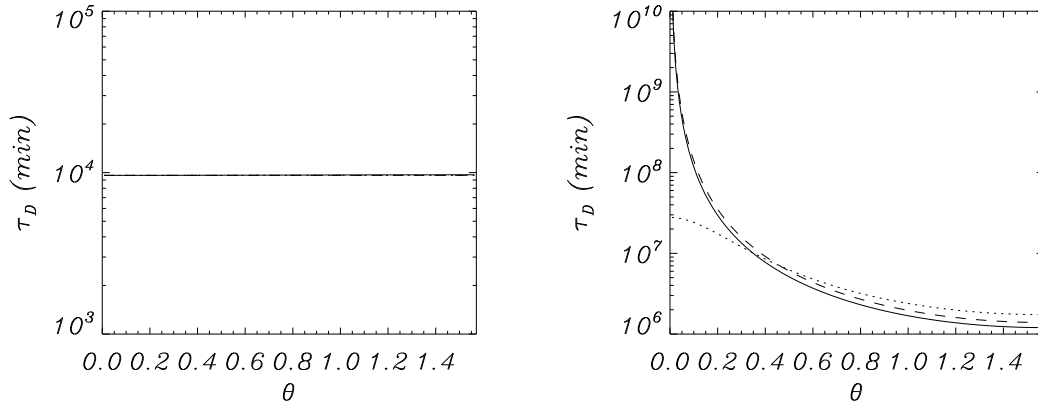
Figure 4.9: Damping time for the fast (*left*) and slow (*right*) waves for an adiabatic partially ionised plasma with $\tilde{\mu} = 0.8$ and $k = 10^{-7}$ m^{-1}. The three different lines correspond to the numerical solutions of Eq. (4.1) (solid line), Braginskii's approximation Eqs. (4.19) and (4.20) (dotted) and results from the aproximate Eqs. (4.15) and (4.16) (dashed).

The damping of fast and slow magneto acoustic waves was derived by Braginskii (1965), Khodachenko et al. (2004) and Khodachenko & Rucker (2005) using the energy equation. Such as we have seen above, the damping rates for fast waves obtained from the energy equation or from a normal mode analysis are the same while for slow waves they do not agree. Recently, Zaqarashvili et al. (2011) have studied MHD waves in a partially ionised plasma using a two-fluid approach, and they have found that for parallel propagation the damping rates for slow waves obtained from Braginskii (1965) and the two-fluid approach are fully coincident. They conclude that the discrepancy is caused by the neglect of the inertial terms in the equation of motion for the relative velocity when the single-fluid MHD equations are derived.

4.3 Alfvén waves

Now we study the behaviour of the Alfvén wave in a partially ionised plasma. This behaviour is described by Eq. (4.2). Since $\Gamma(\theta)$ is a complex quantity, the real and imaginary parts of the Alfvén frequency are given by:

$$\omega_{\mathrm{R}} = \pm k_x \Gamma_{\mathrm{R}},$$

and

$$\omega_{\mathrm{I}} = \pm k_x \Gamma_{\mathrm{I}},$$

with

$$\Gamma_{\mathrm{R}} = \frac{1}{\sqrt{2}} \left(\sqrt{v_a^2 - \omega_I \left(\eta_C + \eta \tan^2 \theta \right)} + \sqrt{\omega_R^2 \left(\eta_C + \eta \tan^2 \theta \right)^2 + \left(-v_a^2 + \omega_I \left(\eta_C + \eta \tan^2 \theta \right) \right)^2} \right)$$
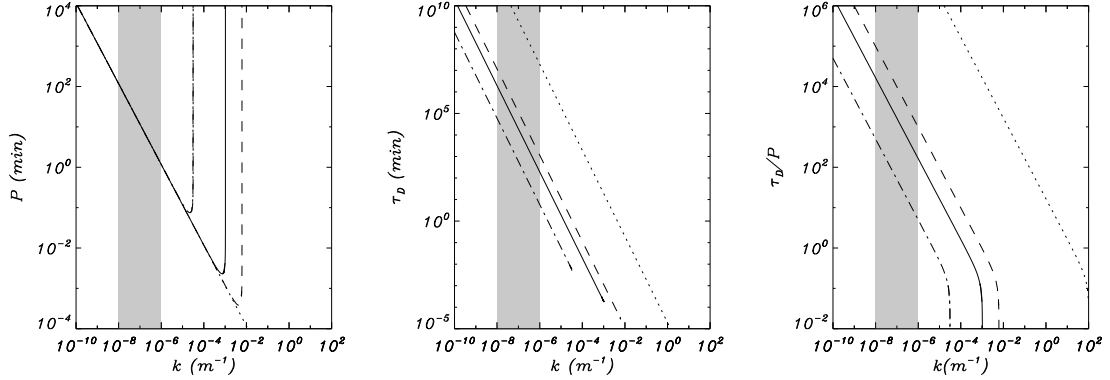
Figure 4.10: Period, damping time and ratio of the damping time to the period for the Alfvén wave in an adiabatic fully ionised resistive plasma (dotted), and in adiabatic partially ionised plasmas with $\tilde{\mu} = 0.6$ (dashed), $\tilde{\mu} = 0.8$ (solid) and $\tilde{\mu} = 0.99$ (dash-dotted). All other parameter values are the same as those in Fig. 4.1.
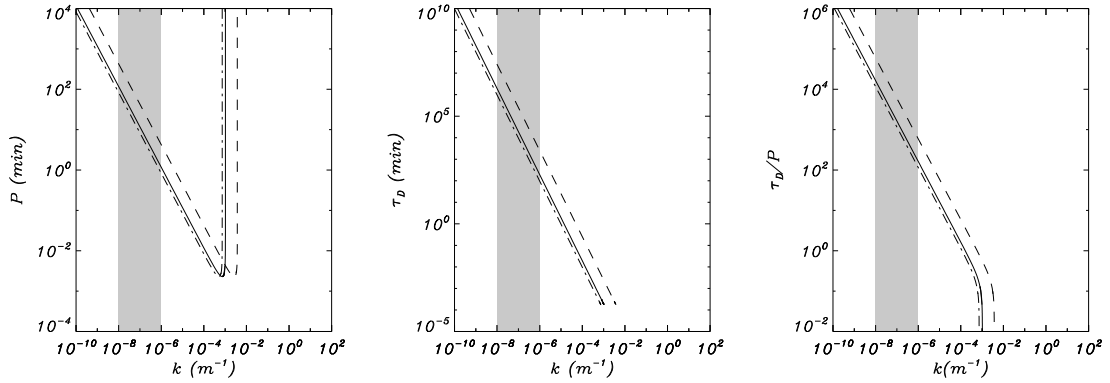

Figure 4.11: Period, damping time and ratio of the damping time to the period for the Alfvén wave in an adiabatic partially ionised plasma with $\theta = 0$ (dash-dotted), $\theta = \pi/4$ (solid) and $\theta = 7\pi/16$ (dashed). All other parameter values are the same as those in Fig. 4.1.

and

$$\Gamma_{\mathrm{I}} = \frac{\omega_R \left(\eta_C + \eta \tan^2 \theta \right)}{\sqrt{2} \left(\sqrt{v_a^2 - \omega_I \left(\eta_C + \eta \tan^2 \theta \right) + \sqrt{\omega_R^2 \left(\eta_C + \eta \tan^2 \theta \right)^2 + \left(-v_a^2 + \omega_I \left(\eta_C + \eta \tan^2 \theta \right) \right)^2}} \right)}.$$

Fig. 4.10 shows the results obtained for the period, the damping time and the ratio of the damping time to the period. In this figure the solution for a fully ionised plasma ($\tilde{\mu} = 0.5$) with Spitzer's magnetic diffusivity (Ferraro & Plumpton 1961; Kendall & Plumpton 1964) is also shown.

The Alfvén wave behavior is similar to that of the fast wave. Fast and Alfvén waves have similar period and damping time and, as for the fast wave, the ratio of the damping time to the period decreases when going to almost neutral plasmas. Also, from Fig. 4.11 one can conclude that the period, damp-
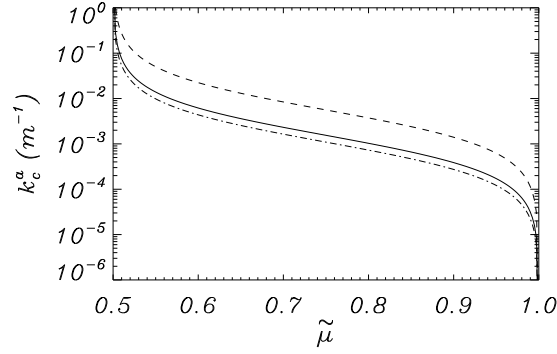
Figure 4.12: Critical wavenumber versus the ionisation fraction for the Alfvén wave for different propagation angles: $\theta = 0$ (dash-dotted), $\theta = \pi/4$ (solid) and $\theta = 7\pi/16$ (dashed). All other parameter values are the same as those in Fig. 4.1.

ing time and damping per period of the Alfvén wave depend slightly on the angle of propagation.

On the other hand, from Eq. (4.2) we can obtain the critical wavenumber, k_c^a, for the Alfvén waves,

$$k_c^a = \frac{2v_a}{\cos\theta\,(\eta_C + \eta\tan^2\theta)}. \tag{4.21}$$

This quantity depends on the ionisation fraction (as the fast wave critical wavenumber does) and on the propagation angle (Fig. 4.12). Usually, k_c^a is bigger than k_c and both critical wavenumbers become equal for parallel propagation. On the other hand, when we consider $\eta_C = \eta$ we can recover from Eq. (4.21) the critical wavenumber, k_c^{FP}, of fully ionised and resistive plasmas (Ferraro & Plumpton 1961; Kendall & Plumpton 1964),

$$k_c^{FP} = \frac{2v_a}{\eta}\cos\theta. \tag{4.22}$$

The ratio between the critical wavenumber for a partially ionised plasma, Eq. (4.21), and that of a fully ionised resistive plasma, Eq. (4.22) is given by

$$\frac{k_c^{FP}}{k_c^a} = \sin^2\theta + \frac{\eta_C}{\eta}\cos^2\theta, \tag{4.23}$$

whose interval of variation is from 1 for a fully ionised resistive plasma ($\eta_C = \eta$) to infinity for a neutral plasma.

Figure 4.13 shows the modified Alfvén speed, Eq. (3.84), computed for different values of the ionisation fraction. One observes that Γ_R is equal to the ideal Alfvén speed, v_a, for wavenumbers smaller than the critical wavenumber, k_c^a, while for wavenumbers larger than k_c^a the modified Alfvén speed falls almost vertically to 0, so there is no propagating wave since $\omega_R = 0$.
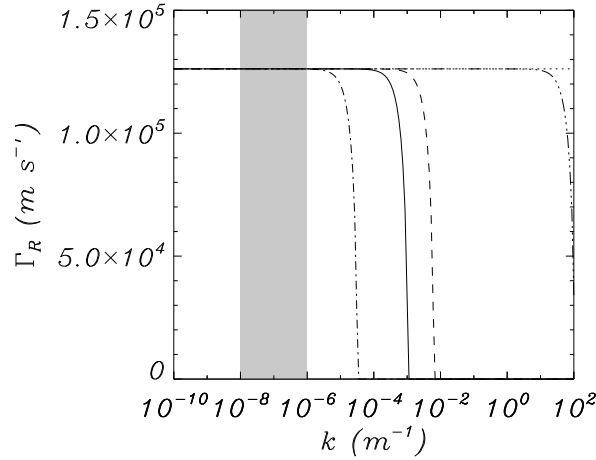
Figure 4.13: Real part of the modified Alfvén speed, Γ_R, in a partially ionised plasma with $\tilde{\mu} = 0.5$ (dash-3-dotted), $\tilde{\mu} = 0.6$ (dashed), $\tilde{\mu} = 0.8$ (solid) and $\tilde{\mu} = 0.99$ (dash-dotted) compared with the ideal Alfvén speed, v_a, (dotted). All other parameter values are the same as those in Fig. 4.1.

4.4 Summary

In this chapter we have studied the time damping of MHD waves in an adiabatic partially ionised plasma, considering an equilibrium model with uniform magnetic field and assuming linear perturbations. The results show that ion-neutral collisions are able to damp the three MHD waves (fast, slow and Alfvén) in different ways.

In prominence conditions the damping by ion-neutral interactions is much stronger for the fast wave than for the slow wave. This is contrary to the effect of other damping mechanisms, such as radiative cooling and conduction, for which the slow wave is strongly attenuated while the fast wave remains almost undamped (Carbonell et al. 2004; Terradas et al. 2002, 2005). A consequence of the present and previous studies is that the observed damped oscillations in prominences could be explained by slow waves attenuated by radiative cooling and thermal conduction or by fast waves attenuated by ion-neutral collisions. The behaviour of Alfvén waves is similar to that of fast waves. For almost neutral plasmas, fast and Alfvén waves are efficiently damped, with values of τ_D/P compatible with observations. The importance of collisions between ions and neutrals grows with the proportion of neutrals in the plasma. This means that this effect is more relevant for small ionisation fractions and that it can be neglected for nearly fully ionised plasmas.

From the magnetoacoustic wave dispersion relation we have obtained an analytical approximation for the real and imaginary parts of the frequency that matches the numerical results for small wavenumbers. This analytical approximation has been compared with the formulae provided by Braginskii

(1965) and a discrepancy between them has been found. The most important difference between the two sets of formulae is the term proportional to k_x^2 in Braginskii's formula for the slow wave damping time, which (according to Braginskii) results in the damping of this wave for propagation nearly parallel to the unperturbed magnetic field. This discrepancy has been recently solved by Zaqarashvili et al. (2011) who have studied MHD waves in a partially ionised plasmas using a two-fluid approach. They have found that for parallel propagation the damping rates for slow waves obtained from Braginskii (1965) and the two-fluid approach are fully coincident, concluding that the discrepancy, when a single-fluid approach is considered, is caused by the neglect of the inertial terms in the equation of motion for the relative velocity when the single-fluid MHD equations are derived.

The existence of a critical wavenumber in fully ionised resistive plasmas was already pointed out by Ferraro & Plumpton (1961), Chandrasekhar (1961), Kendall and Plumpton (1964), while for partially ionised plasmas it was already reported by Balsara (1996), in the context of waves in molecular clouds. In our case, both fast and Alfvén waves present a critical wavenumber. For wavenumbers below the critical one, fast and Alfvén waves exist as damped propagating waves, while for wavenumbers greater than the critical one, we have damped disturbances instead of propagating waves. The critical wavenumber depends on the ionisation fraction and, in the case of Alvén waves, it also depends on the propagation angle. Later on, the presence of critical wavenumbers in partially ionised plasmas has been reported by Singh & Krishan (2010) and (Soler et al. 2009a,b,d) in the case of MHD waves in solar coronal structures. However, Zaqarashvili et al. (2012) have made a thorough analysis of the process of derivation of single-fluid MHD equations. Going from two-fluid to single fluid equations, they have shown that the presence of a cut-off wavenumber in Alfvén waves is due to the neglect of several terms during the derivation process. In particular, the cut-off wavenumber appears when, after neglecting the inertial term, the Hall current term and electron-neutral collisions are also neglected in the induction equation. This points out that the presence of a cut-off wavenumber in Alfvén (and fast) waves in partially ionised plasmas considered under the single-fluid approximation is not connected to any physical process. The cut-off wavenumber is an artifact coming from the approximations made during the derivation of the most commonly used single-fluid MHD equations.

Chapter 5

MHD waves in a non-adiabatic partially ionised prominence plasma[*]

From the theoretical point of view, and as we have stated in previous chapters, small-amplitude prominence oscillations can be interpreted in terms of linear MHD waves. Their attenuation has been studied considering non-adiabatic effects such as radiative losses based on the Newtonian cooling with a constant relaxation time (Terradas et al. 2001), or considering a more complete treatment with the incorporation of optically thin radiation, heating and thermal conduction (Carbonell et al. 2004; Terradas et al. 2005). The main conclusion that arises from these works is that only slow waves are damped by thermal effects in an efficient way, radiation being the dominant attenuation mechanism in the observed range of wavelengths. In contrast, in Chapters 3 and 4 we have proposed ion-neutral collisions as a damping mechanism of prominence oscillations, and it seems to be efficient in attenuating the fast and Alfvén waves in adiabatic plasmas with a small fraction of ions.

In this chapter, our aim is to study the joint effect of ion-neutral collisions and thermal mechanisms on the damping of MHD waves in a partially ionised prominence plasma.

5.1   Dispersion relation

From Eqs. (3.83) and (3.86), and setting the flow velocity to zero, the dispersion relation of non-adiabatic magnetoacoustic waves in a partially ionised plasma is given by,

---

$$\left(\omega^2 - k^2\Lambda^2\right)\left(ik^2\eta_C\omega - \omega^2\right) + k^2v_a^2\left(\omega^2 - k_x^2\Lambda^2\right) + ik^2k_z^2v_a^2\Lambda^2\Xi\rho_0\omega = 0. \qquad (5.1)$$

From Eq. (5.1), and imposing the appropriate conditions, we can obtain already known dispersion relations. For instance, imposing $\Xi = \eta_C = \eta = 0$, we obtain the dispersion relation of non-adiabatic magnetohydrodynamic waves in a fully ionised ideal plasma (Eq. [2.44]); imposing only $A = H = 0$ we obtain the dispersion relation of adiabatic MHD waves in a partially ionised plasma (Eq. [4.1]); and, finally, imposing $\Xi = \eta_C = \eta = A = H = 0$ we obtain the dispersion relation of adiabatic MHD waves in a fully ionised ideal plasma.

On the other hand, since Alfvén waves are not affected by non-adiabatic processes and are decoupled from magnetoacoustic waves, their dispersion relation is given by Eq. (4.2), and their properties are those described in the previous chapter.

5.2   Results

We have numerically solved the dispersion relation (Eq. [5.1]) and Fig. 5.1 shows the results obtained for P, τ_D and τ_D/P corresponding to fast and slow waves. The thermal mode does not correspond to a propagating wave ($\omega_R = 0$) and its behaviour is quite similar to that of the non-adiabatic fully ionised case. For this reason, it is not considered here.

Once again, the fast mode only exists as a damped propagating wave for wavenumbers below a critical wavenumber ($\sim 7 \times 10^{-4}$ m^{-1}). This value is very similar to the value $k_c \sim 7.3 \times 10^{-4}$ m^{-1} that can be obtained from Eq. (4.5). We must remember that Eq. (4.5) has been obtained for an adiabatic partially ionised plasma with parallel propagation. So, after comparing these two values one can conclude that the critical wavenumber, k_c, is not affected significantly by non-adiabatic terms and non-parallel propagation.

5.2.1   Effect of the ionisation degree

Now, we study the effect of the ionisation fraction on the magnetoacoustic waves period and damping time. Figure 5.1 shows the results for fast and slow waves for four different values of the ionisation fraction going from fully ionised plasma ($\tilde{\mu} = 0.5$) to almost neutral plasma ($\tilde{\mu} = 0.99$). In the case of fast waves we observe that, for a fixed wavenumber, the damping time decreases when the ionisation degree is decreased, in agreement with the results obtained in Chapter 4 (Forteza et al. 2007). As expected from Eq. (4.5), the curve representing the period of the fast wave stops at different critical wavenumbers, k_c, when the ionisation fraction is modified.

In the case of slow waves the behaviour is more complex. First, the minimum of τ_D/P at long wavelengths suffers a displacement towards longer wavelengths when $\tilde{\mu}$ is increased, and when $\tilde{\mu} > 0.8$ it is located within the interval
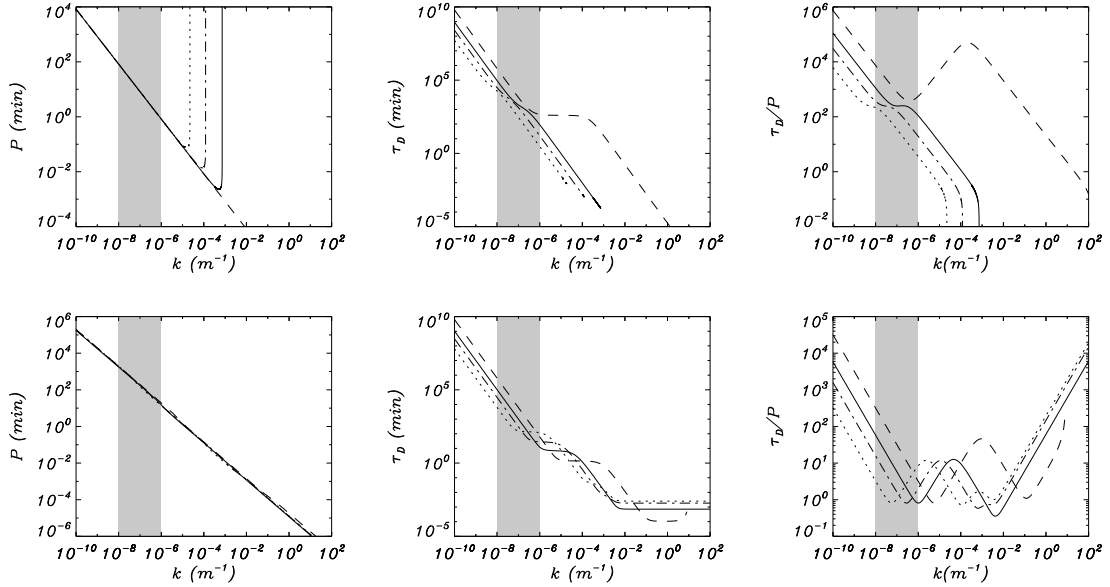
Figure 5.1: Period, damping time and ratio of the damping time to the period for the fast (*top*) and slow (*bottom*) waves for different ionisation fractions: $\tilde{\mu} = 0.5$ (dashed), $\tilde{\mu} = 0.8$ (solid), $\tilde{\mu} = 0.95$ (dash-dotted) and $\tilde{\mu} = 0.99$ (dotted). In all figures, the shaded region corresponds to the interval of observed wavelengths in prominence oscillations. The parameter values are: $T_0 = 8\,000$ K, $\rho_0 = 5 \times 10^{-11}$ kg cm^{-3}, $B_0 = 10$ G and $\theta = \pi/4$.

of observed wavelengths in prominence oscillations. This means that a higher attenuation efficiency is obtained for smaller ionisation degrees. In addition, the minimum of τ_D/P at short wavelengths displays two different features. On one hand, as happens with the other minimum, there is a displacement towards longer wavelengths, although it is less pronounced. On the other hand, for $\tilde{\mu} > 0.8$ this minimum splits in two different minima that become more separated as $\tilde{\mu}$ is increased. The presence of a new minimum in τ_D/P yields the possibility of achieving very large damping rates for three wavelength ranges centered about the three minima.

Finally, in order to assess the effect of ion-neutral collisions on the real part, Λ_R, of the non-adiabatic sound speed Λ (see Eq. [3.87]), we compare its behaviour with and without ion-neutral collisions (Fig. 5.2). This comparison has been performed for two different ionisation degrees and Λ_R shows a similar behavior, with and without ion-neutral collisions, but suffers a displacement towards smaller wavenumbers when ion-neutral collisions are considered. Furthermore, the maximum value of Λ_R decreases when the ionisation degree increases.

5.2.2 Effect of damping mechanisms

In this section we assess the influence of the different damping mechanisms on the ratio of the damping time to the period (τ_D/P). First of all, we focus on
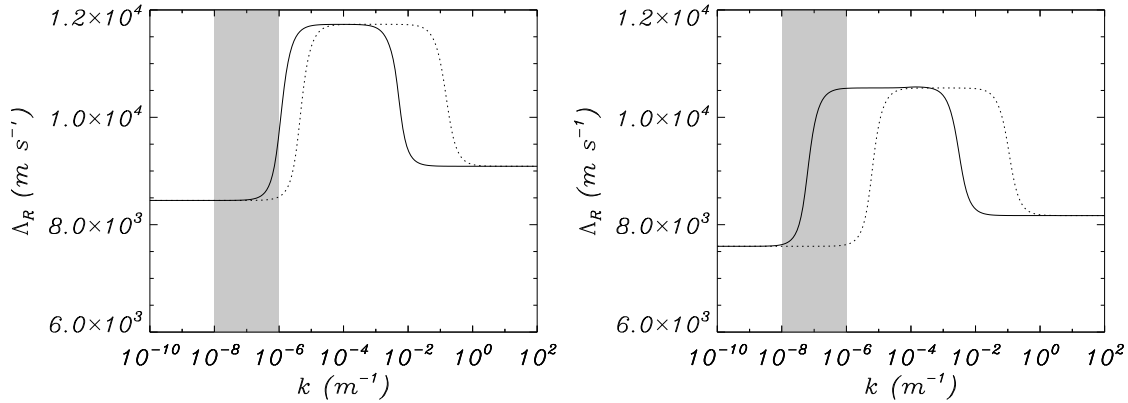
Figure 5.2: Comparison of the real part of modified sound speed as a function of wavenumber k in a non-adiabatic partially ionised plasma (solid) with $\tilde{\mu} = 0.8$ (*left*) and $\tilde{\mu} = 0.99$ (*right*) and in a non-adiabatic fully ionised plasma (dotted). All other parameter values are the same as those in Fig. 5.1.

the fast wave, and according to the top left panel of Fig. 5.3 (corresponding to $\tilde{\mu} = 0.8$) the wavenumber interval considered can be divided in two regions with different dominant damping mechanisms. For small wavenumbers the ratio of the damping time to the period is dominated by radiative cooling, while for large wavenumbers it is dominated by ion-neutral collisions. The behavior is similar for $\tilde{\mu} = 0.99$, but the wavenumber at which the dominant mechanism changes is larger. Thermal conduction by neutrals and electrons does not influence the damping of the fast wave in a significant way.

The slow wave presents a more complex behaviour and we need to consider two different values of the ionisation fraction. For almost neutral plasmas ($\tilde{\mu} = 0.99$) the ratio of the damping time to the period presents three minima of maximum attenuation, each of them corresponding to a different dominant damping mechanism. The first one, situated at long wavelengths, is caused by radiative cooling; the second one, in the mid range of the wavenumber interval, is due to ion-neutral collisions mechanisms; and finally, the last peak, corresponding to short wavelengths, is produced by neutrals thermal conduction. Such as mentioned in Sect. 3.4.2, in a partially ionised plasma the expression of κ has two terms (Eq. [3.41]), corresponding to the contributions of neutrals and electrons. For a typical prominence temperature, the contribution of electrons to thermal conduction is negligible in front of that of neutrals. In Fig. 5.3, the curve corresponding to the neutrals contribution to the thermal conduction is indistinguishable from the curve considering the joint contribution of neutrals and electrons.

For a larger ionisation fraction ($\tilde{\mu} = 0.8$; bottom left panel of Figure 5.3), the separation between the minima caused by ion-neutral collisions and thermal conduction decreases. Because of this, the two minima merge and both effects are important in the same region of the considered wavenumber interval.
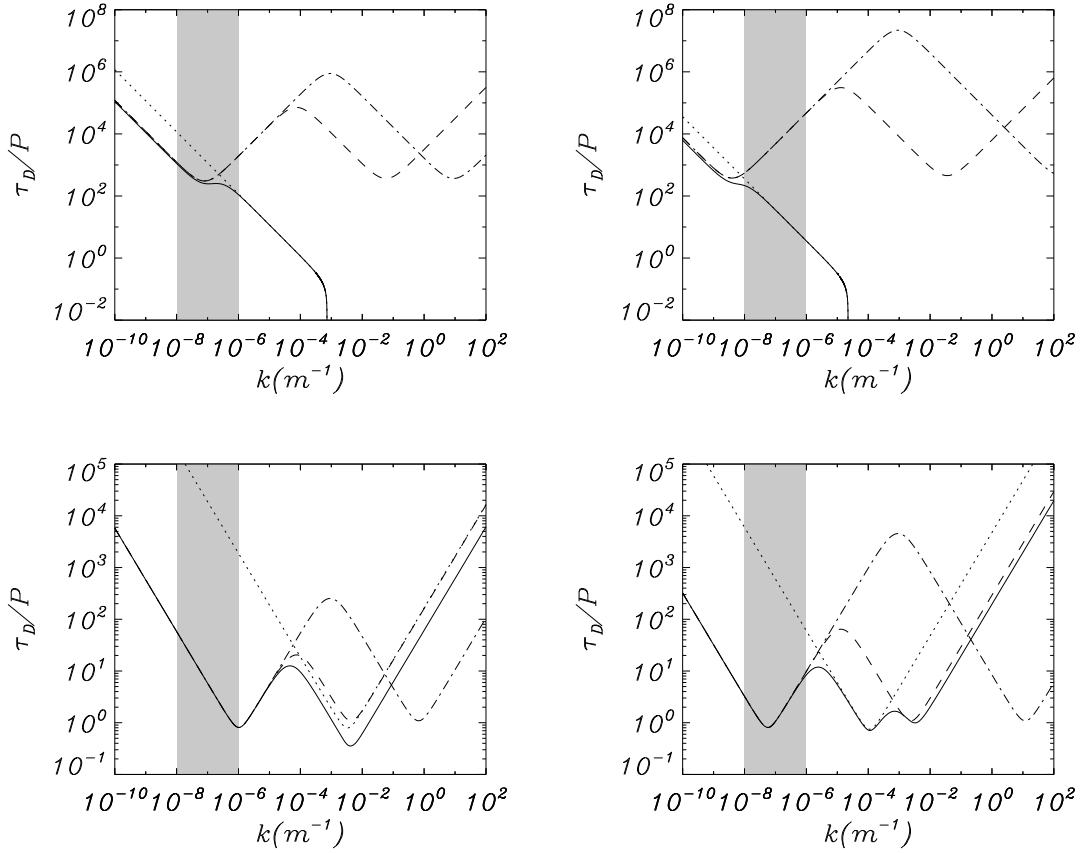
Figure 5.3: Ratio of the damping time to the period for fast (*top*) and slow (*bottom*) waves corresponding to different ionisation fractions, $\tilde{\mu} = 0.8$ (*left*) and $\tilde{\mu} = 0.99$ (*right*). Different line styles correspond to: ion neutral collisions plus thermal mechanisms (solid line), only ion-neutral collisions (dotted line), only thermal mechanisms (dash-dotted line) and only radiation, heating and electronic thermal conduction (dashed line). All other parameter values are the same as those in Fig. 5.1.

5.2.3 Comparison with Carbonell et al. (2004) and Forteza et al. (2007)

Next, we compare our results with previous ones in which non-adiabatic (Carbonell et al. 2004) and partially ionised (Forteza et al. 2007; Chapter 4) effects were considered separately. Figure 5.4 shows the period, damping time and the ratio of the damping time to the period of the magnetoacoustic waves for three different cases: adiabatic partially ionised plasma (dashed line), non-adiabatic fully ionised plasma (dotted line) and non-adiabatic partially ionised plasma (solid line). We can observe that the wavenumber at which the fast wave disappears is not affected by the non-adiabatic terms because it arises from magnetic diffusion and is influenced by partial ionisation effects. On the other hand, while non-adiabatic and partial ionisation effects influence only slightly the period of the waves, which remains basically the
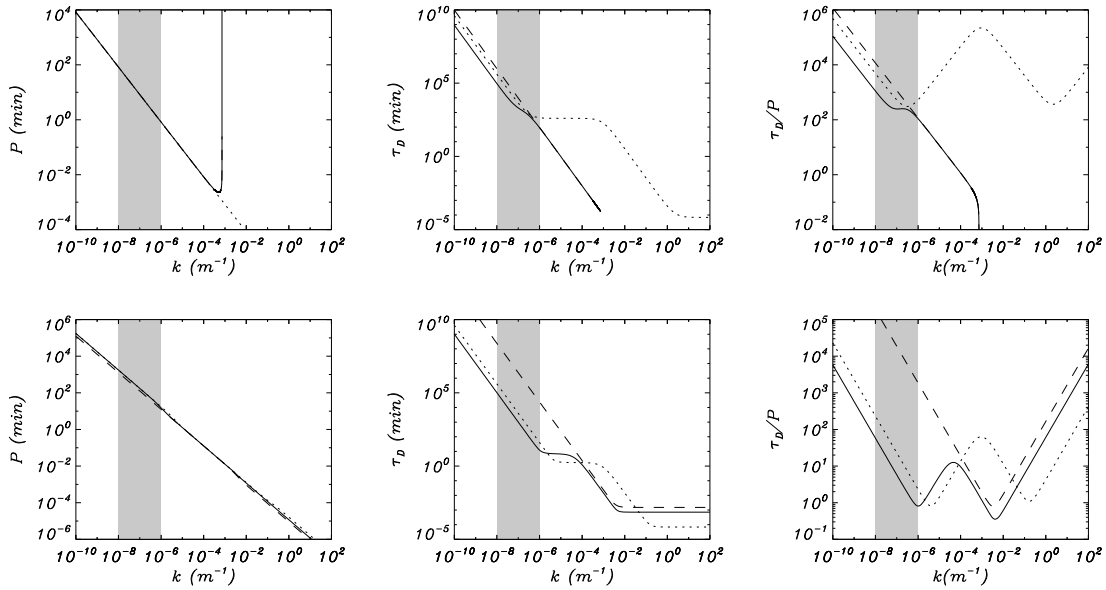
Figure 5.4: Period, damping time and ratio of the damping time to the period for the fast (*top*) and slow (*bottom*) waves. Solid lines: non-adiabatic partially ionised plasma; dashed lines: adiabatic partially ionised plasma; dotted lines: non-adiabatic fully ionised plasma. All other parameter values are the same as those in Fig. 5.1.

same as in the ideal case, the damping time is modified such as can be seen in Fig. 5.4. In particular, for the same wavenumber, and for both magnetoacoustic waves, the damping time is smaller in the case of a non-adiabatic partially ionised plasma, with the only exception of fast waves in a narrow wavenumber interval. As a consequence, the ratio between damping time and period also becomes smaller for both waves, which means that the damping efficiency improves. Furthermore, in Sect. 5.2.2 there is an explanation about the behaviour of the two minima of τ_{D}/P of the slow wave.

We have also studied the differences in the behaviour of the magnetoacoustic waves produced by the change of the parameters χ^* and α corresponding to the different prominence radiative loss regimes. The results are very similar to those of Carbonell et al. (2004) for a fully ionised plasma, and the only difference is that the different prominence regimes only affect the region of the wavenumber interval in which thermal mechanisms are the dominant damping mechanisms.

5.2.4 Dependence with the propagation angle

Figure 5.5 shows the ratio of the damping time to the period for different propagation angles and the three different scenarios considered in Sect. 5.2.3: non-adiabatic fully ionised plasma (Carbonell et al. 2004), adiabatic partially ionised plasma (Chapter 4) and non-adiabatic partially ionised plasma (present chapter).
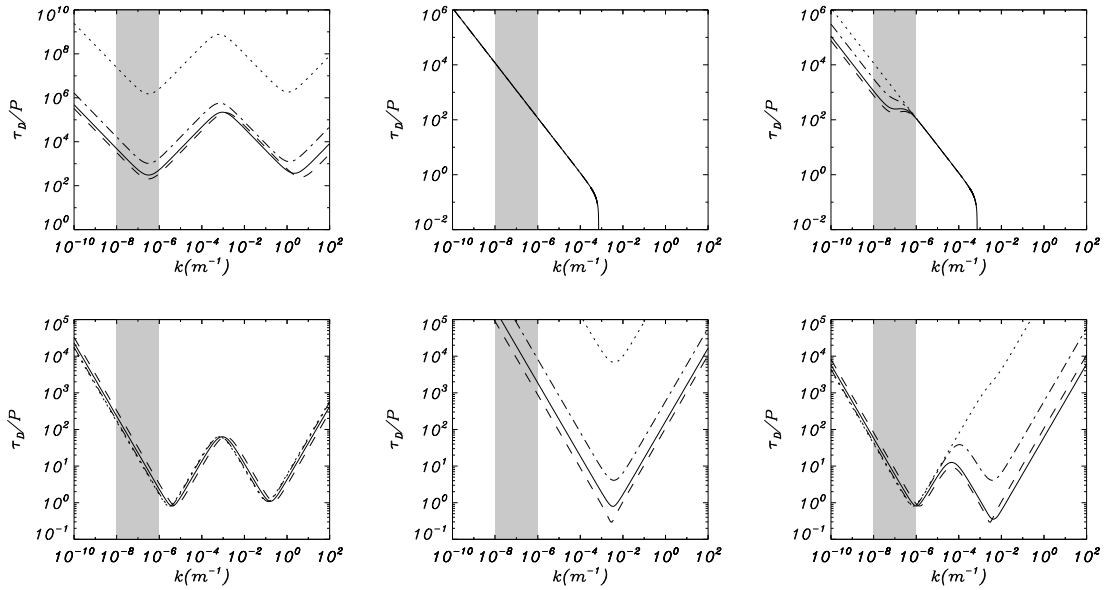
Figure 5.5: Ratio of the damping time to the period for three different scenarios: non-adiabatic fully ionised plasma (*left*), adiabatic partially ionised plasma (*center*) and non-adiabatic partially ionised plasma (*right*). The top panels correspond to the fast wave, while the bottom ones correspond to the slow wave. Different propagation angles have been considered: $\theta = 0.01$ (dotted), $\theta = \pi/8$ (dash-dotted), $\theta = \pi/4$ (solid) and $\theta = \pi/3$ (dashed). All other parameter values are the same as those in Fig. 5.1.

For the non-adiabatic fully ionised plasma (left panels), the damping of the slow wave presents a weak dependence on the propagation angle while the damping of the fast wave is strongly affected by the value of the propagation angle (Carbonell et al. 2006). This behaviour is reversed in an adiabatic partially ionised plasma: the slow wave is considerably affected while the fast wave remains unaffected (center panels).

In the non-adiabatic partially ionised case (right panels) both waves are notably affected by the variation of the propagation angle. Fast waves present a dependence on the propagation angle only in the wavenumber interval in which non-adiabatic effects are the dominant damping mechanisms. Meanwhile, for slow waves, the dependence on the propagation angle is stronger in the region in which ion-neutral collisions and thermal conduction are important. We observe that for large propagation angles the minimum caused by ion-neutral collisions is more pronounced, while for small angles this minimum completely disappears.

5.3 Summary

In this chapter we have studied the time damping of magnetoacoustic waves in a partially ionised plasma considering non-adiabatic effects (thermal con-

duction, radiative losses and heating) in the energy equation. We have assumed small amplitude oscillations, so the linearised non-adiabatic one-fluid MHD equations for a partially ionised plasma have been considered and the dispersion relation for magnetoacoustic waves has been found. While fast and slow waves are more efficiently damped in the non-adiabatic partially ionised case than in the adiabatic partially ionised case, the Alfvén wave is not affected by the non-adiabatic terms, so its behaviour is only affected by the ion-neutral collision mechanism. Because of that, the Alfvén wave is not discused in this chapter since it has been described in Chapter 4.

Looking at the period of the different waves, one can observe that the period of magnetoacoustic waves remains basically the same as in the ideal case. The modification to these ideal values introduced by non-adiabatic terms and ion-neutral collisions is practically negligible. On the contrary, the inclusion of non-adiabatic terms in the partially ionised set of equations decreases the damping time of fast and slow waves in the interval of observed wavelengths as compared with the results obtained for a non-adiabatic fully ionised plasma (Carbonell et al. 2004) and an adiabatic partially ionised plasma (Chapter 4). Moreover, in the case of slow waves, values of the ratio of the damping time to the period similar to those obtained from observations $(1-10)$ can be obtained.

For slow waves, the minima of τ_{D}/P, corresponding to a maximum of attenuation, are displaced to longer wavelengths as compared to the case when only non-adiabatic effects are considered. An increase of the neutral portion in the plasma produces a displacement of these ranges of maximum damping to longer wavelengths. Radiative losses are dominant at long wavelengths while the rest of the wavenumber interval is dominated by thermal conduction and ion-neutral collisions. For ionisation fractions with $\tilde{\mu} < 0.8$ both mechanisms dominate in the considered wavelength interval (a single minimum with maximum damping caused by the combination of the two effects appears), while for $\tilde{\mu} > 0.8$ the minimum splits and ion-neutral collisions dominate in the mid range interval while thermal conduction dominates at short wavelengths.

In the case of fast waves, radiation is the dominant damping mechanism for long wavelengths, while in the rest of the considered wavenumber interval the damping is dominated by the effect of ion-neutral collisions mechanism. As in the adiabatic partially ionised plasma (Chapter 4), fast waves only exist for wavenumbers smaller than a critical wavenumber that depends on the ionisation fraction and that is not affected by the non-adiabatic terms. In spite of this, the value of this critical wavenumber is large in comparison with the typical wavenumbers of waves in prominences. Therefore, our results are completely meaningful within the range of observed wavelengths in prominence oscillations.

In general, for typical prominence temperature values, the contribution of electrons to thermal conduction is negligible in front of the contribution of neutrals. This dominance of neutrals thermal conduction means that in this case thermal conduction is isotropic. Finally, it has been shown by Soler et al.

(2010) that if realistic abundances of helium are taken into account ($\sim 10\%$), this has a minor influence on the wave damping.

Chapter 6

Spatial damping of MHD waves in a flowing and partially ionised prominence plasma*

As we have stated in Sect. 1.3.1.e, there are observational evidences about the presence of flows and mass motions in prominences . These flows can be observed in $H\alpha$, UV and EUV lines (Labrosse et al. 2010). The observed velocities range from 5 to 20 $km \cdot s^{-1}$ for $H\alpha$ quiescent filaments (Zirker et al. 1998; Lin et al. 2003, 2007; Arregui et al. 2012) and the flows seem to be field-aligned. Flow speeds can be higher in the case of active region prominences, and values up to 40-50 $km \cdot s^{-1}$ have been observed. Few observations point out the simultaneous presence of oscillations and mass flows in prominences. Probably, the best example was provided by Okamoto et al. (2007) who observed an active region prominence with Hinode/SOT using Ca II H-line images. In this observation, some prominence threads were flowing along the magnetic field with an apparent velocity on the plane of sky of around 40 $km \cdot s^{-1}$. At the same time, the threads were oscillating in the transverse direction. These observations, displaying oscillations and flows together, were theoretically interpreted by Terradas et al. (2008).

Carbonell et al. (2009) already explored the time damping of non-adiabatic slow and thermal waves in an unbounded and fully ionised prominence medium with a background flow. Therefore, in this chapter we focus basically on the spatial damping of MHD waves in partially ionised plasmas in which a background flow is present. The value of the plasma parameters and propagation angle used in this study are the same as in the previous chapter.

6.1 Spatial damping of MHD waves in a flowing partially ionised prominence plasma

The governing dispersion relations for this case have been derived in Sect. 3.9. However, since we are interested in the spatial damping of MHD waves we consider the frequency, ω, to be real and seek for complex solutions of the wavenumber k expressed as $k = k_R + i k_I$. Therefore, the wavelength of the waves is given by $\lambda = \frac{2\pi}{k_R}$, the damping length by $L_d = \frac{1}{k_I}$ and the damping length per wavelength is $\frac{L_d}{\lambda}$. Furthermore, a uniform field-aligned flow has been considered, with a flow speed, v_0, equal to $10 \ km \cdot s^{-1}$.

On the other hand, depending on the value of $\tilde{\mu}$ and both Spitzer's (η) and Cowling's (η_C) resistivities, we may consider different types of plasmas with the following characteristics:

(1) A fully ionised ideal plasma (FIIP), where $\tilde{\mu} = 0.5$ and $\eta = \eta_C = 0$;

(2) A fully ionised resistive plasma (FIRP), where $\tilde{\mu} = 0.5$ and $\eta = \eta_C$;

(3) A partially ionised plasma (PIP), where $0.5 < \tilde{\mu} < 1$ and $\eta \neq \eta_C$.

6.2 Spatial damping of Alfvén waves in a partially ionised plasma

6.2.1 Spatial damping of Alfvén waves without background flow

In this case, our governing dispersion relation is given by Eq. (4.2), and the wavenumbers are,

$$k = \pm \sqrt{\frac{(\omega \sec \theta)^2}{v_a^2 + i\omega(\eta_C + \eta \tan^2 \theta)}}, \tag{6.1}$$

representing two Alfvén waves propagating in opposite directions. The real part of these wavenumbers is,

$$k_R = \omega \sec \theta \frac{\sqrt{v_a^2 + \sqrt{v_a^4 + \omega^2(\eta_C + \eta \tan^2 \theta)}}}{\sqrt{2\left[v_a^4 + \omega^2(\eta_C + \eta \tan^2 \theta)\right]}}, \tag{6.2}$$

while the imaginary part is,

$$k_I = \frac{-\omega^2 \sec \theta}{\sqrt{2\left[v_a^4 + \omega^2(\eta_C + \eta \tan^2 \theta)\right]}} \times \frac{(\eta_C + \eta \tan^2 \theta)}{\sqrt{v_a^2 + \sqrt{v_a^4 + \omega^2(\eta_C + \eta \tan^2 \theta)}}}. \tag{6.3}$$

Figure 6.1 shows a plot of the damping length, wavelength and the ratio of the damping length to wavelength versus the period for Alfvén waves. The plots have been made for four different ionisation fractions and the shaded

region corresponds to the interval of observed periods in prominence oscillations. When a period within the shaded region is considered, we observe that the damping length decreases in a substantial way when the amount of neutrals in the plasma increases. Then, when ion-neutral collisions are present the spatial damping of Alfvén waves is enhanced for periods greater than 1 s. Also, we can observe that for a FIRP the behaviour of the damping length, wavelength and their ratio versus period is linear, except for periods below 10^{-6} s. However, when a PIP is considered a deviation from the linear behaviour appears for periods below 1 s. This is due to the joint effect of the terms including frequency and resistivities in the real (k_{R}) and imaginary (k_{I}) parts of the wavenumber k since for shorter periods its role becomes more important. The spatial damping of Alfvén waves in prominence PIP with physical properties like those of quiescent prominences is very efficient for periods below 1 s, although, within the interval of periods of interest for prominence oscillations, it is only efficient ($\frac{L_{\mathrm{d}}}{\lambda} \sim 1 - 10$), when almost neutral plasmas are considered.

6.2.2 Spatial damping of Alfvén waves with background flow

Now, our dispersion relation is given by Eq. (3.85) which once expanded becomes a cubic polynomial in the wavenumber k,

$$
\begin{aligned}
i v_0 (\eta_{\mathrm{C}} \cos^2 \theta + \eta \sin^2 \theta) k^3 & \\
+ \left[(v_0^2 - v_{\mathrm{a}}^2 - i \eta_{\mathrm{C}} \omega) \cos \theta - i \eta \omega \sin \theta \tan \theta \right] k^2 & \\
- 2 \omega v_0 k + + \omega^2 \sec \theta = 0. &
\end{aligned}
\tag{6.4}
$$

The increase in the degree of the dispersion relation with respect to the case without flow is produced by the joint presence of flow and resistivities and implies that in the present case we obtain three propagating Alfvén waves. Figure 6.2 shows the numerical solutions of the dispersion relation (6.4) for the three Alfvén waves in a partially ionised plasma with a background flow. For all the interval of periods considered, a strongly damped third Alfvén wave appears, while on the contrary, and like in Sect. 6.2.1, the other two Alfvén waves are very efficiently damped for periods below 1 s. Furthermore, the following approximations for the different wavenumbers corresponding to two of the expected Alfvén waves can be calculated,

$$
k \simeq \pm \sqrt{\frac{(\omega \sec \theta)^2}{(v_0 \pm v_{\mathrm{a}})^2 + i \omega (\eta_{\mathrm{C}} + \eta \tan^2 \theta)}},
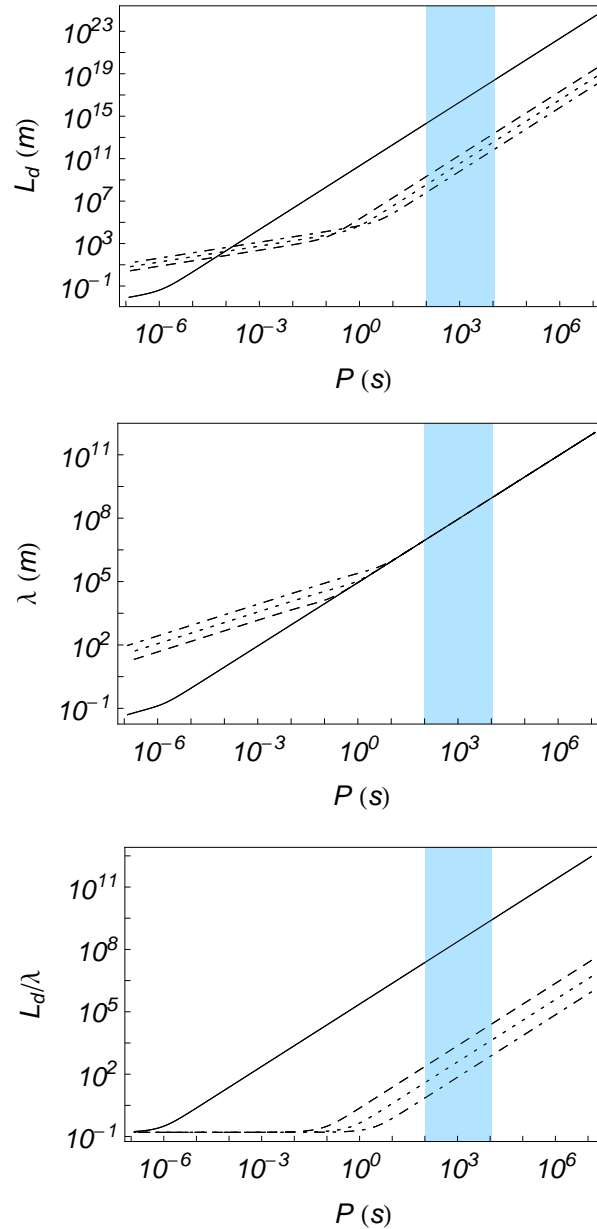\tag{6.5}
$$

Figure 6.1: Damping length, wavelength and ratio of the damping length to the wavelength versus the period for Alfvén waves in a FIRP (solid) and in PIP with $\tilde{\mu} = 0.8$ (dashed), $\tilde{\mu} = 0.95$ (dotted) and $\tilde{\mu} = 0.99$ (dash-dotted). In all figures, the shaded region corresponds to the interval of observed periods in prominence oscillations.
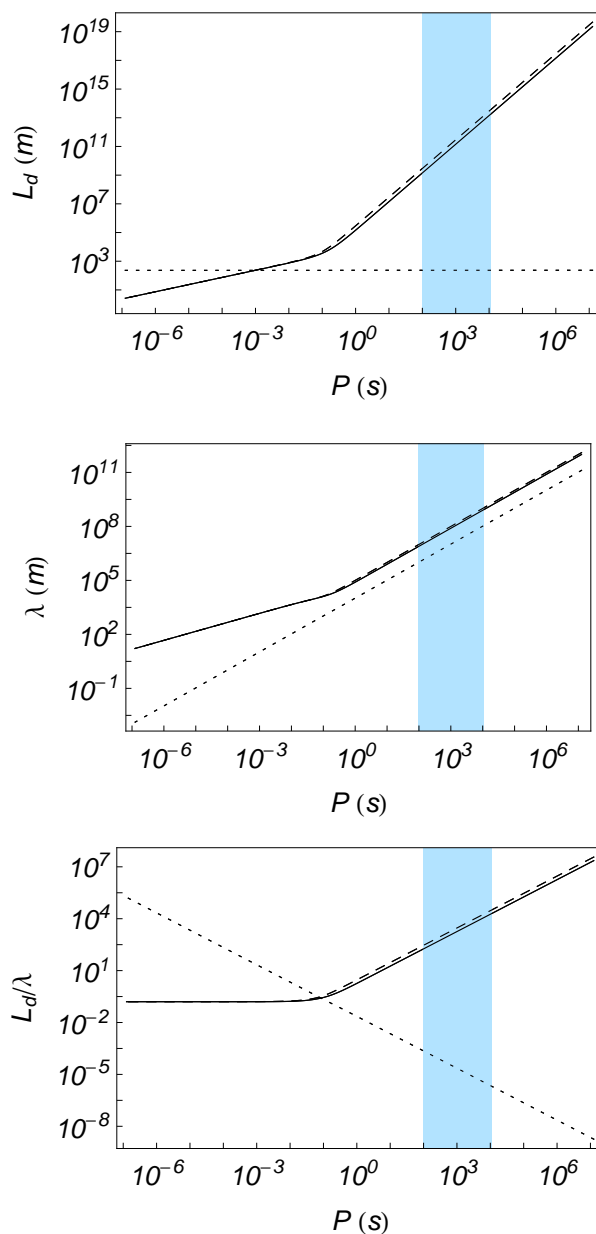
Figure 6.2: Damping length, wavelength and ratio of the damping length to the wavelength versus period for the three (solid, dashed, dotted) Alfvén waves in a PIP with $\tilde{\mu} = 0.8$ and with a background flow of $10 \; km \cdot s^{-1}$. In all figures, the shaded region corresponds to the interval of observed periods in prominence oscillations.

whose real part is given by,

$$k_{\mathrm{R}} \simeq \frac{\sqrt{(v_0 \pm v_{\mathrm{a}})^2 + \sqrt{(v_0 \pm v_{\mathrm{a}})^4 + \omega^2(\eta_{\mathrm{C}} + \eta \tan^2 \theta)}}}{\sqrt{2\left[(v_0 \pm v_{\mathrm{a}})^4 + \omega^2(\eta_{\mathrm{C}} + \eta \tan^2 \theta)\right]}} \times \omega \sec\theta, \qquad (6.6)$$

while the imaginary part is,

$$k_{\mathrm{I}} \simeq \frac{-\omega^2 \sec\theta}{\sqrt{2\left[(v_0 \pm v_{\mathrm{a}})^4 + \omega^2(\eta_{\mathrm{C}} + \eta \tan^2 \theta)\right]}}$$

$$\times \frac{(\eta_{\mathrm{C}} + \eta \tan^2 \theta)}{\sqrt{(v_0 \pm v_{\mathrm{a}})^2 + \sqrt{(v_0 \pm v_{\mathrm{a}})^4 + \omega^2(\eta_{\mathrm{C}} + \eta \tan^2 \theta)}}}. \qquad (6.7)$$

From the above expressions, if we consider a FIIP we recover the dispersion relation for Alfvén waves with a background flow (Carbonell et al. 2009), and if we remove the flow, the well-known dispersion relation for Alfvén waves is recovered. Since the flow speed is much smaller than the Alfvén speed, the effect of the flow on the real and imaginary parts of the wavenumber is very small. Then, the wavelengths and damping lengths are similar to those in Sect. 6.2.1.

The third remaining wavenumber of Eq. (6.4) can be approximated by,

$$k = \frac{\omega}{v_0 \cos\theta} + i\frac{(v_0^2 - v_{\mathrm{a}}^2)\cos\theta}{v_0(\eta_{\mathrm{C}} \cos^2\theta + \eta \sin^2\theta)}, \qquad (6.8)$$

corresponding to the third Alfvén wave. All the above analytical approximations display an excellent agreement with the numerical results, and the presence of the third Alfvén wave, given by Eq. (6.8), fully depends on the join presence of flow and resistivities since, otherwise, the dispersion relation (6.4) would be quadratic. For an external observer to the flowing plasma, this additional wave could be detectable, although its strong spatial damping would make its detection very difficult. For an observer linked to the flow inertial rest frame, only the two usual Alfvén waves, modified by resistivities, would be detected.

6.3   Spatial damping of magnetoacoustic waves in a partially ionised plasma

Our general dispersion relation for non-adiabatic magnetoacoustic waves in presence of a background flow is given by Eq. (3.86). Because of the complexity of this dispersion relation and to help to understand our results, we have divided our study into a sequence of four different cases with dispersion relations of increasing complexity. In the first two cases, the properties

of adiabatic magnetoacoustic waves in a non-flowing (Sect. 6.3.1) and flowing plasma (Sect. 6.3.2) are considered; in the last two cases, the features of non-adiabatic waves in a non-flowing (Sect. 6.3.3) and flowing plasma (Sect. 6.3.4) are studied. Although our main aim is the study of spatial damping of MHD waves in PIP, the case of a FIRP is also considered because it has received almost no attention in the literature. The variation in the sound speed due to the ionisation fraction (Sect. 3.10) can be important since, depending on the flow speed and ionisation fraction chosen, the flow speed could be greater than, smaller than or equal to the sound speed, which affects the direction of propagation of slow and thermal waves (Carbonell et al. 2009). In our case, the flow speed is both subsonic and subalfvénic, which seems to be a typical feature of flows observed in quiescent filaments.

6.3.1 Adiabatic magnetoacoustic waves without background flow

Setting $A = H = 0$ in Eq. (3.87), $v_0 = 0$ in expression (3.72) and substituting in Eq. (3.86), we obtain the dispersion relation for adiabatic magnetoacoustic waves in a PIP without background flow, which is,

$$(\omega^2 - k^2 c_s^2)(ik^2 \eta_C \omega - \omega^2) + k^2 v_a^2 (\omega^2 - k_x^2 c_s^2) + ik^2 k_z^2 v_a^2 c_s^2 \Xi \rho_0 \omega = 0. \qquad (6.9)$$

which is equivalent to Eq. (4.1) already found in Chapter 4. Since in this case we do not consider the presence of flow, the main difference with respect to the research reported in Chapter 4 is that in the following paragraphs we study spatial damping instead of time damping, and that this study has also been performed for a fully ionised resistive plasma.

6.3.1.a *Fully ionised resistive plasma*

Now, imposing FIRP conditions, the dispersion relation given by Eq. (6.9) simplifies to,

$$(\omega^2 - k^2 c_s^2)(ik^2 \eta \omega - \omega^2) + k^2 v_a^2 (\omega^2 - k_x^2 c_s^2) = 0, \qquad (6.10)$$

which once expanded gives a fourth degree polynomial in the wavenumber k,

$$k^4 c_s^2 (v_a^2 \cos^2 \theta + i\omega\eta) - k^2 \omega^2 (c_s^2 + v_a^2 + i\omega\eta) + \omega^4 = 0. \qquad (6.11)$$

Furthermore, when only longitudinal propagation is allowed ($\theta = 0$), the dispersion relation (6.10) can be factorized as,

$$(\omega^2 - k^2 c_s^2)\left[\omega^2 - k^2 (v_a^2 + i\omega\eta)\right] = 0, \qquad (6.12)$$

giving place to two undamped slow waves with a dispersion relation given by,

$$k^2 = \frac{\omega^2}{c_s^2}.$$

In addition, since fast waves become Alfvén waves for longitudinal propagation, we also obtain two Alfvén waves damped by resistivity, whose dispersion relation is,

$$k^2 = \frac{\omega^2}{v_a^2 + i\eta\omega}.$$

For these Alfvén waves, the real and imaginary parts of the wavenumber k can be obtained from expressions (6.2) and (6.3) setting $\theta = 0$.

Then, in the case of a FIRP and for parallel propagation, resistivity does not affect slow waves, which propagate undamped, and only affects fast waves.

Next, if we allow oblique propagation ($0 < \theta < \pi/2$) in the dispersion relation (6.11), the solutions for the wavenumbers squared are given by,

$$k_1^2 = \frac{\omega^2(v_a^2 + c_s^2 + i\eta\omega)}{2ic_s^2(\eta\omega - iv_a^2\cos^2\theta)} + \frac{\omega^2\sqrt{(v_a^2 + c_s^2 + i\eta\omega)^2 - 4ic_s^2(\eta\omega - iv_a^2\cos^2\theta)}}{2ic_s^2(\eta\omega - iv_a^2\cos^2\theta)}, \quad (6.13)$$

and

$$k_2^2 = \frac{\omega^2(v_a^2 + c_s^2 + i\eta\omega)}{2ic_s^2(\eta\omega - iv_a^2\cos^2\theta)} - \frac{\omega^2\sqrt{(v_a^2 + c_s^2 + i\eta\omega)^2 - 4ic_s^2(\eta\omega - iv_a^2\cos^2\theta)}}{2ic_s^2(\eta\omega - iv_a^2\cos^2\theta)}, \quad (6.14)$$

where k_1 and k_2 are the wavenumbers corresponding to two coupled and damped fast and slow waves propagating in opposite directions. Figure 6.3 displays the behaviour of the damping length, the wavelength and their ratio versus the period for fast and slow waves. In these figures it is clearly observed that the behaviour of the wavelength is the same for a FIRP and a FIIP, and that the only difference occurs at periods below 10^{-6} s due to resistivity. Moreover, the ratio of the damping length to the wavelength shows that in a FIRP, and within the interval of periods of interest, the spatial damping of both waves is negligible.

6.3.1.b Partially ionised plasma

The dispersion relation is given by Eq. (6.9), and considering only longitudinal propagation we obtain,

$$(\omega^2 - k^2c_s^2)\left[\omega^2 - k^2(v_a^2 + i\omega\eta_C)\right] = 0. \quad (6.15)$$

This expression is formally identical to Eq. (6.12), this could suggest that the consideration of longitudinal propagation in a FIRP or in a PIP leads to the same dispersion relation. However, there is an important difference between a FIRP for which both resistivities have the same numerical value, and a PIP, for which the numerical value of Cowling's resistivity is much greater than that of Spitzer's resistivity. Furthermore, for longitudinal propagation slow waves are not influenced by Cowling's resistivity.
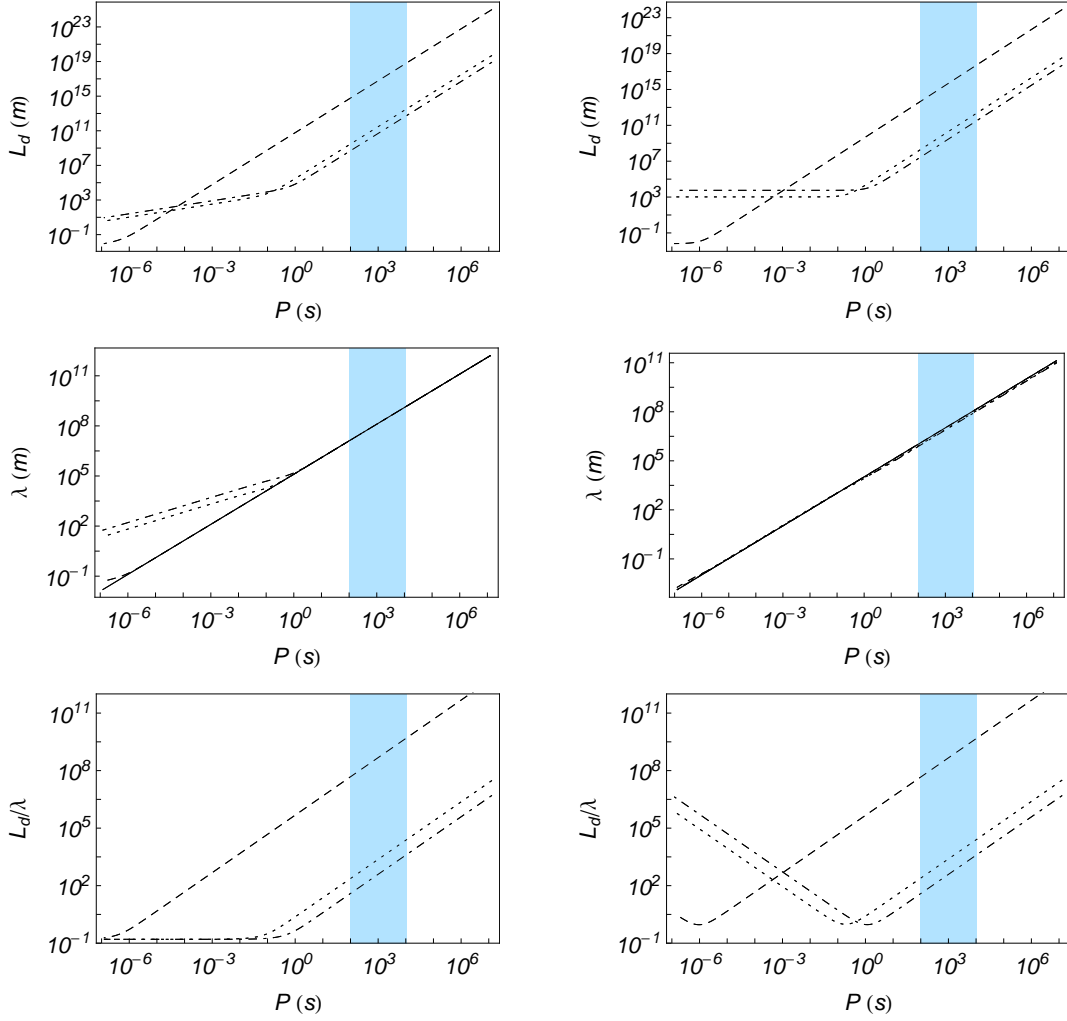
Figure 6.3: Damping length, wavelength and ratio of the damping length to the wavelength versus period for the adiabatic fast (*left*) and slow (*right*) waves in a FIIP (solid), a FIRP (dashed) and a PIP with $\tilde{\mu} = 0.8$ (dotted) and $\tilde{\mu} = 0.95$ (dash-dotted). Note that waves in a FIIP are undamped, so L_d tends to infinity and so there are no solid lines in the top and bottom panels.

Once expanded, Eq. (6.9) gives the following fourth degree polynomial in the wavenumber k,

$$ik^4 c_s^2 \left[\eta_C \omega - i v_a^2 \cos^2 \theta + v_a^2 \rho_0 \omega \Xi (\cos^2 \theta - 1) \right] -$$
$$- k^2 \omega^2 (v_a^2 + c_s^2 + i \eta_C \omega) + \omega^4 = 0. \tag{6.16}$$

After solving this biquadratic dispersion relation, we obtain,

$$q_m^2 = \frac{B + \sqrt{C}}{D}, \tag{6.17}$$

$$q_n^2 = \frac{B - \sqrt{C}}{D}, \tag{6.18}$$

with

$$
\begin{aligned}
B &= (v_a^2 + c_s^2 + i\eta_C\omega), \\
C &= (v_a^2 + c_s^2 + i\eta_C\omega)^2 - 4ic_s^2\left[\eta_C\omega - iv_a^2\cos^2\theta - v_a^2\rho_0\Xi(\cos^2\theta - 1)\right], \\
D &= 2ic_s^2\left[\eta_C\omega - iv_a^2\cos^2\theta - v_a^2\rho_0\Xi(\cos^2\theta - 1)\right],
\end{aligned}
$$

and the wavenumbers are,

$$
k_1 = \pm\sqrt{\omega^2 q_m^2} \tag{6.19}
$$

$$
k_2 = \pm\sqrt{\omega^2 q_n^2} \tag{6.20}
$$

Figure 6.3 displays the behaviour of the damping length, the wavelength and the ratio of damping length to wavelength versus period for fast and slow waves in a PIP. The damping length of both slow and fast waves is severely influenced by ion-neutral collisions and shows a strong dependence on the period for values greater than 1 s, while for shorter periods the dependence becomes weaker. This figure also shows that compared with that of a FIIP, the wavelength of fast waves is slightly affected by partial ionisation, deviating from the linear behaviour for periods below 1 s, while the wavelength of slow waves is not affected at all. Within the interval of observed periods in prominence oscillations, when the ionisation degree is decreased the ratio between the damping length and the wavelength also decreases for both waves and the spatial damping becomes more efficient. The maximum efficiency of the spatial damping for fast waves is attained for periods below 1 s while for slow waves the maximum of efficiency is attained at a period which depends on the ionisation fraction. The location of this maximum moves towards long periods when the ionisation of the plasma decreases, but when almost neutral plasmas are considered it is still located at a period slightly greater than 1 s, ouside the region of interest. Finally, comparing Figs. 6.1 and 6.3 it becomes obvious that the behaviour of Alfvén and fast waves is quite similar.

6.3.2 Adiabatic magnetoacoustic waves with background flow

Setting $A = H = 0$ in Eq. (3.87) and substituting in Eq. (3.86), we obtain the dispersion relation for adiabatic magnetoacoustic waves in a partially ionised plasma with a background flow, which is

$$
\left(\Omega^2 - k^2c_s^2\right)\left(ik^2\eta_C\Omega - \Omega^2\right) + k^2v_a^2\left(\Omega^2 - k_x^2c_s^2\right) + ik^2k_z^2v_a^2c_s^2\Xi\rho_0\Omega = 0. \tag{6.21}
$$

6.3.2.a *Fully ionised resistive plasma*

Considering fully ionised resistive plasma conditions, the dispersion relation (6.21) becomes,

$$(\Omega^2 - k^2 c_s^2)(ik^2\eta\Omega - \Omega^2) + k^2 v_a^2(\Omega^2 - k_x^2 c_s^2) = 0. \tag{6.22}$$

The dispersion relation is a fifth degree polynomial of the wavenumber k, and we therefore expect two slow waves and two fast waves that, for the considered flow speed, propagate in opposite directions, plus an additional wave. When only longitudinal propagation is considered, the above dispersion relation becomes

$$(\Omega^2 - k^2 c_s^2)\left[k^2(i\eta\Omega + v_a^2) - \Omega^2\right] = 0, \tag{6.23}$$

so that slow waves are decoupled from fast waves and propagate undamped, while fast waves are damped by resistivity. The wavenumbers corresponding to the undamped slow waves are given by

$$k = \frac{\omega}{v_0 \pm c_s}. \tag{6.24}$$

For the fast waves, which become Alfvén waves because of longitudinal propagation, the corresponding dispersion relation, given by the second factor in Eq. (6.23), is equivalent to Eq. (6.4) when $\theta = 0$. The solutions to this dispersion relation are given by Eqs. (6.5) and (6.8) with $\theta = 0$, and we obtain three Alfvén waves similar to those studied in Sect. 6.2.2. The expected additional wave mentioned above is then a fast wave that, for longitudinal propagation and when a background flow is present, becomes the third Alfvén wave already found in Sect. 6.2.2. As in Sect. 6.2.2, the presence of this third fast wave fully depends on the join presence of flow and resistivities since, otherwise, the dispersion relation given by Eq. (6.22) would be of fourth order. Since its strong spatial damping would make its detection very difficult, its is not shown in the figures displaying the behaviour of magnetoacoustic waves.

When oblique propagation is allowed, fast and slow waves become coupled and the dispersion relation given by Eq. (6.22) is solved numerically. Figure 6.4 displays the behaviour of the damping length, wavelength and the ratio of the damping length to the wavelength versus period for fast and slow waves in a FIRP. Because of the strong difference between Alfvén and flow speeds, in the case of fast waves the unfolding in wavelength and damping length caused by the flow is not evident, while for slow waves it is clearly seen. In both cases, the behaviour of the wavelength versus period is linear, similar to what happens for a FIIP and the only difference is provided by the unfolding produced by the flow. The damping length also behaves linearly with the period and for slow waves the unfolding in wavelength and damping length produces two different curves for the ratio L_d/λ. In both curves,
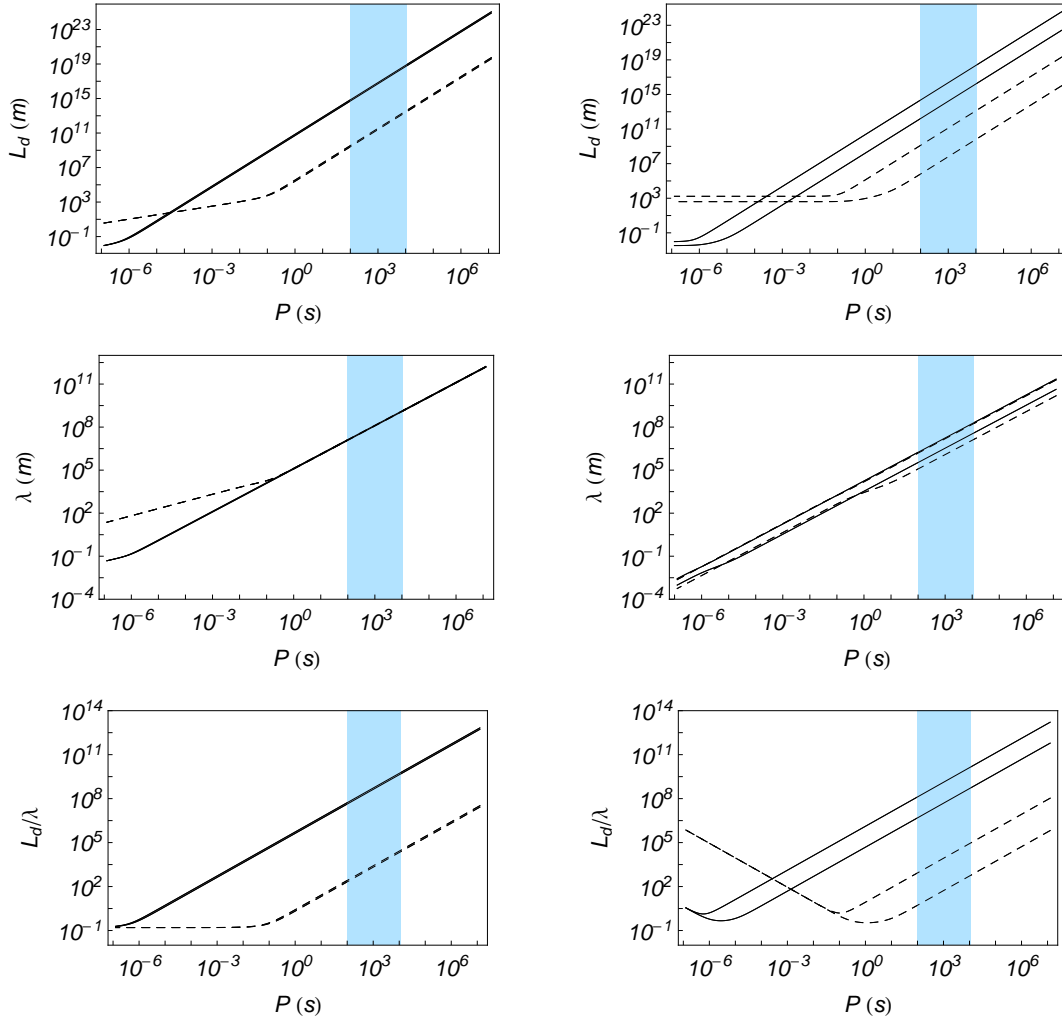
Figure 6.4: Damping length, wavelength and ratio of the damping length to the wavelength versus period for the adiabatic fast (*left*) and slow (*right*) waves in a FIIP (solid) and in a PIP with $\tilde{\mu} = 0.8$ (dashed). The background flow speed is $10 \; km \cdot s^{-1}$.

the most efficient spatial damping appears for periods far away from those of interest in prominence oscillations. For fast waves, the ratio L_d/λ behaves linearly with period and its value is very large within the region of periods of interest. The behaviour of the third fast wave is quite different from the other two fast waves and very similar to that of the third Alfvén wave shown in Section 6.2.2, being strongly damped within the interval of periods considered.

6.3.2.b Partially ionised plasma

Our dispersion relation is given by Eq. (6.21), which is a fifth degree polynomial in k, and when longitudinal propagation is considered we recover the results of Sect. 6.3.2.a with slight differences due to the different numerical value of Cowling's resistivity adopted. As shown in Fig. 6.4, at periods longer

than 0.1 s, the damping lengths of both slow and fast waves increase linearly with the period. However, for periods below 0.1 s the damping length slowly decreases in the case of fast waves and becomes constant for slow waves. Furthermore, the wavelength of fast waves for periods below 0.1 s increases relative to the FIRP case, while the wavelengths corresponding to slow waves are only slightly modified. For the ratio of the damping length to the wavelength, the unfolding in wavelength caused by the flow and the change in the damping length due to the partial ionisation produces fast waves that are far more efficiently attenuated than in a FIRP, for any period, but especially at periods below 0.1 s. In contrast, the peak of maximum efficiency for slow waves is displaced towards long periods when the ionisation decreases, and for almost neutral plasmas it would approach the region of periods usually observed in prominence oscillations. The behaviour of the remaining third fast wave is again very similar to that found for the third Alfvén wave discussed in Sect. 6.2.2.

In absence of flow, the dispersion relation given by Eq. (6.22) becomes a fourth degree polynomial in k and the third fast wave disappears. Such as happens for Alfvén waves with background flow, this third fast wave is produced by the joint action of flow and resistivity, since when a FIIP with a background flow is considered, the dispersion relation also becomes a fourth degree polynomial in k and the third fast wave is absent.

6.3.3   Non-adiabatic magnetoacoustic waves without background flow

Setting $v_0 = 0$ in Eq. (3.72) and substituting this into Eq. (3.86), we obtain the dispersion relation for non-adiabatic magnetoacoustic waves in a PIP without background flow, which is,

$$(\omega^2 - k^2\Lambda^2)(ik^2\eta_C\omega - \omega^2) + k^2v_a^2(\omega^2 - k_x^2\Lambda^2) + ik^2k_z^2v_a^2\Lambda^2\Xi\rho_0\omega = 0. \qquad (6.25)$$

which is the dispersion relation (Eq. [5.1]) obtained in Chapter 5. Again, since in this case we do not consider the presence of flow, the main difference with respect to the research reported in Chapter 5 is that in the following paragraphs we study spatial damping instead of time damping, and that this study has also been performed for a fully ionised resistive plasma.

6.3.3.a   Fully ionised resistive plasma

After imposing the conditions corresponding to a FIRP, the following dispersion relation, a sixth degree polynomial in the wavenumber k, is obtained,

$$(\omega^2 - k^2\Lambda^2)(ik^2\eta\omega - \omega^2) + k^2v_a^2(\omega^2 - k_x^2\Lambda^2) = 0, \qquad (6.26)$$

which describes coupled fast, slow and thermal waves. When only longitudinal propagation is allowed, the above dispersion relation becomes

$$(\omega^2 - k^2\Lambda^2)\left[k^2(i\eta\omega + v_a^2) - \omega^2\right] = 0. \qquad (6.27)$$
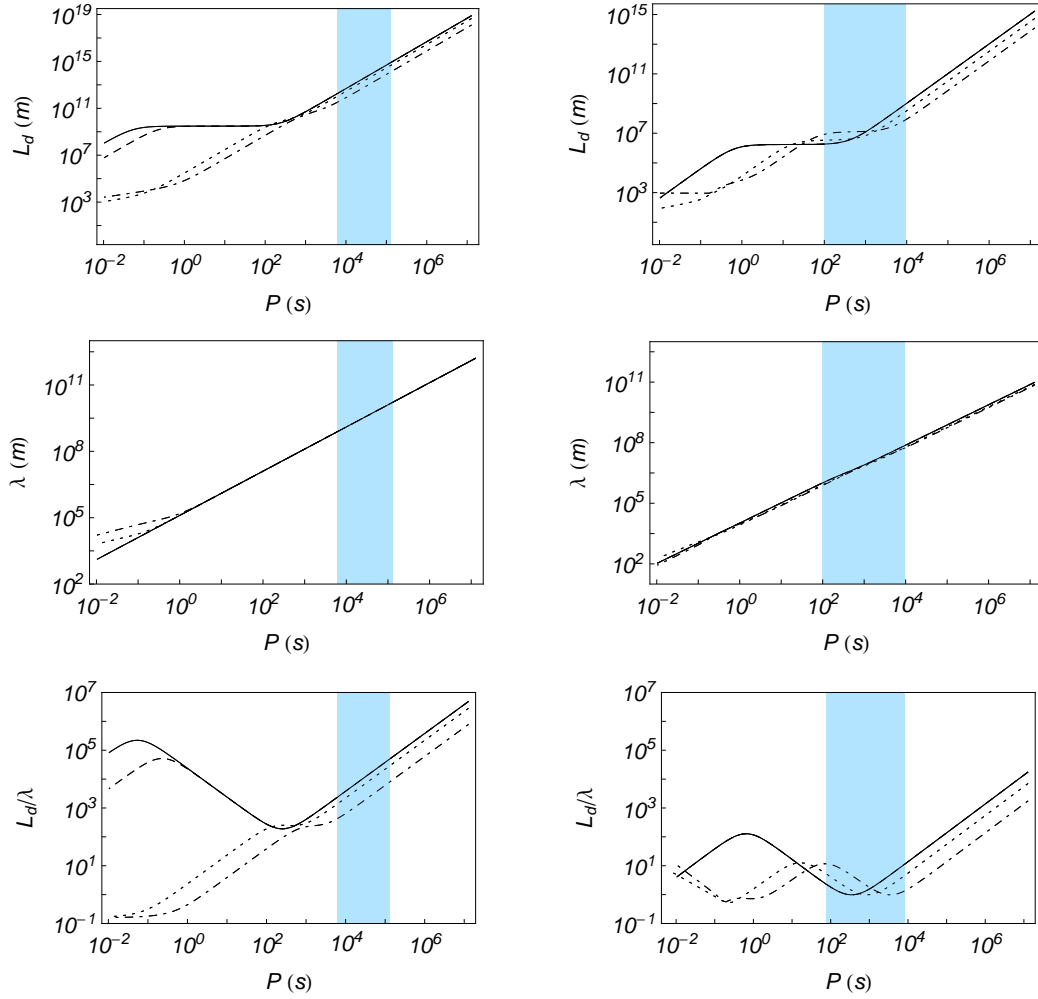
Figure 6.5: Damping length, wavelength and ratio of the damping length to the wavelength versus period for the non-adiabatic fast (*left*) and slow (*right*) waves. Solid lines correspond to a FIIP; dashed lines to a FIRP; dotted lines to a PIP with $\tilde{\mu} = 0.8$; and dash-dotted lines to a PIP with $\tilde{\mu} = 0.95$.

As in Sect. 6.2.1, we then obtain two decoupled Alfvén waves, damped by resistivity, whose dispersion relation is given by

$$k^2 = \frac{\omega^2}{v_{\mathrm{a}}^2 + i\omega\eta} \tag{6.28}$$

and another dispersion relation

$$k^2 = \frac{\omega^2}{\Lambda^2}, \tag{6.29}$$

Because of the dependence of Λ on k, this expression yields to a fourth degree polynomial in k describing coupled propagating thermal and slow waves, damped only by thermal effects. The dispersion relation given by Eq. (6.26) has been solved numerically and the results are presented in Figs. 6.5 (for
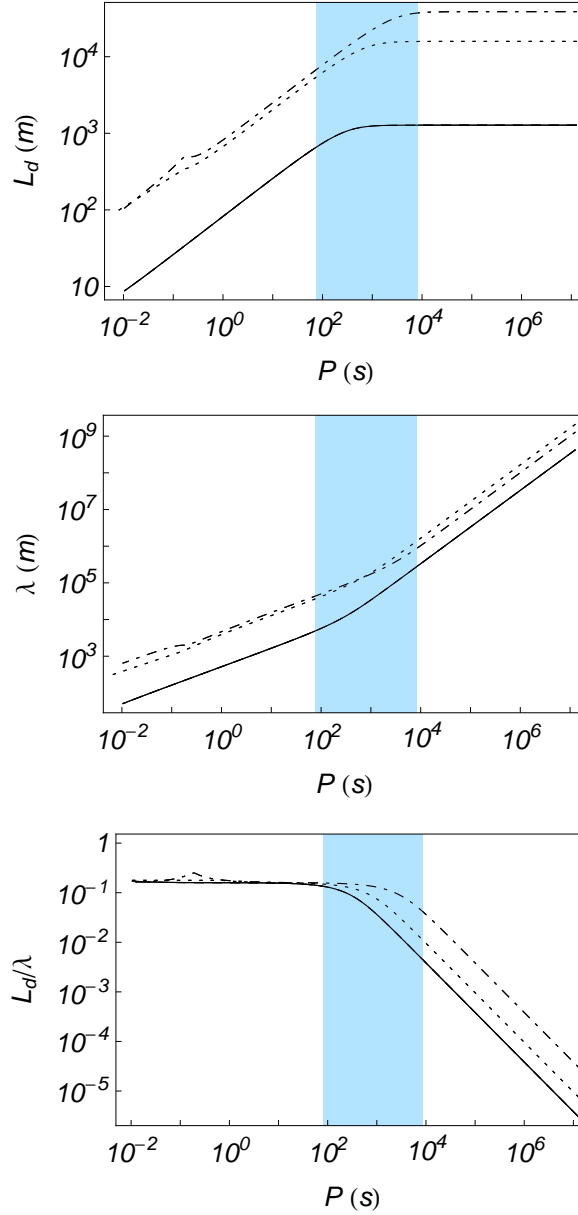
Figure 6.6: Damping length, wavelength and ratio of the damping length to the wavelength versus period for the non-adiabatic thermal wave in a FIIP (solid), a FIRP (dashed) and a PIP with $\tilde{\mu} = 0.8$ (dotted) and $\tilde{\mu} = 0.95$ (dash-dotted).

fast and slow waves) and 6.6 (for thermal waves). Starting with Fig. 6.5, we have only considered an interval of periods between 10^{-2} and 10^7 s, since for periods shorter than 10^{-2} s, much shorter than those of interest, the curves become very entangled. When an FIIP is considered, the spatial damping of the fast wave is governed by radiative losses and thermal conduction (Carbonell et al. 2006) in the interval of periods from 10^{-2} to 10^7 s. However, in a FIRP we observe a slight change in the damping length of fast waves around a period of 1 s. This change tells us that the dominance of thermal conduction appears for slightly shorter periods than for the ideal case. As for the ratio of

the damping length to the wavelength, we observe that the efficiency of the fast wave damping is higher for a FIRP than for a FIIP, for periods below 1 s. For slow waves, no differences appear between the behaviours of FIIP and FIRP. The behaviour of thermal waves (Fig. 6.6) is exactly the same in FIIP and FIRP.

6.3.3.b   *Partially ionised plasma*

In this case, our dispersion relation is given by Eq. (6.25) and when only longitudinal propagation is allowed the expression is similar to that of Sect. 6.3.3.a, although the numerical value of Cowling's resistivity is different and the results for fast waves differ. When oblique propagation is considered, Eq. (6.25) is solved numerically and a strong distortion of the damping length and wavelength curves corresponding to fast waves (Fig. 6.5, left panels) appears. The changes affect the radiative plateau, between periods 10^3 and 10^{-2} s, and partial ionisation decreases the damping length of fast waves in this region. For slow waves (Fig. 6.5, right panels), a similar behaviour is found in the same regions, although the distortion is not so important since a very short radiative plateau, between 10^2 and 10^3 s, remains, together with a region, between 1 and 10^2 s, where thermal conduction is dominant. Compared to a FIRP, the ratio L_d/λ for fast waves decreases substantially for periods below 10^3 s, although for the periods of interest in prominences, this ratio remains very large. For slow waves, partial ionisation causes the ratio L_d/λ to reach a maximum efficiency of ~ 1 for periods similar to those involved in prominence oscillations, and this maximum is displaced towards longer periods when ionisation is decreased. The changes in the wavelengths of slow and fast waves are similar to those shown in the adiabatic case (Sect. 6.3.1.b). In the case of thermal waves (Fig. 6.6), partial ionisation increases both the damping length and wavelength of these waves, although the behaviour of the ratio L_d/λ is similar to that of previous cases. Since a thermal wave is always strongly damped, which makes its detection very difficult, in the following we avoid additional comments on it.

To understand the effects of radiation and thermal conduction by neutrals and electrons on fast and slow waves, in Fig. 6.7 we represent the same quantities but with optically thin radiation and heating removed, i.e., only thermal conduction is at work. We can observe that the most efficient damping for both waves occurs for partially ionised plasmas, which suggests that the inclusion of isotropic thermal conduction due to neutrals plays a very important role for all the periods considered. However, we must take into account that when the ionisation fraction decreases, radiation also decreases and that, because of neutrals, thermal conduction is favoured, which makes it difficult to establish meaningful comparisons between plasmas with different degrees of ionisation.

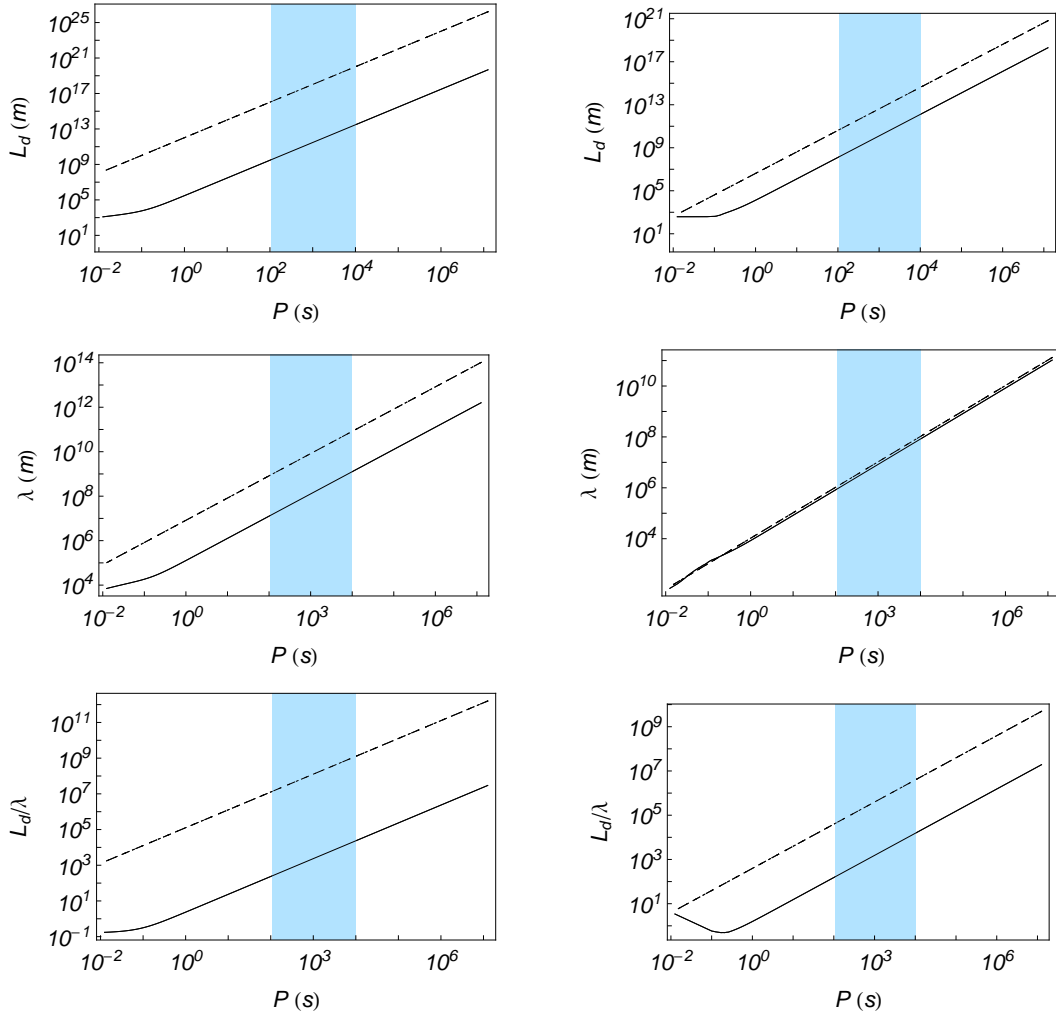In Fig. 6.8 we plot the behaviour of fast and slow waves when thermal

Figure 6.7: Damping length, wavelength and ratio of the damping length to the wavelength versus period for the non-adiabatic fast (*left*) and slow (*right*) waves, without radiation, in a FIIP (dashed), a FIRP (dotted) and a PIP with $\tilde{\mu} = 0.8$ (solid).

conduction has been removed, i.e. only radiation and heating remain. In this case, and within the interval of periods of interest, the behaviour of fast waves is similar when different types of plasma are considered. However, when periods below 100 s are considered, FIIP and FIRP are strongly affected by the lack of thermal conduction. For slow waves, a similar behaviour appears and the most important conclusion after comparing Figs. 6.7 and 6.8 is that, within the interval of periods of interest, a very efficient damping is caused by optically thin radiation.

On the other hand, when non-adiabatic magnetoacoustic waves are considered, the importance of radiation and thermal conduction can also be quantified in terms of two dimensionless numbers (De Moortel and Hood 2004). The first one is the thermal ratio, which in the case of partial ionisation becomes
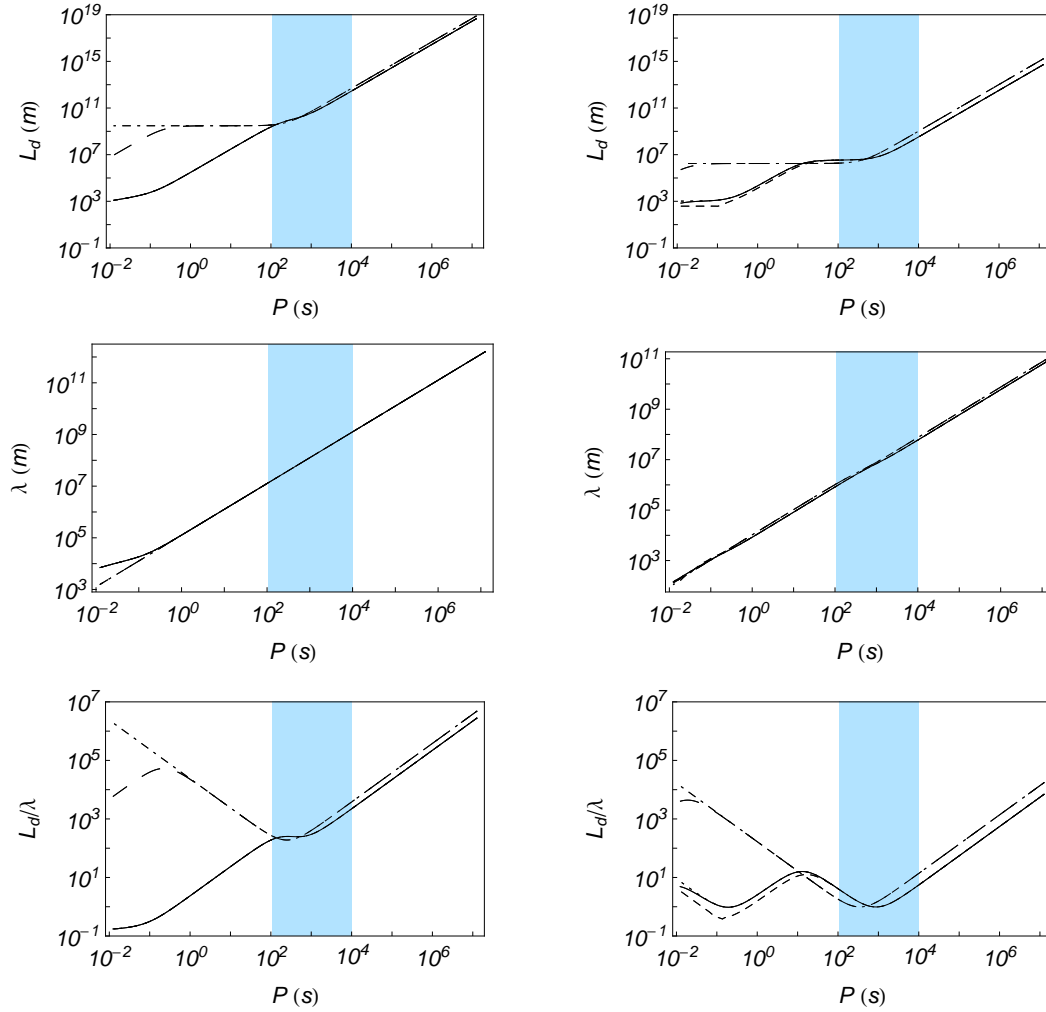
Figure 6.8: Damping length, wavelength, and ratio of the damping length to the wavelength versus period for the non-adiabatic fast (*left*), slow (*right*) waves in a PIP ($\tilde{\mu} = 0.8$) without neutrals thermal conduction (solid); without electronic thermal conduction (dashed) and without thermal conduction (dotted); in a FIIP without thermal conduction (dash-dotted) and in a FIRP without thermal conduction (long-dashed).

$$d = \frac{(\gamma - 1)(\kappa_{e\parallel} + \kappa_{n})T_0\rho_0}{\gamma^2 p_0^2 \tau_{s}} = \frac{1}{\gamma}\frac{\tau_{s}}{\tau_{\text{cond}}}, \qquad (6.30)$$

with $\tau_{s} = l/c_{s}$ the sound travel time and $\tau_{\text{cond}} = l^2 p_0 / \left[(\gamma - 1)(\kappa_{e\parallel} + \kappa_{n})T_0\right]$ the thermal conduction timescale. $\kappa_{e\parallel}$ and κ_{n} are the thermal conduction coefficients corresponding to anisotropic thermal conduction by electrons and to isotropic thermal conduction by neutrals, respectively, l is a characteristic wavelength while the meaning of the rest of parameters have been already defined in previous sections. The second dimensionless number is the radiation ratio

$$r = \frac{(\gamma - 1)\tau_{s}\xi_i\rho_0^2\chi^* T_0^{\alpha}}{\gamma p_0} = \frac{\tau_{s}}{\tau_{r}}, \qquad (6.31)$$

which is the ratio of the sound travel time to the radiation timescale, $\tau_r = \gamma p_0 / \left[(\gamma - 1) \xi_i \rho_0^2 \chi^* T_0^\alpha \right]$. From the equilibrium parameters, we can compute the value of l at which the condition $d = r$ is satisfied

$$l = \sqrt{\frac{\kappa_{e\parallel} + \kappa_n}{\xi_i \rho_0^2 \chi^* T_0^{\alpha-1}}}. \tag{6.32}$$

Then, when the spatial length of the perturbation, the wavelength, is of the order of l or shorter, thermal conduction becomes dominant. For the slow wave, Fig. 6.5 (right panels) shows that the transition from a regime dominated by radiation to another dominated by conduction can be clearly seen in the plot of the damping length versus period. For a FIIP, this transition occurs at a period of 1 s, while for a PIP, with $\tilde{\mu} = 0.8$, it occurs at a period between 10 and 100 s, and with $\tilde{\mu} = 0.95$, at a period close to 100 s. Using the values assumed for prominence parameters, for a FIIP we obtain $l \approx 4\,700$ m, for a PIP ($\tilde{\mu} = 0.8$), $l \approx 40\,000$ m, and for a PIP ($\tilde{\mu} = 0.95$), $l \approx 100\,000$ m. Then, putting these periods in the plot of the wavelength versus period in Fig. 6.5 (right panels), we can check that the numerical value of the wavelength is almost coincident with the above analytical determinations for l. The reason for this increase in the numerical value of l is that for a PIP, thermal conduction is enhanced because of the contribution from neutrals, that increases when the ionisation fraction decreases, while the denominator of l decreases when the ionisation fraction decreases. To summarize, when ionisation decreases the period at which the dominant damping mechanism changes from radiation to thermal conduction increases and, consequently, the wavelength also increases.

6.3.4 Non-adiabatic magnetoacoustic waves with background flow

6.3.4.a Fully ionised ideal plasma

Setting in Eq. (3.86) conditions corresponding to FIIP, we obtain

$$(\Omega^2 - k^2 \Lambda^2)(-\Omega^2) + k^2 v_a^2 (\Omega^2 - k_x^2 \Lambda^2) = 0, \tag{6.33}$$

which is a sixth degree polynomial in the wavenumber k. When only longitudinal propagation is allowed, we obtain two undamped Alfvén waves given by

$$k^2 = \frac{\Omega^2}{v_a^2}, \tag{6.34}$$

whose solutions for the wavenumbers are

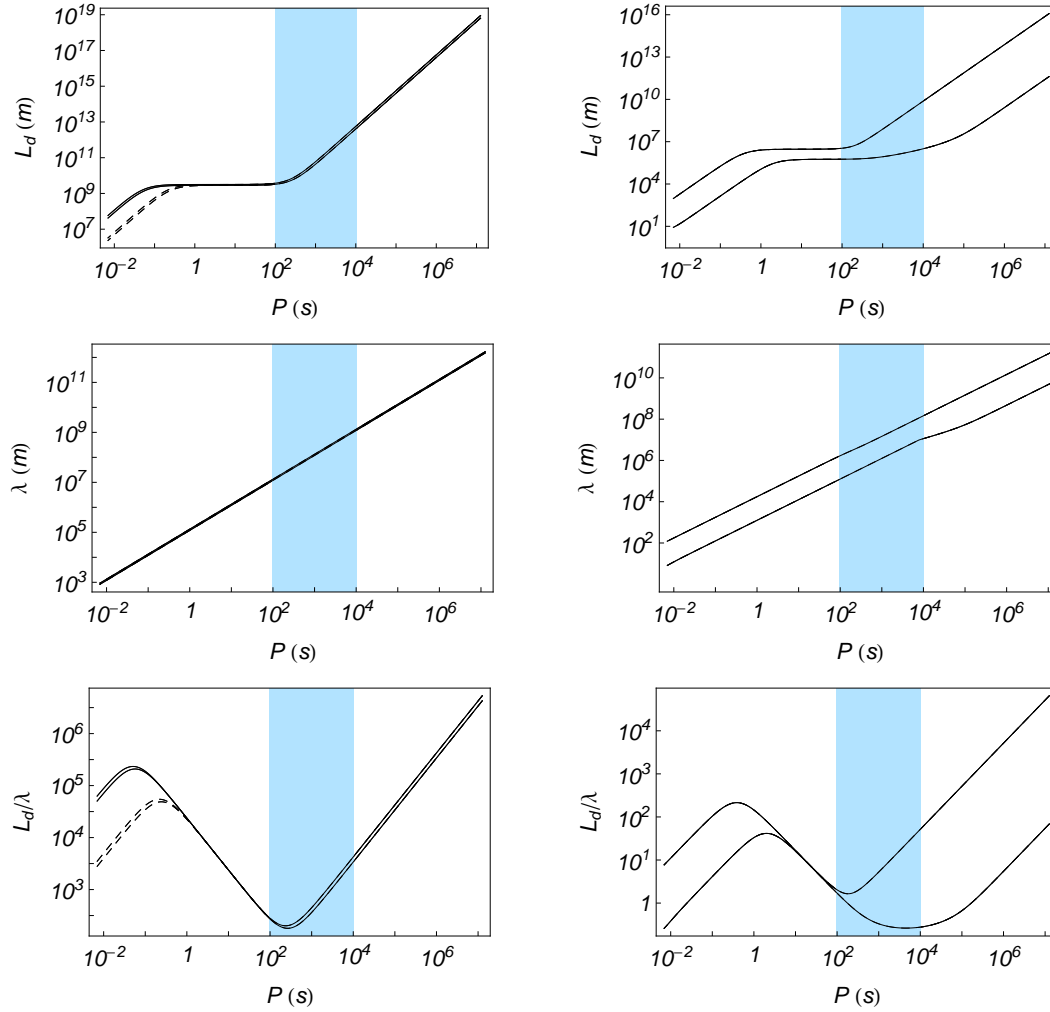$$k = \frac{\omega}{v_0 \pm v_a} \tag{6.35}$$

Figure 6.9: Damping length, wavelength and ratio of the damping length to the wavelength versus period for the non-adiabatic fast (*left*) and slow (*right*) waves in a FIIP (solid) and in a FIRP (dashed). The flow speed is $10 \; km \cdot s^{-1}$.

as in Carbonell et al. (2009). Moreover, the dispersion relation

$$\Omega^2 = k^2 \Lambda^2, \tag{6.36}$$

describes coupled slow and thermal waves modified by the flow and damped by thermal effects. In the case of oblique propagation, Eq. (6.33) is solved numerically and the behaviour of fast and slow waves is shown in Fig. 6.9. When a flow is present the unfolding of wavelengths and damping lengths appears. Since the considered flow speed is much lower than the Alfvén speed, the separation of the curves corresponding to the fast wave is very small, while the curves corresponding to slow waves separate substantially because the flow speed and sound speed are comparable. This effect strongly affects the behaviour of the damping length versus wavelength for slow waves, since one of them has a very efficient spatial damping for periods observed in prominence

oscillations. In the case considered in this section, the damping of fast and slow waves is strictly due to thermal effects.

6.3.4.b *Fully ionised resistive plasma*

In this case, considering FIRP conditions, the dispersion relation becomes

$$(\Omega^2 - k^2\Lambda^2)(ik^2\eta\Omega - \Omega^2) + k^2 v_a^2(\Omega^2 - k_x^2\Lambda^2) = 0, \tag{6.37}$$

which is a seventh degree polynomial in the wavenumber k. Considering only longitudinal propagation, again we find coupled slow and thermal waves modified by the flow and damped by thermal effects, and three Alfvén waves given by the dispersion relation (6.4), with $\theta = 0$, and its solutions. Therefore, when we solve the dispersion relation given by Eq. (6.37), we expect three fast, two slow, and two thermal propagating waves. In Fig. 6.9, the wave features of fast and slow waves have been plotted and compared with the previous case. As shown, for fast and slow waves no important differences in the behaviour with respect to the ideal case are seen. Thermal waves, as well as the third fast wave, are strongly damped after a very short distance.

6.3.4.c *Partially ionised plasma*

The dispersion relation is now given by Eq. (3.86) which, once expanded, becomes a seventh degree polynomial in the wavenumber k. Figure 6.10 displays the behaviour of the damping length, wavelength and ratio of damping length to wavelength for fast and slow waves. The most interesting results are those related to the ratio L_d/λ. For fast waves, this ratio decreases with the period and becomes small for periods below 10^{-2} s, while for one of the slow waves, the ratio becomes very small for periods typically observed in prominence oscillations. When the ionisation is decreased, slight changes in the above described behaviour occur, the most important being the displacement towards longer periods of the peak for the most efficient damping corresponding to slow waves. As pointed out before, a third fast wave is, again, produced by the joint action of flow and resistivity. In the absence of flow or resistivity, the dispersion relation becomes a sixth order polynomial of the wavenumber and this wave is absent.

6.4 Summary

We have analysed the spatial damping of Alfvén and non-adiabatic magnetoacoustic waves in a flowing partially ionised prominence plasma. Several different cases, with dispersion relations of increasing complexity, have been considered, and our results are summarized below

As it is well known, Alfvén waves are difficult to damp because they are insensitive to non-adiabatic effects. However, when Alfvén waves in a partially
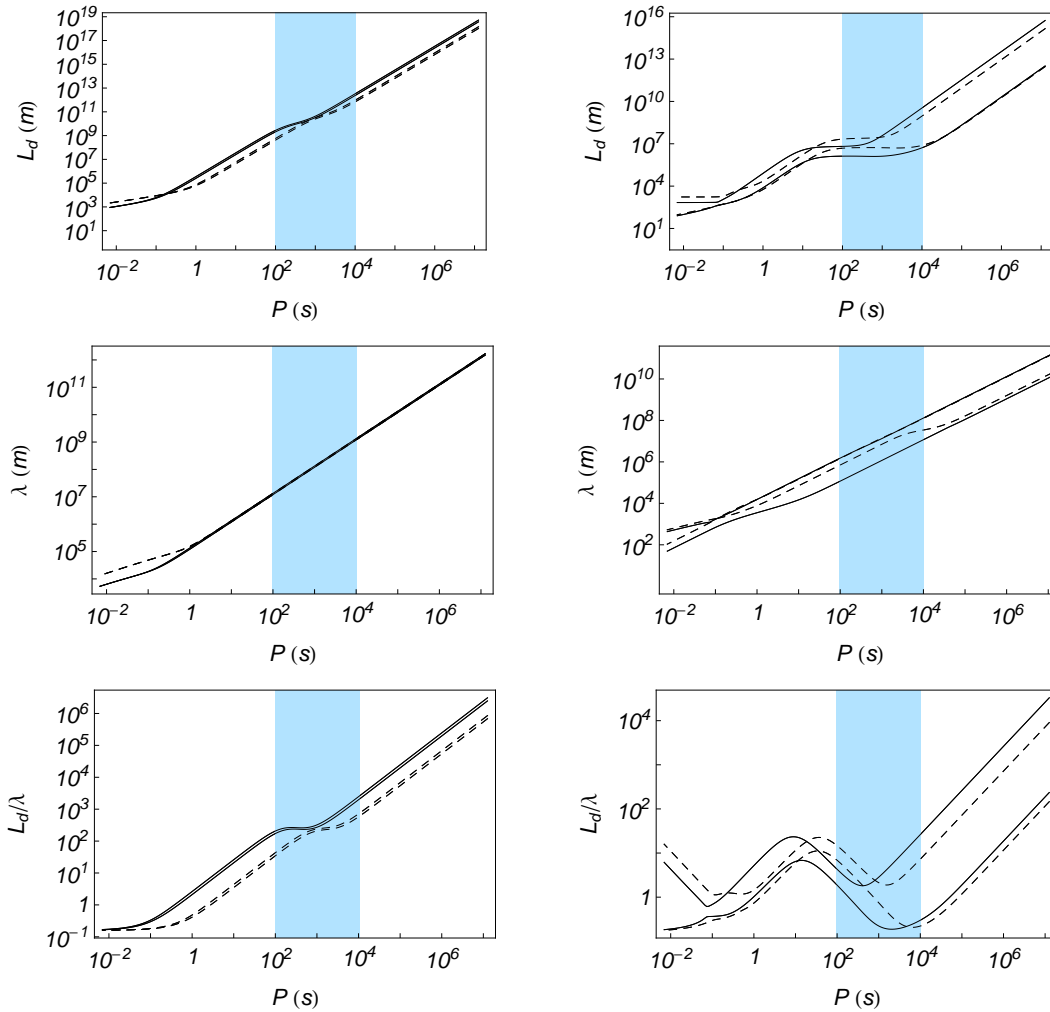
Figure 6.10: Damping length, wavelength and ratio of the damping length to the wavelength versus period for the non-adiabatic fast (*left*) and slow (*right*) waves in a PIP with $\tilde{\mu} = 0.8$ (solid) and $\tilde{\mu} = 0.95$ (dashed). The flow speed is $10 \; km \cdot s^{-1}$.

ionised plasma are considered, they can be spatially damped and analytical expressions describing their spatial damping can be obtained. When the ionisation decreases, the damping length of these waves also decreases and the efficiency of their spatial damping in the range of periods of interest is improved, although the most efficient damping is attained for periods below 1 s. A new feature is that when a flow is present a new third Alfvén wave, strongly attenuated, appears. This wave depends on the joint action of flow and resistivities, since in the absence of flow, or for a FIIP, the dispersion relation becomes quadratic and only the two well-known Alfvén waves are present. Furthermore, this third wave could only be detected by an observer not moving with the flow.

When adiabatic magnetoacoustic waves are considered and the effect of partial ionisation is taken into account, some new features appear. When a

FIRP is considered and only longitudinal propagation is allowed, slow waves are decoupled from fast waves, propagating undamped, while fast waves propagate with a modified Alfvén speed and are damped by resistivity. When a PIP plasma is studied and only longitudinal propagation is allowed, the same occurs but then the numerical value of Cowling's resistivity is greater than for a FIRP, thus enhancing the damping. The behaviour of slow waves is then only influenced by partial ionisation when oblique propagation is allowed. Furthermore, when a PIP is considered the behaviour of fast waves is very similar to that of Alfvén waves and the damping becomes very efficient for periods below 1 s, while for slow waves the peak denoting the most efficient damping moves towards higher periods as the plasma ionisation decreases. When a flow is considered in the adiabatic case, the main difference is the unfolding of the damping length, wavelength and damping length to wavelength curves, and the apparition of a third fast wave, strongly damped, caused by the join presence of flow and resistivities.

For non-adiabatic magnetoacoustic waves, when partial ionisation is present the behaviour of fast, slow and thermal waves is strongly modified. Comparing with non-adiabatic fast waves in a FIIP, which are damped by electronic thermal conduction and radiation, the damping length of a fast wave in a PIP is strongly diminished by neutrals thermal conduction for periods between 0.01 and 100 s, and, at the same time, the radiative plateau present in FIIP and FIRP disappears. The behaviour of slow waves is not so strongly modified as for fast waves, although thermal conduction by neutrals also diminishes the damping length for periods below 10 s, and a short radiative plateau remains for periods between 10 and 1000 s. Finally, thermal waves are only slightly modified, although the effect of partial ionisation is to increase the damping length of these waves, the converse of what happens for the other waves. When a background flow is included, a new third fast wave appears, which is again, due to the joint action of flow and resistivities. As we already know, wavelengths and damping lengths are modified by the flow, and since for slow waves the sound speed and observed flow speeds are comparable, the change in wavelength and damping length are important and lead to an improvement in the efficiency of the damping. The maximum of efficiency is also displaced towards long periods when the ionisation decreases, and for ionisation fractions from 0.8 to 0.95, it is clearly located within the range of periods typically observed in prominence oscillations, with a value of L_{d}/λ smaller than 1. This means that for a typical period of 10^3 s, the damping length is between 10^2 and 10^3 km, the wavelength around 10^3 km and, as a consequence, the slow wave would be strongly attenuated in a distance smaller than a wavelength. On the other hand, during our calculations, we have found that the different heating mechanisms usually considered (Sect. 3.4.1) do not affect the results.

In conclusion, the joint effect of non-adiabaticity, flows and partial ionisation allows slow waves to damp in an efficient way within the interval of

periods typically observed in prominences. Thermal waves are attenuated very efficiently within the interval of interest but their observational detection is probably very difficult, and fast waves are very unefficiently attenuated within the considered interval. We also note that the new fast and Alfvén waves are only detectable in a reference system external to the flow, although their short damping length should make their detection very difficult. As we have seen, even in the most simple case of an unbounded medium threaded by a uniform magnetic field, the inclusion of non-adiabatic effects, partial ionisation and flows complicates the study of the spatial damping of prominence oscillations because of the apparition of new waves and the difficulty in distinguishing between the different effects. From observations, this implies that because of the entanglement of the different effects, it is extremely difficult to properly interpret the observed oscillations in terms of MHD waves.

On the other hand, and such as we stated in Chapter 4, Zaqarashvili et al. (2011) have studied MHD waves in partially ionised plasmas using a two-fluid approach. In this study they have focused in the time damping of Alfvén and magnetoacoustic waves and they have compared their results with those obtained using the single-fluid approach. The comparison shows that while for very low or low frequencies the behaviours of the period and damping time are the same, for high frequencies these behaviours, in particular for fast and Alfvén waves, are quite different. Zaqarashvili et al. (2011) did not make any study about the spatial damping of MHD waves in the two-fluid approach, therefore, it is adventurous to predict whether or not the results obtained using both approaches are going to be very different.

Chapter 7

Summary and Conclusions

This last chapter is intended to provide a summary of the thesis and of the most important conclusions obtained, and to highlight new problems which could be addressed in future works.

7.1   Summary

1. Single-fluid MHD equations for a partially ionised plasma with a non-adiabatic energy equation have been derived.

2. From these MHD equations, and assuming a magnetostatic equilibrium in which a background flow is present, the dispersion relations for linear non-adiabatic magnetoacoustic and Alfvén waves have been derived.

3. A modified Alfvén speed which includes resistive effects has been defined and its behavior has been studied.

4. A non-adiabatic sound speed for the case of partially ionised plasmas with a background flow has been defined and its behaviour has been studied.

5. The time damping of adiabatic and non-adiabatic linear MHD waves in a partially ionised prominence plasma has been studied.

6. The spatial damping of non-adiabatic linear MHD waves in different types of prominence plasmas, having a background flow, has been studied.

7.2 Conclusions

7.2.1 Time damping of adiabatic partially ionised prominence plasmas

1. The damping by ion-neutral interactions is much stronger for the fast wave than for the slow wave, unlike what happens with other damping mechanisms, such as radiative cooling and conduction, for which the slow wave is strongly attenuated while the fast wave remains almost undamped.

2. For almost neutral plasmas the fast and Alfvén waves are efficiently damped, with values of τ_{D}/P compatible with those of observations.

3. Both fast and Alfvén waves present a critical wavenumber. For wavenumbers below these critical values, the fast and Alfvén modes only exist as damped propagating waves. For wavenumbers greater than these values, we have damped disturbances instead of propagating waves.

7.2.2 Time damping of non-adiabatic partially ionised prominence plasmas

1. The period of magnetoacoustic waves remains basically the same as in the ideal case. The modification to these ideal values introduced by non-adiabatic terms and ion-neutral collisions is practically negligible.

2. Fast and slow waves are more efficiently damped in the non-adiabatic partially ionised case than in the adiabatic partially ionised case, and the values of the ratio of the damping time to the period are similar to those obtained in observations. On the contrary, Alfvén waves are not affected by the non-adiabatic terms.

3. For slow waves, radiative losses are dominant at short wavenumbers while the rest of the wavenumber interval is dominated by thermal conduction and ion-neutral collisions. For $\tilde{\mu} > 0.8$, ion-neutral collisions dominate in the mid range interval while thermal conduction dominates at long wavenumbers.

4. In the case of fast waves, radiation is the dominant damping mechanism for long wavelengths, while ion-neutral collisions dominate for short wavelengths. The critical wavenumber for fast waves is not affected by the non-adiabatic terms. In spite of this, the value of this critical wavenumber is large in comparison with the typical wavenumbers derived from observations of prominence oscillations.

5. For typical prominence temperature values, the contribution of electrons to thermal conduction is negligible in front of the contribution of neutrals.

7.2.3 Spatial damping of partially ionised prominence plasmas

1. Alfvén waves in a partially ionised plasma can be spatially damped. When the ionisation decreases, the damping length of these waves also decreases and the efficiency of their spatial damping in the range of periods of interest is improved, although the most efficient damping is attained for periods below 1 s.

2. In presence of flow, a new third Alfvén wave, strongly attenuated, appears. This wave depends on the joint action of flow and resistivities.

3. For non-adiabatic magnetoacoustic waves, when partial ionisation is present the behaviour of fast, slow and thermal waves is strongly modified. Comparing with non-adiabatic fast waves in a fully ionised ideal plasma (FIIP), which are damped by electronic thermal conduction and radiation, the damping length of a fast wave in a partially ionised plasma is strongly diminished by neutrals thermal conduction for periods between 0.01 and 100 s, and, at the same time, the radiative plateau present in fully ionised ideal plasma and fully ionised resistive plasma disappears. The behaviour of slow waves is not so strongly modified as for fast waves, although thermal conduction by neutrals also diminishes the damping length for periods below 10 s, and a short radiative plateau remains for periods between 10 and 1000 s. Finally, thermal waves are only slightly modified, although the effect of partial ionisation is to increase the damping length of these waves, the converse of what happens for the other waves.

4. Wavelengths and damping lengths are modified by the flow, and since, for slow waves the sound speed and the observed flow speeds are comparable, the change in wavelength and damping length are important leading to an improvement in the efficiency of the damping. The maximum of efficiency is also displaced towards long periods when the ionisation decreases, and for ionisation fractions from 0.8 to 0.95, it is clearly located within the range of periods typically observed in prominence oscillations with a value of L_{d}/λ smaller than 1.

7.3 Final comments

The research and results reported in this thesis have been developed using the single-fluid MHD approach. However, other approaches could be also consid-

ered for this kind of studies. For instance, Zaqarashvili et al. (2011) have used the two-fluid approach to study the time damping of MHD waves in partially ionised plasmas and they have found some differences with respect to the results reported here. Using this approach, they have found the reason for the discrepancy between our results for the damping rates of slow modes, when parallel propagation is considered, and Braginskii's results. This discrepancy is caused by the neglect of the inertial terms in the equation of motion for the relative velocity when the single-fluid MHD equations are derived.

On the other hand, we have found a cut-off wavenumber in fast and Alfvén waves, when fully ionised resistive and partially ionised plasmas are considered. For wavenumbers below the cut-off, fast and Alfvén waves exist as damped propagating waves, while for wavenumbers greater than this cut-off, we have damped disturbances instead of propagating waves. Zaqarashvili et al. (2012) have made a thorough analysis of the process of derivation of single-fluid MHD equations. Going from two-fluid to single fluid equations, they have shown that the presence of a cut-off wavenumber in Alfvén waves is due to the neglect of several terms during the derivation process. In particular, the cut-off wavenumber appears when, after neglecting the inertial term, the Hall current term and electron-neutral collisions are also neglected in the induction equation. This points out that the presence of a cut-off wavenumber in Alfvén (and fast) waves in partially ionised plasmas considered under the single-fluid approximation is not connected to any physical process. The cut-off wavenumber is an artifact coming from the approximations made during the derivation of the most commonly used single-fluid MHD equations.

Zaqarashvili et al. (2011) did not study the spatial damping of MHD waves in partially ionised plasmas, and for this reason our results can not be compared. However, it could be possible that if such approach is used the behaviour of the spatial damping of MHD waves would be different from our results obtained with the single-fluid approach.

7.4 Future work

As always happens, science is a way to give an answer to a question while two or three new questions arise in the process. This is why the work of the scientific community will never stop.

This thesis provides with basic knowledge about the behaviour of linear MHD waves in a partially ionised solar prominence and puts the basis for future studies. In the following we would like to suggest several aspects in which the research done in this thesis can be used as a starting basis for more in-depth studies.

First of all, recent observations of quiescent prominences made by HINODE show a complicated plasma dynamics within the prominence body with the presence of flows, ripples, plumes, etc. which could be easily related with the development of instabilities. MHD instabilities in fully ionised plasmas

have been already studied, although, the study of MHD instabilities in partially ionised plasmas remains to be done. This topic is a natural extension of this thesis and would have an immediate application to the understanding of prominence dynamics.

Next, the inclusion of the additional terms needed to study partially ionised plasmas in MHD numerical codes would allow the study of the time evolution of linear and non-linear disturbances in partially ionised plasmas. The study of non-linear MHD waves in partially ionised plasmas could be of application to large amplitude oscillations in filaments (winking filaments).

On the other hand, to represent a prominence in terms of a static equilibrium background is very unrealistic since we know about the complex dynamics of prominences.

Therefore, another topic of interest is the consideration of a dynamic equilibrium background on which MHD waves are superimposed. These dynamic equilibrium backgrounds could be modeled in different ways: spatial and time dependent flows, time dependent equilibrium parameters, etc.

Finally, we cannot resist to point out that since prominences are made of partially ionised plasmas, an explanation about how are they supported by magnetic fields is needed.

In summary, and related with prominences, partially ionised plasmas will become in the next future one of the most interesting research areas.

Appendix A

Derivation of the momentum equation

In Sect. 3.3 the main steps to obtain the momentum equation for the whole partially ionised plasma have been described. This appendix is a more detailed derivation in which the algebraic manipulations are shown.

We start from Eq. (3.24),

$$n_i m_i \frac{d_i \mathbf{v}_i}{dt} + n_n m_i \frac{d_n \mathbf{v}_n}{dt} = -\nabla p + \frac{1}{c} \mathbf{j} \times \mathbf{B}, \tag{A.1}$$

and we concentrate only in the left-hand side of the equation

$$n_i m_i \frac{d_i \mathbf{v}_i}{dt} + n_n m_i \frac{d_n \mathbf{v}_n}{dt} = \rho_i \frac{\partial \mathbf{v}_i}{\partial t} + \rho_n \frac{\partial \mathbf{v}_n}{\partial t} + \rho_i \mathbf{v}_i \cdot \nabla \mathbf{v}_i + \rho_n \mathbf{v}_n \cdot \nabla \mathbf{v}_n. \tag{A.2}$$

Considering

$$\rho_\alpha \frac{\partial \mathbf{v}_\alpha}{\partial t} = \frac{\partial \rho_\alpha \mathbf{v}_\alpha}{\partial t} - \mathbf{v}_\alpha \frac{\partial \rho_\alpha}{\partial t}, \tag{A.3}$$

and taking into account the continuity equation,

$$\frac{\partial \rho_\alpha}{\partial t} + \nabla \cdot (\rho_\alpha \mathbf{v}_\alpha) = 0, \tag{A.4}$$

one obtains the following expression

$$\rho_\alpha \frac{\partial \mathbf{v}_\alpha}{\partial t} = \frac{\partial \rho_\alpha \mathbf{v}_\alpha}{\partial t} + \mathbf{v}_\alpha \nabla \cdot (\rho_\alpha \mathbf{v}_\alpha), \tag{A.5}$$

that allows us to write the right-hand side of Eq. (A.2) in the following form

$$\frac{\partial \rho \mathbf{v}}{\partial t} + \mathbf{v}_i \nabla \cdot (\rho_i \mathbf{v}_i) + \mathbf{v}_n \nabla \cdot (\rho_n \mathbf{v}_n) + \rho_i \cdot \nabla \mathbf{v}_i + \rho_n \cdot \nabla \mathbf{v}_n. \tag{A.6}$$

We use the relative ion-neutral velocity (Eq. [3.19]) and introduce the centre of mass velocity

$$\mathbf{v} = \xi_i \mathbf{v}_i + \xi_n \mathbf{v}_n, \tag{A.7}$$

in order to obtain expressions for the ion and neutral velocities

$$\mathbf{v}_i = \xi_n \mathbf{w} + \mathbf{v}, \tag{A.8}$$

$$\mathbf{v}_n = -\xi_i \mathbf{w} + \mathbf{v}. \tag{A.9}$$

Inserting these formulaes in Eq.(A.6) it can be expressed as

$$\frac{\partial \rho \mathbf{v}}{\partial t} + (\xi_n \mathbf{w} + \mathbf{v})\nabla \cdot (\rho_i \mathbf{v}_i) + \rho_i \mathbf{v}_i \cdot \nabla(\xi_n \mathbf{w} + \mathbf{v})$$
$$+ (-\xi_i \mathbf{w} + \mathbf{v})\nabla \cdot (\rho_n \mathbf{v}_n) + \rho_n \mathbf{v}_n \cdot \nabla(-\xi_i \mathbf{w} + \mathbf{v}). \tag{A.10}$$

Next we consider the following identity

$$\nabla \cdot (\alpha \mathbf{A} \mathbf{B}) = \alpha \mathbf{A} \cdot \nabla \mathbf{B} + \mathbf{B} \nabla \cdot (\alpha \mathbf{A}) \equiv \mathbf{A} \cdot \nabla(\alpha \mathbf{B}) + \alpha \mathbf{B} \nabla \cdot \mathbf{A}, \tag{A.11}$$

to write Eq.(A.10) in the form

$$\frac{\partial \rho \mathbf{v}}{\partial t} + \mathbf{w}\nabla \cdot (\xi_n \rho_i \mathbf{v}_i) + \xi_n \rho_i \mathbf{v}_i \cdot \nabla \mathbf{w} + \mathbf{v}\nabla \cdot (\rho_i \mathbf{v}_i + \rho_n \mathbf{v}_n)$$
$$+ (\rho_i \mathbf{v}_i + \rho_n \mathbf{v}_n) \cdot \nabla \mathbf{v} - \mathbf{w}\nabla \cdot (\xi_i \rho_n \mathbf{v}_n) - \xi_i \rho_n \mathbf{v}_n \cdot \nabla \mathbf{w}, \tag{A.12}$$

and considering $\rho_i \mathbf{v}_i + \rho_n \mathbf{v}_n \approx \rho \mathbf{v}$ one can write the previous expression as

$$\frac{\partial \rho \mathbf{v}}{\partial t} + \mathbf{v}\nabla \cdot (\rho \mathbf{v}) + \rho \mathbf{v} \cdot \nabla \mathbf{v} + \mathbf{w}\nabla \cdot (\xi_i \xi_n \rho \mathbf{w}) + \xi_n \xi_i \rho \mathbf{w} \cdot \nabla \mathbf{w}. \tag{A.13}$$

After some algebraic manipulations, splitting the first term and combining the last two terms, we end up with the following expression for the left-hand side of Eq. (A.1)

$$\rho\frac{\partial \mathbf{v}}{\partial t} + \rho \mathbf{v} \cdot \nabla \mathbf{v} + \nabla \cdot (\xi_i \xi_n \rho \mathbf{w} \mathbf{w}). \tag{A.14}$$

So, the momentum equation for the whole partially ionised plasma is

$$\rho\frac{d\mathbf{v}}{dt} = -\nabla p + \frac{1}{c}\mathbf{j} \times \mathbf{B} - \nabla \cdot (\xi_i \xi_n \rho \mathbf{w} \mathbf{w}). \tag{A.15}$$

Appendix B

Derivation of the energy equation

In Sect. 3.4 the main steps to obtain the energy equation for the whole partially ionised plasma have been given. This appendix is a more detailed derivation in which the algebraic manipulations are shown.

To derive the energy equation the starting point are the individual energy equations as given by Braginskii (1965) or in the more convenient form of Eq. (2.63) of Goedbloed & Poedts (2004), where viscosity and conduction are neglected. These equations are added and we get

$$\frac{\partial p}{\partial t} + \sum_\alpha (\mathbf{v}_\alpha \cdot \nabla p_\alpha + \gamma p_\alpha \nabla \cdot \mathbf{v}_\alpha) = (\gamma - 1) \sum_\alpha Q_\alpha. \tag{B.1}$$

From Eqs. (3.3), (3.19) and (3.20) one can write the velocities of each species as

$$\mathbf{v}_e = \mathbf{v} + \xi_n \mathbf{w} - \frac{\mathbf{j}}{en_e}, \tag{B.2}$$

$$\mathbf{v}_i = \xi_n \mathbf{w} + \mathbf{v}, \tag{B.3}$$

$$\mathbf{v}_n = -(1 - \xi_n)\mathbf{w} + \mathbf{v}. \tag{B.4}$$

Considering the former equations, the first term of the sum in Eq. (B.1) can be written as

$$\sum_\alpha \mathbf{v}_\alpha \cdot \nabla p_\alpha = \mathbf{v} \cdot \nabla p + \xi_n \mathbf{w} \cdot \nabla (p_e + p_i) - \xi_i \mathbf{w} \cdot \nabla p_n - \frac{\mathbf{j}}{en_e} \cdot \nabla p_e, \tag{B.5}$$

and taking into account the expression for the pressure function (Eq. [3.51]), we end up with

$$\sum_{\alpha} \mathbf{v}_{\alpha} \cdot \nabla p_{\alpha} = \mathbf{v} \cdot \nabla p + \mathbf{w} \cdot \mathbf{G} - \frac{\mathbf{j}}{en_i} \cdot \nabla p_i. \tag{B.6}$$

To obtain the second term of the sum in Eq. (B.1) we follow the same procedure. Thus, first of all we use Eqs. (B.2)–(B.4),

$$\sum_{\alpha} p_{\alpha} \nabla \cdot \mathbf{v}_{\alpha} = p_e \nabla \cdot \left(\mathbf{v} + \xi_n \mathbf{w} - \frac{\mathbf{j}}{en_e} \right) + p_i \nabla \cdot (\xi_n \mathbf{w} + \mathbf{v}) + p_n \nabla \cdot (\mathbf{v} - \xi_i \mathbf{w}), \tag{B.7}$$

and now one can write this term as follows

$$\sum_{\alpha} p_{\alpha} \nabla \cdot \mathbf{v}_{\alpha} = p \nabla \cdot \mathbf{v} + 2 p_i \nabla \cdot (\xi_n \mathbf{w}) - \frac{p_i}{en_i} \nabla \cdot \mathbf{j} - p_n \nabla \cdot (\xi_i \mathbf{w}). \tag{B.8}$$

Once we have obtained this equation, we need the following vectorial identity

$$\nabla \cdot (f \mathbf{A}) = \nabla f \cdot \mathbf{A} + f \nabla \cdot \mathbf{A}, \tag{B.9}$$

that allows us to write Eq. (B.8) as

$$\sum_{\alpha} p_{\alpha} \nabla \cdot \mathbf{v}_{\alpha} = p \nabla \cdot \mathbf{v} + 2 \nabla \cdot (\xi_n p_i \mathbf{w}) - 2 \xi_n \mathbf{w} \cdot \nabla p_i$$

$$- \nabla \cdot (\xi_i p_n \mathbf{w}) + \xi_i \mathbf{w} \cdot \nabla p_n - \nabla \cdot \left(\frac{p_i \mathbf{j}}{en_i} \right) + \frac{\mathbf{j}}{en_i} \cdot \nabla p_i, \tag{B.10}$$

so the second term of the sum in Eq. (B.1) can be cast in the form,

$$\sum_{\alpha} p_{\alpha} \nabla \cdot \mathbf{v}_{\alpha} = p \nabla \cdot \mathbf{v} - \mathbf{w} \cdot \mathbf{G} + \frac{\mathbf{j}}{en_i} \cdot \nabla p_i + 2 \nabla \cdot (\xi_n p_i \mathbf{w}) - \nabla \cdot (\xi_i p_n \mathbf{w}) - \nabla \cdot \left(\frac{p_i \mathbf{j}}{en_i} \right). \tag{B.11}$$

Now, the left-hand side of Eq. (B.1) can be written as

$$\frac{\partial p}{\partial t} + \sum_{\alpha} (\mathbf{v}_{\alpha} \cdot \nabla p_{\alpha} + \gamma p_{\alpha} \nabla \cdot \mathbf{v}_{\alpha}) = \frac{\partial p}{\partial t} + \mathbf{v} \cdot \nabla p + \gamma p \nabla \cdot \mathbf{v}$$

$$- (\gamma - 1) \left(\mathbf{w} \cdot \mathbf{G} - \frac{\mathbf{j}}{en_i} \cdot \nabla p_i \right) + \gamma \nabla \cdot \left(2 \xi_n p_i \mathbf{w} - \xi_i p_n \mathbf{w} - \frac{\mathbf{j}}{en_i} p_i \right). \tag{B.12}$$

For the right-hand side we take $Q_{\alpha} = \sum_{\beta} Q_{\alpha\beta}$, where $Q_{\alpha\beta}$ is the heat generated in a gas of particles of species α as a consequence of collisions with particles of species β. Considering

$$Q_{\alpha\beta} + Q_{\beta\alpha} = -\mathbf{R}_{\alpha\beta} \cdot (\mathbf{v}_{\alpha} - \mathbf{v}_{\beta}), \tag{B.13}$$

and Eqs. (B.2)–(B.4), we obtain

$$\sum_\alpha Q_\alpha = \frac{\alpha_e}{e^2 n_i^2} j^2 + \alpha_n w^2 - 2\frac{\alpha_{en}}{e n_i} \mathbf{w} \cdot \mathbf{j}. \tag{B.14}$$

So, upon considering Eqs. (B.12) and (B.14), the energy equation can be written in the following form

$$\frac{dp}{dt} + \gamma p \nabla \cdot \mathbf{v} + \gamma \nabla \cdot (2\xi_n p_i \mathbf{w} - \xi_i p_n \mathbf{w}) - \gamma \nabla \cdot \left(\frac{\mathbf{j} p_i}{e n_i}\right)$$
$$= (\gamma - 1)\left[\frac{\alpha_e}{e^2 n_i^2} j^2 + \alpha_n w^2 - 2\frac{\alpha_{en}}{e n_i}\mathbf{w} \cdot \mathbf{j} + \mathbf{w} \cdot \mathbf{G} - \frac{\mathbf{j}}{e n_i} \cdot \nabla p_i\right]. \tag{B.15}$$

Now, considering the expressions for $\mathbf{w}$ (Eq. [3.50]), with the inertial term neglected)

$$\mathbf{w} \approx -\frac{\mathbf{G}}{\alpha_n} + \frac{\xi_n}{c\alpha_n}\mathbf{j} \times \mathbf{B} + \frac{\alpha_{en}}{\alpha_n}\frac{\mathbf{j}}{e n_i}, \tag{B.16}$$

and for the Joule heating term (Eq. [3.57]), the energy equation for the whole partially ionised plasma is

$$\frac{dp}{dt} + \gamma p \nabla \cdot \mathbf{v} + \gamma \nabla \cdot (2\xi_n p_i \mathbf{w} - \xi_i p_n \mathbf{w}) - \gamma \frac{\mathbf{j}}{e n_i} \cdot \nabla p_i = (\gamma - 1)q_{\text{Joule}}. \tag{B.17}$$

Bibliography

Anzer, U. 2009, A&A, 497, 521

Arregui, I. & Ballester, J. L. 2010, Space Sci. Rev., 59

Arregui, I., Oliver, R., & Ballester, J. L. 2012, Living Reviews in Solar Physics, 9, 2

Arregui, I., Terradas, J., Oliver, R., & Ballester, J. L. 2008, ApJ, 682, L141

Aschwanden, M. J. 2004, Physics of the Solar Corona. An Introduction (Springer)

Ballester, J. L. 2005, Space Science Reviews, 121, 105

Ballester, J. L. 2006, Philos. Trans. R. Soc. A, 364, 405

Ballester, J. L. 2010, Advances in Space Research, 46, 364

Balsara, D. S. 1996, ApJ, 465, 775

Balthasar, H., Wiehr, E., Schleicher, H., & Wohl, H. 1993, A&A, 277, 635

Banerjee, D., Erdélyi, R., Oliver, R., & O'Shea, E. 2007, Sol. Phys., 246, 3

Bashkirtsev, V. S. & Mashnich, G. P. 1984, Sol. Phys., 91, 93

Bashkirtsev, V. S. & Mashnich, G. P. 1993, A&A, 279, 610

Berger, T. E., Shine, R. A., Slater, G. L., et al. 2008, ApJ, 676, L89

Bommier, V. & Leroy, J. L. 1998, in Astronomical Society of the Pacific Conference Series, Vol. 150, IAU Colloq. 167: New Perspectives on Solar Prominences, ed. D. F. Webb, B. Schmieder, & D. M. Rust, 434

Braginskii, S. I. 1965, Reviews of Plasma Physics, 1, 205

Carbonell, M., Forteza, P., Oliver, R., & Ballester, J. L. 2010, A&A, 515, A80+

Carbonell, M., Oliver, R., & Ballester, J. L. 2004, A&A, 415, 739

Carbonell, M., Oliver, R., & Ballester, J. L. 2009, New Astronomy, 14, 277

Carbonell, M., Terradas, J., Oliver, R., & Ballester, J. L. 2006, A&A, 460, 573

Chae, J., Ahn, K., Lim, E., Choe, G. S., & Sakurai, T. 2008, ApJ, 689, L73

Chen, F. F. 1974, Introduction to plasma physics (New York: Plenum Press, 1974)

Cowling, T. G. 1976, Magnetohydrodynamics (Monographs on Astronomical Subjects, Bristol: Adam Hilger, 1976)

Cox, D. P. & Tucker, W. H. 1969, ApJ, 157, 1157

Dahlburg, R. B. & Mariska, J. T. 1988, Sol. Phys., 117, 51

Díaz, A. J. 2004, Ph. D. Thesis: Fast Magnetohydrodynamic Waves in a Line-tied Solar Coronal Flux Tube (Universitat de les Illes Balears)

Díaz, A. J., Oliver, R., & Ballester, J. L. 2002, ApJ, 580, 550

Díaz, A. J., Oliver, R., & Ballester, J. L. 2003, A&A, 402, 781

Díaz, A. J., Oliver, R., & Ballester, J. L. 2005, A&A, 440, 1167

Díaz, A. J., Oliver, R., Erdélyi, R., & Ballester, J. L. 2001, A&A, 379, 1083

Dodson, H. W. 1949, ApJ, 110, 382

Edlén, B. & Swings, P. 1942, ApJS, 95, 532

Engvold, O. 2001, in INTAS Workshop on MHD Waves in Astrophysical Plasmas, ed. J. L. Ballester & B. Roberts (Spain: Universitat de les Illes Balears), 123

Engvold, O. 2008, in IAU Symposium, Vol. 247, IAU Symposium, ed. R. Erdélyi & C. A. Mendoza-Briceño, 152–157

Eto, S., Isobe, H., Narukage, N., et al. 2002, PASJ, 54, 481

Ferraro, V. C. A. & Plumpton, C. 1961, An introduction to magneto-fluid mechanics (Oxford University Press)

Field, G. B. 1965, ApJ, 142, 531

Forteza, P., Oliver, R., & Ballester, J. L. 2008, A&A, 492, 223

Forteza, P., Oliver, R., Ballester, J. L., & Khodachenko, M. L. 2007, A&A, 461, 731

Foullon, C., Verwichte, E., & Nakariakov, V. M. 2004, A&A, 427, L5

Gilbert, H., Hansteen, V., & Holzer, T. 2002, ApJ, 577, 464

Goedbloed, J. P. H. & Poedts, S. 2004, Principles of Magnetohydrodynamics (CUP)

Goossens, M. 2003, An introduction to plasma astrophysics and magnetohydrodynamics (Astrophysics and Space Science Library, Vol. 294. Dordrecht: Kluwer Academic Publishers)

Harvey, J. W. 1969, PhD thesis, University of Colorado

Hildner, E. 1974, Sol. Phys., 35, 123

Hyder, C. L. 1966, ZAp, 63, 78

Ibáñez, S. M. H. & Mendoza, B. C. A. 1990, Ap&SS, 164, 193

Isobe, H. & Tripathi, D. 2006, A&A, 449, L17

Isobe, H., Tripathi, D., Asai, A., & Jain, R. 2007, Sol. Phys., 246, 89

Jing, J., Lee, J., Spirock, T. J., & Wang, H. 2006, Sol. Phys., 236, 97

Jing, J., Lee, J., Spirock, T. J., et al. 2003, ApJ, 584, L103

Joarder, P. S., Nakariakov, V. M., & Roberts, B. 1997, Sol. Phys., 173, 81

Joarder, P. S. & Roberts, B. 1992a, A&A, 256, 264

Joarder, P. S. & Roberts, B. 1992b, A&A, 261, 625

Joarder, P. S. & Roberts, B. 1993, A&A, 273, 642

Kendall, D. C. & Plumpton, C. 1964, Magnetohydrodynamics with hydrodynamics, vol. 1 (Pergamon Press)

Khodachenko, M. L., Arber, T. D., Rucker, H. O., & Hanslmeier, A. 2004, A&A, 422, 1073

Khodachenko, M. L. & Rucker, H. O. 2005, Advances in Space Research, 36, 1561

Khodachenko, M. L., Rucker, H. O., Oliver, R., Arber, T. D., & Hanslmeier, A. 2006, Advances in Space Research, 37, 447

Kippenhahn, R. & Schlüter, A. 1957, Zeitschrift fur Astrophysik, 43, 36

Kleczek, J. & Kuperus, M. 1969, Sol. Phys., 6, 72

Labrosse, N., Heinzel, P., Vial, J., et al. 2010, Space Science Reviews, 151, 243

Landman, D. A., Edberg, S. J., & Laney, C. D. 1977, ApJ, 218, 888

Leake, J. E. & Arber, T. D. 2006, A&A, 450, 805

Leake, J. E., Arber, T. D., & Khodachenko, M. L. 2005, A&A, 442, 1091

Leroy, J. L. 1989, in Astrophysics and Space Science Library, Vol. 150, Dynamics and Structure of Quiescent Solar Prominences, ed. E. R. Priest, 77–113

Lin, Y. 2004, Ph. D. Thesis: Magnetic Field Topology Inferred from Studies of Fine Threads in Solar Filaments (Institute of Theoretical Astrophysics, University of Oslo)

Lin, Y., Engvold, O., Rouppe van der Voort, L., Wiik, J. E., & Berger, T. E. 2005, Sol. Phys., 226, 239

Lin, Y., Engvold, O., Rouppe van der Voort, L. H. M., & van Noort, M. 2007, Sol. Phys., 246, 65

Lin, Y., Engvold, O. R., & Wiik, J. E. 2003, Sol. Phys., 216, 109

Lin, Y., Martin, S. F., & Engvold, O. 2008, in Astronomical Society of the Pacific Conference Series, Vol. 383, Subsurface and Atmospheric Influences on Solar Activity, ed. R. Howe, R. W. Komm, K. S. Balasubramaniam, & G. J. D. Petrie , 235–+

Lin, Y., Soler, R., Engvold, O., et al. 2009, ApJ, 704, 870

Mackay, D. H., Karpen, J. T., Ballester, J. L., Schmieder, B., & Aulanier, G. 2010, Space Science Reviews, 151, 333

Mashnich, G. P., Bashkirtsev, V. S., & Khlystova, A. I. 2009, Astronomy Letters, 35, 253

McWhirter, R. W. P., Thonemann, P. C., & Wilson, R. 1975, A&A, 40, 63

Menzel, D. H. 1951, in Proc. Conf. on Dynamics of Ionised Media (London)

Milne, A. M., Priest, E. R., & Roberts, B. 1979, ApJ, 232, 304

Molowny-Horas, R., Heinzel, P., Mein, P., & Mein, N. 1999, A&A, 345, 618

Moreton, G. E. 1960, AJ, 65, 494

Ning, Z., Cao, W., Okamoto, T. J., Ichimoto, K., & Qu, Z. Q. 2009, A&A, 499, 595

Okamoto, T. J., Nakai, H., Keiyama, A., et al. 2004, ApJ, 608, 1124

Okamoto, T. J., Tsuneta, S., Berger, T. E., et al. 2007, Science, 318, 1577

Oliver, R. 1999, in ESA SP-448: Magnetic Fields and Solar Processes, ed. A. Wilson & et al., 425

Oliver, R. 2004, in ESA SP-547: SOHO 13 Waves, Oscillations and Small-Scale Transients Events in the Solar Atmosphere: Joint View from SOHO and TRACE, ed. H. Lacoste, 175

Oliver, R. 2009, Space Science Reviews, 39

Oliver, R. & Ballester, J. L. 2002, Sol. Phys., 206, 45

Oliver, R., Ballester, J. L., Hood, A. W., & Priest, E. R. 1992, ApJ, 400, 369

Oliver, R., Ballester, J. L., Hood, A. W., & Priest, E. R. 1993, ApJ, 409, 809

Oliver, R., Hood, A. W., & Priest, E. R. 1996, ApJ, 461, 424

Paletou, F. & Aulanier, G. 2003, in Astronomical Society of the Pacific Conference Series, Vol. 307, Solar Polarization, ed. J. Trujillo-Bueno & J. Sanchez Almeida, 458

Pandey, B. P. & Wardle, M. 2008, MNRAS, 385, 2269

Parker, E. N. 1953, ApJ, 117, 431

Patsourakos, S. & Vial, J.-C. 2002, Sol. Phys., 208, 253

Poland, A. & Anzer, U. 1971, Sol. Phys., 19, 401

Priest, E. R. 1984, Solar magneto-hydrodynamics (Geophysics and Astrophysics Monographs, Dordrecht: Reidel)

Ramsey, H. E. & Smith, S. F. 1966, AJ, 71, 197

Raymond, J. C. & Smith, B. W. 1977, ApJS, 35, 419

Roberts, B. 1991, in Advances in Solar System Magnetohydrodynamics, ed. E. R. Priest & A. W. Hood, 105

Roberts, B., Edwin, P. M., & Benz, A. O. 1984, ApJ, 279, 857

Roberts, B. & Joarder, P. S. 1994, in Lecture Notes in Physics, Berlin Springer Verlag, Vol. 432, Advances in Solar Physics, ed. G. Belvedere, M. Rodono, & G. M. Simnett, 173–178

Rosner, R., Tucker, W. H., & Vaiana, G. S. 1978, ApJ, 220, 643

Schmieder, B., Chandra, R., Berlicki, A., & Mein, P. 2010, A&A, 514, A68+

Singh, K. A. P. & Krishan, V. 2010, New A, 15, 119

Soler, R., Oliver, R., & Ballester, J. L. 2007, A&A, 471, 1023

Soler, R., Oliver, R., & Ballester, J. L. 2008, ApJ, 684, 725

Soler, R., Oliver, R., & Ballester, J. L. 2009a, New A, 14, 238

Soler, R., Oliver, R., & Ballester, J. L. 2009b, ApJ, 699, 1553

Soler, R., Oliver, R., & Ballester, J. L. 2009c, ApJ, 693, 1601

Soler, R., Oliver, R., & Ballester, J. L. 2009d, ApJ, 707, 662

Soler, R., Oliver, R., & Ballester, J. L. 2010, A&A, 512, A28+

Soler, R., Oliver, R., Ballester, J. L., & Goossens, M. 2009e, ApJ, 695, L166

Suetterlin, P., Wiehr, E., Bianda, M., & Kueveler, G. 1997, A&A, 321, 921

Tandberg-Hanssen, E., ed. 1995, Astrophysics and Space Science Library, Vol. 199, The nature of solar prominences

Terradas, J., Arregui, I., Oliver, R., & Ballester, J. L. 2008, ApJ, 678, L153

Terradas, J., Carbonell, M., Oliver, R., & Ballester, J. L. 2005, A&A, 434, 741

Terradas, J., Molowny-Horas, R., Wiehr, E., et al. 2002, A&A, 393, 637

Terradas, J., Oliver, R., & Ballester, J. L. 2001, A&A, 378, 635

Tripathi, D., Isobe, H., & Jain, R. 2009, Space Science Reviews, 149, 283

Tsubaki, T. & Takeuchi, A. 1986, Sol. Phys., 104, 313

Tucker, W. H. & Koren, M. 1971, ApJ, 168, 283

Uchida, Y. 1970, PASJ, 22, 341

Vernazza, J. E., Avrett, E. H., & Loeser, R. 1981, ApJS, 45, 635

Vial, J.-C. 1998, in Astronomical Society of the Pacific Conference Series, Vol. 150, IAU Colloq. 167: New Perspectives on Solar Prominences, ed. D. F. Webb, B. Schmieder, & D. M. Rust, 175

Vršnak, B., Veronig, A. M., Thalmann, J. K., & Žic, T. 2007, A&A, 471, 295

Wiehr, E. 2004, in ESA Special Publication, Vol. 547, SOHO 13 Waves, Oscillations and Small-Scale Transients Events in the Solar Atmosphere: Joint View from SOHO and TRACE, ed. H. Lacoste, 185

Yi, Z. & Engvold, O. 1991, Sol. Phys., 134, 275

Yi, Z., Engvold, O., & Keil, S. L. 1991, Sol. Phys., 132, 63

Zaqarashvili, T. V., Carbonell, M., Ballester, J. L., & Khodachenko, M. L. 2012, A&A, 544, A143

Zaqarashvili, T. V., Khodachenko, M. L., & Rucker, H. O. 2011, A&A, 529, A82

Zirker, J. B., Engvold, O., & Martin, S. F. 1998, Nature, 396, 440